Δισδιάστατα και τρισδιάστατα in vitro NSC34 κυτταρικά μοντέλα για την ALS και για φαρμακολογικές μελέτες

Όνομα φοιτητή: Όλγα Σαρλίδου
Εργαστήριο Neural Tissue Engineering, IMBB-ITE
Υπεύθυνος καθηγητής: Α. Γραβάνης
Μεταπτυχιακό Πρόγραμμα: “Μοριακή Βάση των Νοσημάτων του Ανθρώπου”
Ιατρική σχόλη, Πανεπιστήμιο Κρήτης
Νοέμβρης, 2018

Two and Three-dimensional in vitro NSC34 models for ALS and pharmacological studies

By

Olga Sarlidou

Neural Tissue Engineering Laboratory, IMBB-FORTH
Supervisors: Prof. A. Gravanis
This dissertation is submitted for the degree of Master of
The Molecular Basis of Human Diseases
School of Medicine, University of Crete
November, 2018

Table of Contents

List of Tables

List of Figures

List of Acronyms and Abbreviations

ALS	Amyotrophic lateral sclerosis
AMPA	α-amino-3-hydroxy-5-methyl-4-isoxazole propionic acid
Ara-C	Cytarabine - Cytosine arabinoside
Bax	Bcl-2-associated X protein
BBB	Blood–brain barrier
Bcl-2	B cell lymphoma-2
BDNF	Brain-derived neurotrophic factor
CTNF	Ciliary neurotrophic factor
DHEA	*Dehydroepiandrosterone*
EGF	Epidermal Growth Factor
FDA	Food and Drug Administration
FTD	Frontotemporal Dementia
GDNF	Glial cell-derived neurotrophic factor
Ḧ	Hoechst fluorescent dye
H2DCFDA	2´,7´-Dichlorodihydrofluorescein diacetate
H_2O_2	Hydrogen peroxide
IFN-γ	Interferon gamma
IL-1$^{\alpha}$	Interleukin 1 alpha
NGF	Nerve Growth Factor
NMDA	N-methyl-D-aspartate
PI	Propidium iodide
ROS	Reactive oxygen species
SMA	Spinal muscular atrophy
SOD1	Superoxide dismutase 1

Abstract

Amyotrophic Lateral Sclerosis (ALS) is a fatal multifactorial neurodegenerative disorder with most patients dying within 5 years. Despite progress made in unraveling the pathophysiological mechanisms of ALS, no effective treatment has been found. So far *only two drugs have received FDA approval for ALS (Riluzole, Edaravone), though both have limited effect on life expectancy. With most human clinical trials failing to demonstrate clinical efficacy, better pre-clinical models are required to save lives. This thesis utilizes a novel systems-level culture platform based on the NSC34 motor neuron-like cell like to evaluate various pro-apoptotic stimuli that mimic aspects of ALS pathophysiology (oxidative stress, excitotoxicity neuroinflammation) were investigated. Then, the effect of ALS FDA-approved or candidate drugs (Edaravone, BNN20) was evaluated. Experimental data based on high-content fluorescent imaging were consistent and reproducible. 24h or 48h serum deprivation and 48h of 100 ng/ml TNFα induced apoptosis and could be further incorporated to screen for novel neuroprotective compounds including novel microneurotrophins. NSC34 apoptosis induced by 100 μM H_2O_2 was not reversed upon Edaravone, BNN20 or BDNF treatment. The expression of TrkB and $p75^{NTR}$ receptors was confirmed in NSC34 cells, underling the potential of NSC34 utilization in TrkB - mediated pharmacological studies. Finally, this thesis presents the first steps towards developing* a more physiologically relevant *in vitro 3D cell culture model based on growing and studying NSC34 inside porous collagen scaffolds. Transition of NSC34 cell to 3D platform required seeding of C2C12 muscle cell line, as no NSC34 cell attachment to collagen occurred in the absence of C2C12. Further optimization of the NSC34 and C2C12 co-culture parameters (including cell differentiation, number, ratio and seeding as cell spheres or as single cells) demonstrated that differentiated single cells of both NSC34 and C2C12 provided the best results in terms of NSC34 adhesion to collagen and axonal growth.*

Keywords: ALS, Neurotrophins, Microneurotrophins, TRK Receptors, TrkB, NSC34, C2C12, 2D Sandwich Matrigel Culture, 3D Collagen I Scaffolds

Περίληψη

Η Αμυοτροφική πλευρική σκλήρυνση (ALS) είναι μια θανατηφόρα πολυπαραγοντική νευροεκφυλιστική νόσος με τους περισσότερους ασθενείς να υποκύπτουν μέσα σε διάστημα πενταετίας. Παρά την πρόοδο που έχει σημειωθεί στην διερεύνηση των μηχανισμών που συμβάλλουν στην παθοφυσιολογία της ALS, δεν έχει βρεθεί ακόμα κάποια αποτελεσματική θεραπεία. Μέχρι στιγμής μόνο δύο φάρμακα έχουν εγκριθεί από την FDA (Riluzole, Edaravone), όμως και τα δύο παρέχουν περιορισμένη αποτελεσματικότητα στο προσδόκιμο ζωής. Με την πλειονότητα των κλινικών δοκιμών να μην φέρουν κλινική αποτελεσματικότητα, καλύτερα προκλινικά μοντέλα είναι απαραίτητα για την επιβίωση των ασθενών. Σε αυτή τη μεταπτυχιακή εργασία, χρησιμοποιήθηκε μια καινοτόμος πλατφόρμα για συστημικές κυτταρικές μελέτες που βασίζεται στην καλλιέργεια της κυτταρικής σειράς NSC34 (μοντέλο κινητικών νευρώνων) για να διερευνηθούν οι επιδράσεις διάφορων προ-αποπτωτικών διεγέρσεων που προσομοιάζουν διάφορες πτυχές της παθοφυσιολογίας της νόσου (οξειδωτικό στρες, νευροφλεγμονή, διεγερτοτοξικότητα). Η πλατφόρμα χρησιμοποιήθηκε για να αξιολογηθεί η αποτελεσματικότητα ενός εγκεκριμένου από την FDA και ενός νέου υποψήφιου φαρμάκου για το ALS (Edaravone, BNN20 αντίστοιχα). Παρόλο που τα αποτελέσματα βρίσκονται σε πρωταρχικό στάδιο, παρατηρείται επαναληψιμότητα στα πειραματικά δεδομένα. Βρέθηκε ότι τόσο η αφαίρεση όρου από το θρεπτικό της καλλιέργειας για 24h ή 48h όσο και η διέγερση για 48h από 100 ng/ml TNFα προκαλούν αυξημένο κυτταρικό θάνατο και μπορούν να χρησιμοποιηθούν σε περαιτέρω μελέτες ουσιών ή φαρμάκων με νευροπροστατευτική δράση (Νευροτροφίνες, Μικρονευροτροφίνες). Η απόπτωση που προκλήθηκε από τη διέγερση με 100 μM H_2O_2 δεν μπόρεσε να αντιστραφεί με τη χορήγηση Edaravone, BNN20 ή BDNF στα κύτταρα NSC34. Επιπλέον, η επιβεβαίωση της έκφρασης των υποδοχέων TrkB και $p75^{NTR}$ στα NSC34 κύτταρα, ανέδειξε τη δυνατότητα χρήσης των NSC34 κυττάρων σε φαρμακολογικές μελέτες του TrkB υποδοχέα. Τέλος έγιναν τα πρώτα βήματα για την ανάπτυξη μιας in vitro 3D κυτταρικής πλατφόρμας για μελέτες φαρμάκων με βάση την καλλιέργεια των NSC34 μέσα σε πορώδη ικριώματα κολλαγόνου με στόχο την καλύτερη προσομοίωση των in vivo συνθηκών. Η εισαγωγή των κυττάρων NSC34 στην 3D πλατφόρμα απαιτεί τη χρήση της κυτταρικής σειράς C2C12, καθώς απουσία της δεν παρατηρήθηκε προσκόλληση των NSC34 κυττάρων στα ικριώματα κολλαγόνου. Συνεπώς, διεξήχθη βελτιστοποίηση του συστήματος συν-καλλιέργειας των δύο κυτταρικών σειρών. Παράμετροι σχετικοί με την κυτταρική διαφοροποίηση, τον αριθμό, την αναλογία και τη μορφολογία (σφαίρες ή μεμονωμένα κύτταρα) εξετάστηκαν με τα αποτελέσματα να υποδηλώνουν ότι οι συν-καλλιέργειες διαφοροποιημένων μεμονωμένων κυττάρων είναι οι πιο αποτελεσματικές όσον αφορά την προσκόλληση των NSC34 στο ικρίωμα και το μήκος των νευραξόνων των NSC34 κυττάρων.

Λέξεις-κλειδιά: ALS, *Νευροτροφίνες, Μικρονευροτροφίνες* , TRK υποδοχείς, TrkB, NSC34, C2C12, 2D Sandwich Matrigel καλλιέργεια, Πορώδη Ικριώματα Κολλαγόνου τύπου Ι

Chapter 1: Introduction

1.1. Amyotrophic Lateral Sclerosis (ALS)

1.1.1. Introduction to ALS

ALS is a multifactorial heterogenous adult-onset neurodegenerative disease that attacks the motor system leading to a focal and unilateral limb weakness or bulbar dysfunction and eventually to fatal paralysis (Van Damme et al., 2017; Hardiman et al., 2017). The motor system is comprised from the upper (corticospinal) motor neurons in the motor cortex and the lower (bulbar and spinal) motor neurons in the spinal cord and brain stem that innervate muscles (Brown & Al-Chalabi, 2017). Although identified for the first time as a specific disease 1869 in by the French neurologist Jean Martin Charcot (Charcot & Joffroy, 1869), ALS became more known in 1939 when a famous baseball player, Lou Gehrig was diagnosed with this disease. Therefore, ALS may as well be referred as both Charcot's sclerosis or Lou Gehrig disease (Cleveland & Rothstein, 2001).

ALS is the third most common neurodegenerative disease and the first most common adult-onset motor neuron disease (Renton et al., 2013). The average survival of individuals diagnosed with ALS is 2-5 years with many patients collapse due to respiratory failure (Van Damme et al., 2017). 15-20% of patients have progressive cognitive abnormalities and show behavioural changes indicating as well Frontotemporal Dementia (FTD or Prick's disease) (Brown & Al-Chalabi, 2017; Al-Chalabi et al., 2016). In the case of the Nobel-prize-winning astrophysicist Stephen Hawking the disease had an unusual slow progression with nearly complete muscle paralysis, but without cognitive impairment (Cleveland & Rothstein, 2001).

As with many other neurodegenerative diseases, the mechanisms underlying the pathophysiology of ALS remain unclear, despite the discovery of more than 20 mutated genes in patients with hereditary ALS (Van Damme et al., 2017). Animal and cellular models that aim to recapitulate some of the aspects of ALS disease pathology have contributed to better understanding of the pathogenic processes that cause ALS (Van Damme et al., 2017). Such processes include oxidative stress, mitochondrial dysregulation, protein aggregation, excitotoxicity and neuroinflammation caused by microglia and astrocytes. These aspects will be further analysed in the following sections. Consistent with a study that suggested that sensory and spinocerebellar pathways as well as specific substantia nigra and hippocampal dentate granule layer neurons were implicated in disease pathology (Ince et al., 2008), new imaging and neuropathological data demonstrated again a non-motor neuraxis contribution, hence classifying the disease as a multisystemic disorder (Ferraiuolo et al., 2011; Hardiman et al., 2017).

1.1.2. Epidemiological Features

According to European ALS Epidemiology Consortium, in Europe the incidence rate is 2 to 3 cases per 100,000 individuals. However, when epidemiological study was performed based on ancestral origin, the incidence rate was more than 3 cases per 100,000 individuals. Incidence rate in both East and South Asia (0.8 and 0.7 per 100,000 respectively) were lower than the one found in Europe. Guam and the Kii peninsula of Japan showed high incidence rates possibly due to an environmental toxin (β-methylamino-L-alanine) that have been reduced in recent years. Countries with homogenous populations such as Ireland demonstrated as well high incidence rates (2.6 per 100,000) (Hardiman et al., 2017). Sex is a non-genetic risk factor for ALS as several studies have revealed a 1.5:1 male:female ratio. However, this could be an artefact as in younger groups of studied patients, men were predominant (Brown & Al-Chalabi, 2017). An interesting fact is that in Europe most men have spinal-onset ALS, while women have bulbar-onset ALS (Hardiman et al., 2017). The incidence and prevalence of disease increase with age (Brown & Al-Chalabi, 2017). The age of onset is 65 years in Europe, which is higher that Asia or South America (Hardiman et al., 2017). Approximately ~10% of ALS cases are

classified as familiar ALS (fALS) when inherited in a dominant manner, whereas the remaining ~90% of cases with no apparent genetic linkage are classified as sporadic (sALS) (Renton et al., 2013).

1.1.3 Pathological Characteristics

The major clinical manifestation of ALS is motor neuron death that eventually results in respiratory failure. Increased muscle tone, stiffness, spasticity, hyperreflexia and slowing of voluntary movements are characteristic for upper motor neuron loss. Signs like muscle weakness and atrophy, cramps and fasciculations (spontaneous muscle twitching) are associated with lower motor neuron degeneration. Spinal-onset disease, typically starting with a weakness in limb muscle, affects 2 out of 3 patients. 1 out of 3 patients present bulbar-onset disease where bulbar muscle weakness results in dysphagia (difficulty in chewing and swallowing) and dysarthria (difficulty in speaking) (Brown & Al-Chalabi, 2017; Hardiman et al., 2017; Van Damme et al., 2017). When disease progresses, it may affect as well neurons that innervate the eyes or sphincter muscle (Brown & Al-Chalabi, 2017). Moreover, half of the patients develop non-motor neuron symptoms due to degeneration of the frontal and anterior temporal lobes. Such symptoms include progressive cognitive and behavior impairment (Hardiman et al., 2017; Van Damme et al., 2017). 10-13% of these patients demonstrate Frontotemporal Dementia (FTD) (Hardiman et al., 2017; Van Damme et al., 2017). ALS is diagnosed based on El Escorial and Airlie House criteria (Hardiman et al., 2017; Gordon, 2013). ALS diagnosis requires history and clinical examination of upper and lower motor neuron findings. Neuron denervation is confirmed and evaluated by electromyography, MRI and further laboratory tests. These tests exclude the possibility of other diseases such as multifocal motor neuropathy (MMN) with conduction block or cervical spondylosis (Gordon, 2013).

***Figure 1.1.3.*: ALS pathology**. *Lateral atrophy and furrowing of the tongue in an ALS patient on the left, and the flail-arm syndrome with thinned arms and shoulders on the right. (Brown & Al-Chalab, New Eng. Journal of Med. 2017)*

1.1.4 Genetic Features

Through years many genes associated with variant forms of ALS have been identified. The Superoxide dismutase 1 (SOD1) is the first gene identified as mutated in ALS and is responsible for 15% of the familiar and 1-2% of the sporadic ALS cases (Rosen, 1993). SOD1 gene encodes the Cu/Zn superoxide dismutase enzyme that plays a major role in destroying free superoxide radicals in the body, produced primarily by errors of mitochondrial oxidative phosphorylation to water and hydrogen peroxide. This action is mediated through a two-step catalytic reaction: the reduction of an essential copper atom and oxidation by superoxide (Figure 1.1.3) (Cleveland & Rothstein, 2001). SOD1 is a ubiquitously expressed, 153-amino-acid protein with more than 120 mutations identified in over 60 residues (Andersen, 2000; Taylor et al., 2017). The majority of mutations are amino-acid point mutations, while few induce protein C-terminal truncations (Andersen et al., 2003). The mutant form of human SOD1 ($hSOD1^{G93A}$) that is widely used in many animal and cell models (see Table 1.3.3.) arose by a point mutation in the 93^{th} position where alanine substituted glycine (Menzies, 2002).

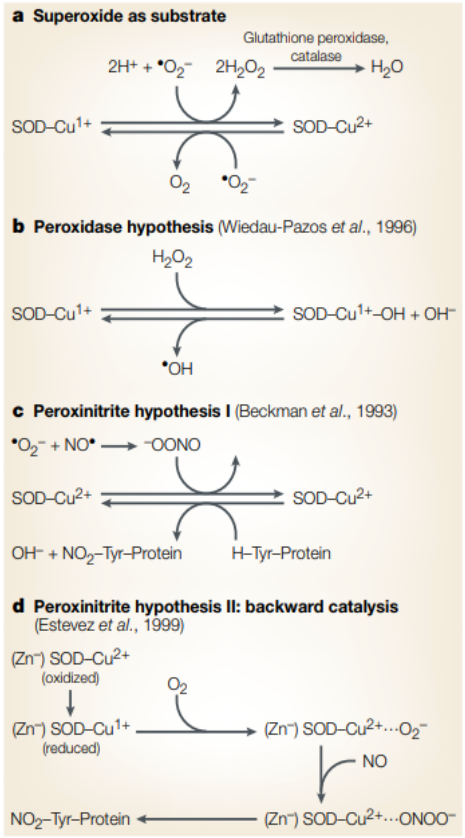

***Figure 1.1.4.1.*: SOD1 chemistry**. *a. SOD1-mediated dismutation of superoxide in two asymmetric steps. b. Hydroxyl radical formation when hydrogen peroxide acts as substrate. c,d. Protein nitration models (Cleveland & Rothstein, Nature Rev. Neur, 2001)*

Other genes highly associated with ALS include noncoding GGCCCC repeat-expansions of the C9orf72 (DeJesus-Hernandez et al., 2011; Renton et al., 2011), TAR DNA binding protein 43 (TDP-43) (Rutherford et al., 2008; Sreedharan, et al., 2008), fused in sarcoma/translated in liposarcoma (FUS/TLS) (Kwiatkowski, et al., 2009; Vance et al., 2009), UBQLN2 (Deng et al., 2011), p62 (Fecto et al., 2011), Valosin Containing Protein (VCP) (Johnson et al., 2010), Vascular Endothelial Growth Factor (VEGF) (Oosthuyse, et al., 2001) and Matrin 3 (Johnson et al., 2014). A recent review summarizes all the genes implicated in ALS, in association with their inheritance and role in ALS pathogenesis (Hardiman et al., 2017). Despite progress in understanding ALS biology, the exact genetic and molecular pathways responsible for neuronal degeneration in most ALS cases are still largely unknown (Boillée, et al, 2006). Moreover, neurodegenerative disorders such as the FTD and the Spinocerebellar ataxia share similar mutations in C9orf72 and in Ataxin2 genes respectively with ALS (Robberecht & Philips, 2013), implying a common mechanism. Although the expansion repeats of the C9orf72 gene intron accounts for 40% of ALS cases and 25% of FTD cases, such repeats could not be detected until recently (Renton et al., 2013) – as sequencing tools currently used miss large repetitive sequences (Brown & Al-Chalabi, 2017). The rate of gene discovery in ALS, summarized in Figure 1.1.4.2., is doubling every 4 years (Brown & Al-Chalabi, 2017).

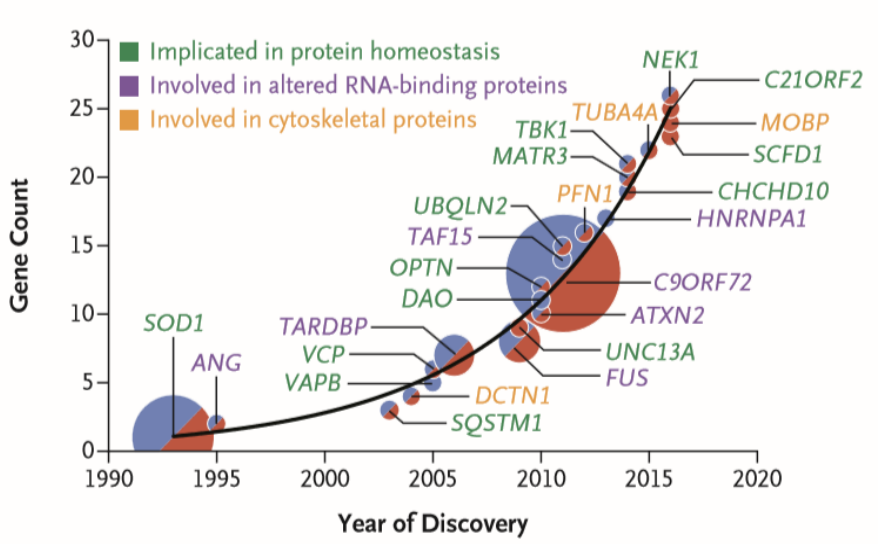

***Figure 1.1.4.2.:* Gene discovery in ALS**. *The timeline starts with the discovery of the first ALS associated gene, SOD1, and follows an exponential growth. The size of each circle represents the proportion of the gene in ALS cases, where blue corresponds to fALS and red to sALS. (Brown & Al-Chalab, New Eng. Journal of Med. 2017)*

1.1.5. Mechanisms in ALS Pathogenesis

ALS pathogenesis is a result of the interplay between several genetic and environmental factors. The similarities in pathological and clinical features observed in both fALS and sALS suggest a common pathway involved in motor neuron death (Brown & Al-Chalabi, 2017). Many different interacting mechanisms that are impaired, are involved in the overall pathophysiology of the disease. Such mechanisms include oxidative stress, excitotoxicity, neuroinflammation, mitochondrial dysregulation, protein homeostasis and transport impairment, DNA repair, abnormal RNA metabolism and axonopathy (Brown & Al-Chalabi, 2017; Hardiman et al., 2017). Furthermore, other non-neuronal cells, including microglia, astrocytes and oligodendrocytes, contribute to ALS pathophysiology. However, due to ALS heterogeneity, not all mechanisms involved in each ALS are known (Hardiman et al., 2017). Figure 1.1.5. illustrates the known mechanisms of ALS, which are further discussed in the following sections.

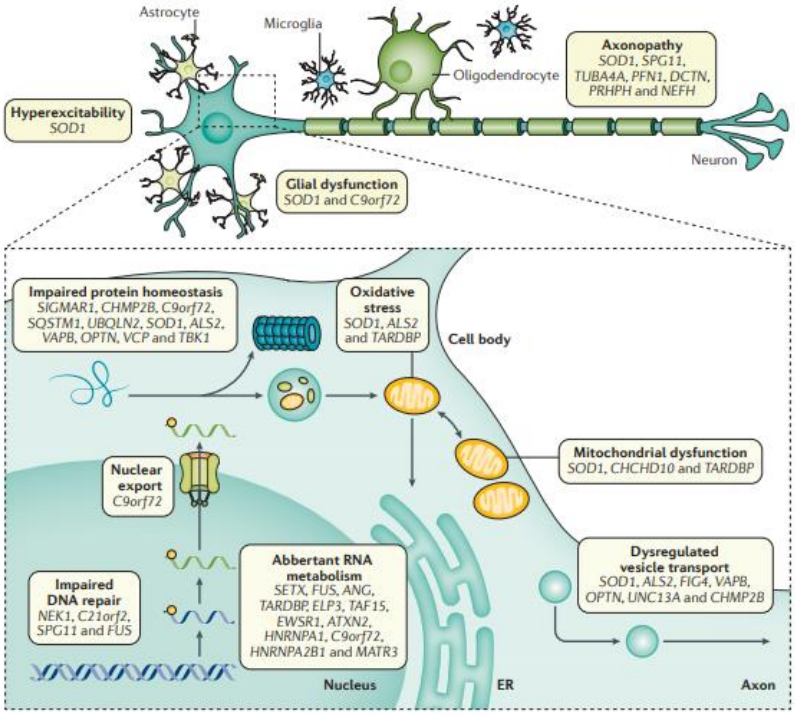

Figure 1.1.5.: ***Mechanisms involved in ALS pathophysiology****. Mechanisms are often interlinked, with mutations in several genes causing neuronal injury through activation of more than one pathophysiological mechanisms. (Hardiman et al., Nature Reviews/Disease Primers. 2017)*

1.1.5.1. Oxidative stress

Oxidative damage observed in spinal cord and cerebrospinal fluid of ALS patients as well as SOD1 mutations in 20% of familial ALS cases prove that oxidative stress is a central mechanism for neuronal degeneration (Barber & Shaw, 2010). However, whether oxidative stress is a primary cause of degeneration or just a consequence of impaired cellular homeostasis, remains unclear (Ferraiuolo et al., 2011).

Oxidative stress is a result of accumulation of by-products of the aerobic metabolism, known as reactive oxygen species (ROS), when the balance between ROS and anti-oxidants is impaired (Liu et al., 2017). ROS are also produced naturally in small proportions by cellular oxidative enzymes. Free radicals (superoxide and nitric oxide, NO·) are involved in signal transduction as second messengers, are also produced in immune cells (Barber & Shaw, 2010). Superoxide and hydrogen peroxide are not highly reactive, in contrast to their derivatives peroxynitrite (ONOO−) and hydroxyl radical (·OH) respectively (Barber & Shaw, 2010), which can lead to protein and DNA damage, lipid peroxidation, and apoptosis (Liu et al., 2017).

Besides being a superoxide radical (O^{2}•-) scavenger, SOD1 is involved in cellular respiration, energy metabolism and posttranslational modification (Saccon et al., 2013). SOD1 convers O2•– into H_2O_2 and molecular oxygen (Figure 1.1.4.1.). Gain-of-function of mutant SOD1 protein has been significantly implicated in motor neuron disease pathogenesis. For instance, mutant SOD1 can lead to mitochondrial dysfunction (D'Amico et al., 2013) with subsequent consequences. Two predominant hypotheses explain this mutant SOD1 function. According to the first hypothesis, abnormal copper catalysis or metal binding alter enzyme activity by altering configuration of the active channel (Pasinelli & Brown, 2006). Thus, the enzyme performs a backward catalysis, where SOD1 converts H_2O_2 into hydroxyl radicals through the Fenton reaction (Yim et al., 1996). According to the second hypothesis, unproper zinc binding results in rapid reduction of SOD1-bound copper, producing superoxide anion that subsequently reacts with nitric oxide, generating peroxynitrite and eventually tyrosine

nitration (Barber and Shaw, 2010). Although both hypotheses can contribute to the toxicity of mutated SOD1, they are unable to explain why copper depletion had no change on disease onset or progression of $SOD1^{G93A}$ mice (Subramaniam et al., 2002). Furthermore, down-regulation of genes involved in the antioxidant responses was evident in mutant SOD1 neuron cells through microarrays (Kirby et al., 2005).

1.1.5.2. Excitotoxicity

Calcium influx due to excessive glutamate-induced stimulation can lead to the activation of calcium-dependent enzymatic pathways that disrupt mitochondrial function. Mitochondrial dysfunction can result in generation of free radicals that eventually cause neuronal injury (Van Den Bosch et al., 2000; Blasco et al., 2014). Two families of ionotropic ligand-gated cation channels (Lodge, 2009) are mainly involved in this process (Van Den Bosch et al., 2000): AMPA and NMDA glutamate receptors, named after their non-natural preferred agonists. Motor neurons contain more AMPA receptors with less GluR2 subunits - making them more Ca^{2+} permeable - comparing to other neuronal cells, and hence, are more susceptible to Ca^{2+} influx. Moreover, motor neurons have lower expression of calcium-buffering proteins (Ferraiuolo et al., 2011). Moreover, loss of the astroglia protein transporter - the excitatory amino acid transporter 2; EAAT2 - responsible for reuptake of synaptic glutamate, results in overstimulation of neuron cells, promoting neuronal injury and toxicity (Hardiman et al., 2017). Both rodent models and ALS patients showed loss of EAAT2 transporter with subsequent elevation of glutamate in CSF (Hardiman et al., 2017; Wijesekera & Leigh, 2009).

1.1.5.3. Neuroinflammation

Imaging studies of ALS patients reveal signs of neuroinflammation (Corcia et al., 2012), with pro-inflammatory molecules, such as TNFα, present in patient CSF (Ferraiuolo et al., 2011). Moreover, in early stages of neurodegeneration recruited regulatory T_{REG} cells and monocytes are evident (Ferraiuolo et al., 2011). T_{REG} cells stimulate the secretion of anti-inflammatory cytokines in microglia to attenuate neuroinflammation (Kipnis, 2004). When mutated SOD1 was depleted from astrocytes and microglia, which produce both protective and hazardous factors, mice survival was increased and disease progression was attenuated (Wang et al., 2010). Moreover, ALS mouse models demonstrated a microglial switch from the resting M2 phenotype (associated with neuroprotection) at the disease onset, to activated-primed M1 phenotype (associated with neurotoxicity) at the final stage of disease (Liao et al., 2012). Release of anti-inflammatory cytokines, neurotrophins and growth factors activates microglia to induce neuronal repair and controlled synaptic stripping. Release of pro-inflammatory cytokines as TNFα and MCP-1, though, promotes microglial-induced neuronal injury (Moisse & Strong, 2006). On the other hand, mutated SOD1 astrocytes released lactate, activated the $p75^{NTR}$ pathway and were unable to release trophic factors and support motor neurons (Ferraiuolo et al. 2011). Finally, ROS-induced glial cells further promote the release of ROS and pro-inflammatory cytokines that subsequently activate more glial cells, inducing therefore neurotoxicity (Barber & Shaw, 2010). The potential role of TNFα in ALS pathophysiology is demonstrated in Figure 1.1.5.3.

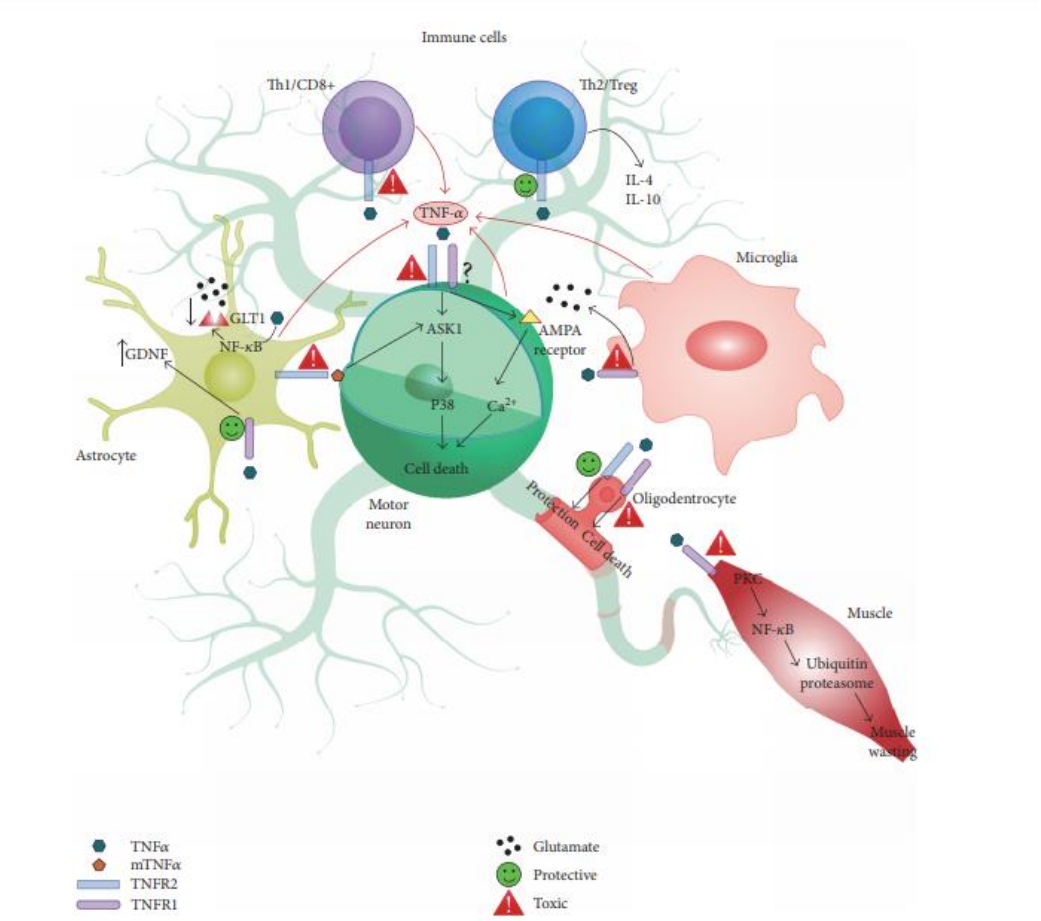

Figure 1.1.5.3.: ***Potential mechanisms of TNFα involved in the ALS pathophysiology****. TNFα and its receptors TNFR1 and TNFR2 have both neuroprotective and neurotoxic functions depending on cell type. (Tortarolo et al., 2017)*

1.1.5.4. Other mechanisms involved in ALS pathophysiology

One of the hallmarks of ALS pathophysiology is the accumulation of ubiquitylated proteinaceous inclusions found as well in other neurodegenerative diseases (amyloid plaques in Alzheimer and synuclein-containing Lewy bodies in Parkinson) (Xiao et al., 2006; Hardiman et al., 2017). In ALS, cytoplasmic inclusions contain the RNA-binding TDP43 protein – a protein that normally is located in the nucleus - in almost 97% of ALS patients, despite the fact that mutations in the TDP43 gene that encodes this protein are rare in ALS (Kabashi et al., 2008). These TDP43 inclusions are not restricted to motor neurons (Ferraiuolo et al., 2011) and may self-assemble to form prion-like aggregates (Kim et al., 2013). Furthermore, Bunina Bodies that are small, 2–4μm diameter, granular eosinophilic inclusions with immunoreactivity for the cysteine proteinase inhibitor, cystatin C and transferrin, were found in 85% of ALS cases (Xiao et al., 2006). Some of the inclusions have Lewy body-like morphology, however unlike Parkinson's disease, are alpha-synuclein negative (Xiao et al., 2006). Moreover, in specific subtypes of ALS other proteins like misfolded SOD1 or neurofilamentous hyaline conglomerate inclusions (argyrophilic structures found within the neuronal perikaryal) may accumulate (Xiao et al., 2006; Hardiman et al., 2017). Misfolded SOD1 is characteristic for SOD1-linked fALS as mouse and cellular models of mutant SOD1 demonstrated (Shibata N et al., 1994). In contrast to wild-type SOD1, mutant SOD1 in the course of time leads to the formation of small structures with similarities to β-amyloid protein (Matsumoto et al., 2006). Moreover, misfolded SOD1 was associated with reduced expression of factors involved in the ubiquitin – proteasome

system (Urushitani et al., 2002). The exact role of these inclusions in ALS pathogenesis still remains a mystery. These aggregates may be innocent by-products or a result of a cell defence mechanism for the reduction of toxic protein concentrations (Wijesekera & Leigh, 2009). The fact that both sALS and fALS share this hallmark implies that a common pathway in involved, despite the heterogeneity of disorder (Xiao et al., 2006).

Another hallmark of ALS pathophysiology is mitochondrial dysfunction, as abnormalities in morphology and biochemistry of mitochondria are present in both ALS patients and SOD1 transgenic mice models (Velde et al., 2011; Magrane et al., 2014). Such abnormalities include the formation of mutated SOD1 containing vacuoles in inter-membrane space that lead to protein import impairment (Higgins et al., 2003). Additionally, reduction in electron transport chain activity and mitochondrial membrane potential, impairment of calcium homeostasis and reduced antioxidant defence mechanism are as well present (Barber & Shaw, 2010). Oxidative damage due to leaks of electrons that convert into molecular oxygen in the respiratory chain, leads to ROS production and mitochondrial DNA damage (Barber & Shaw, 2010).

Many mutations in RNA-binding proteins (e.g. FUS, TDP43) found in rare cases of ALS imply that abnormal RNA metabolism and trafficking contributes to ALS pathogenesis. Specifically, mis-localization to cytoplasm is implied to the loss of their target-RNA processing (transcription, splicing, mRNA transport) (Hardiman et al., 2017). Nevertheless, dysregulation of nucleocytoplasmic, endosomal and vesicle transport as well as impaired DNA repair are as well contribute to the disease pathogenesis (Hardiman et al., 2017).

1.2 *In vitro* and *in vivo* models of ALS

Based on identified mutations, a wide range of different ALS models that mimic aspects of ALS have been developed (Philips & Rothstein, 2015). Such cellular and animal ALS models offer essential tools for understanding ALS pathophysiology and hence can contribute to the identification of novel therapeutic targets (Van Damme et al., 2017).

Although cellular systems are too simple in mimicking the complexity of human disease, they offer important information regarding gene and protein function. For instance, *in vitro* cellular systems as oligomerization and aggregation assays help in unravelling of the biophysical properties of protein aggregates (Van Damme et al., 2017). Additionally, the simplicity of budding yeast (*Saccharomyces cerevisiae*) suits in cytotoxicity ALS models, while various cell lines are utilized in ALS-associated-gene function studies (Van Damme et al., 2017). Protocols for the isolation of motor neurons from newborn or embryonic murine spinal cord (Gingras et al., 2007; Wiese et al, 2010), organotypic cultures (Ferraiuolo et al., 2014) and stem-cell technologies (Lee & Huang, 2017) have been developed. The poor proliferation of motor neuron culture after its differentiation is a technical difficulty that was solved by the development of immortalized cell lines transfected with ALS-associated genes as NSC34 (Cashman et al., 1992).

The complex interplay between motor neurons and their surrounding environment inside a living organism, something that cellular models are unable to provide, is recapitulated by using small animal models. Such models include the *Drosophila melanogaster*, *C. elegans*, Zebrafish (*Danio rerio*) and rodents. Van Damme et al., 2017 in their review summarize all the different model systems as also their contribution in current knowledge of ALS disease (Van Damme et al., 2017).

It is important to mention that animals do not naturally develop ALS. Only dogs experience an ALS-like neuromuscular disease (Clerc et al., 2016). Animals of ALS models are subjected to artificial expression of a mutant human ALS-associated gene (Clerc et al., 2016). Although animal models have provided significant information regarding ALS biology, they are not the ideal system for modelling this complex human condition with adequate fidelity (Serio & Patani, 2017). Several reviews address the lack of clinical translation from rodent models to humans and their inability to predict efficacy, safety and toxicity in humans (Mcgonigle & Ruggeri,

2014; Clerc et al., 2016; Serio & Patani, 2017). Animal models fail to face validity as they are incapable to fully replicate the complete spectrum of ALS symptoms in humans with the same progression and neurobiological mechanism of action. Moreover, animal models generated by human gene overexpression may carry hundreds of copies of the human transgene and express it several-folds higher than endogenous animal gene expression. This overload may result to toxic effects that resemble an ALS-like phenotype, but do not associate with ALS disease progression. Furthermore, ALS is a strongly age-related disease: differences in lifespan, tissue-specific cellular turnover rates, oxidative stress responses and gene expression patters among the species, as well as, environmental and dietary factors may result to different progression of the disease. The spinal cord anatomy and the unique gene expression profile of human brain may further contribute to the inability of animal models to recapitulate disease phenotype (Clerc et al., 2016). The aforementioned reasons explain partially why preclinical drug studies have not managed to successfully translate into human clinical trials (Clerc et al., 2016).

A promising strategy is the integration of human experimental models that utilize patient-specific induced Pluripotent Stem Cells (iPSCs). In 2008, Dimos and his colleagues first managed to generate patient-specific iPSCs using skin fibroblasts collected from an 82-year-old woman with fALS. The collected cells maintained stem cell potency and were differentiated successfully into motor neurons (Dimos, et al., 2008). The integration of iPSC-based models to 3D platforms holds a great potential to be used not only in high throughput drug screening and therapy design, but also in conducting physiological and mechanistic studies. Such studies can potentially improve the understanding of interactions between neuronal cells and their surrounding environment, as well as, aid in a better understanding of the ALS pathogenesis without the use of animal models. A recent review provides a comprehensive summary of ALS and FTD studies that utilize iPSC-derived neurons and their potential in drug screening are analysed (Lee & Huang, 2017).

1.3 The NSC34 cell line

The NSC34 cell line is a fusion of motor-neuron-enriched embryonic mouse spinal cord cells and mouse neuroblastoma (Cashman et al., 1992). In this section NSC34 derivatives, growth and differentiation protocols, cell markers and properties, as well as ALS related studies that are reported in literature will be analyzed.

1.3.1. The NSC34 Cell Line and Its Derivatives

The majority of studies on the functionality and trafficking of neurotrophic growth factor receptors have exploited the potential of the non-neuronal rat PC12 pheochromocytoma cell line that expresses TrkA and $p75^{NTR}$ receptors. Since TrkA is not expressed in several CNS neuron types, including motor neurons, and due to the lack of a well-characterized 'easy-to-maintain' primary neuron culture, there was a need to develop an equivalent immortalized motor neuron-like cell line that would exceed the morphology and the physiology of primary motor neurons. Cashman et al., 1992 developed such a cell line by fusing mouse aminopterin-sensitive N18TG2 neuroblastoma and motor neuron-enriched primary embryonic day 12–14 spinal cord cells. The resulting NSC34 cell line kept several parental properties of the original primary motor neurons. Since then, the NSC34 cell line has been widely used, solving the problem of the low yields of motor neuron cultures and becoming the most stable motor neuron cell line for modelling the ALS pathophysiology (Veyrat-Durebex et al., 2014).

Upon seeding, NSC34 cells remain round with many neurite-like processes appearing over the course of time. NSC34 culture contains two distinct cell populations: small, undifferentiated, highly proliferating cells and larger, multi-nucleate, non-dividing motor neuron-like cells (Eggett et al., 2000). Undifferentiated (immature) NSC34 cells (denoted as NSC34) include both proliferating and non-proliferating cell populations whereas differentiated (mature) NSC34 cells (denoted as $NSC34_D$) obtained through the differentiation of undifferentiated NSC34 cells, consist mainly of non-dividing motor neuron cells. Work on the development of an experimental

model for glutamate-mediated excitotoxicity pointed out the inability to produce cultures consisting only of differentiated cells (Hounoum et al., 2016). In this study Hounoum et al., 2016, assessed if the all-trans retinoic acid (atRA) responded differently - in terms of neurite outgrowth - depending on the differentiation conditions. Therefore, they investigated three different differentiation media with or without the atRA addition: the classical DMEM cell medium, the 1:1 DMEM/Ham's F12 that is commonly used for NSC34 differentiation (Johann et al., 2011) and the α-MEM medium that was previously used for another neuron-like cell line (P19) (MacPherson et al., 1997). Using Sholl's method for quantification of dendritic branching in hippocampal neurons (Sholl, 1956) they classified cells with neurites longer than 50 μm as differentiated. By adding 1 μM atRA to the differentiation protocol of Johann et al., 2011, they observed a 60–70% reduction in NSC34 proliferation in 4 days, with approximately 80% of surviving NSC34 having a motor neuron-like phenotype. After 4 weeks of NSC34 culture, average neurite outgrowth was increased by 55% with α-MEM medium plus atRA, decreased by 20% with DMEM/Ham's F12 media plus atRA and had no significant change with DMEM plus atRA. Moreover, studying the expression profile of all glutamate receptors promoted by NSC34 differentiation, they found that the DMEM/Ham's F12 medium without RA generated the most glutamate receptors - all AMPR subunits (GluA1–4) and half of the NMDAR subunits (GluN1, GluN2A, and GluN2D) - and the less heterogeneity bias (Hounoum et al., 2016). This work is an example of how the various differentiation conditions affect the resulting mixture and phenotype of cells. Several other differentiation protocols reported in literature are listed in Table 1.3.1 below.

Table 1.3.1.: Published growth and differentiation protocols for NSC34.

Medium	Recipe	Subculture	Differentiation	Reference
Growth	DMEM,10% FBS, 1% PSG	3-4 days	-	Cashman et al., 1992
	DMEM, 10% FCS, 0.5% P/S	2–3 days	-	Johann et al., 2011
	DMEM 1X GlutaMAX-I, 10% heat-inactivated FBS, 1% P/S	ND	-	Bonafede et al. 2016
Differentiation	1:1 DMEM/F12 (Ham), 1% FBS, 1% PSG, NEAA	2 times	7 days	Eggett et al., 2000
	1:1 DMEM/F12, 1% FCS, NEAA, 0.5% P/S, 1μM atRA	-	8 days	Johann et al., 2011; Hounoum et al., 2016
	Neurobasal medium, no FBS	-	24 or 48 h	Benavente et al., 2012
	α-MEM, 1% FCS, 1% P/S, 1% NEAA, w/wo 1μM atRA	-	4 weeks	Hounoum et al., 2016
	DMEM,1% FCS,1% P/S, w/wo 1μM atRA	-	4 weeks	Hounoum et al., 2016

* Abbreviations: Dulbecco's modified Eagle's medium (DMEM), Fetal Bovine Serum (FBS), Fetal calf serum (FCS), penicillin/streptomycin (P/S), penicillin/streptomycin/glutamine solution (PSG), Modified Eagle's medium nonessential amino acids (NEAA), all-trans retinoic acid (atRA), Not Determined (ND)

Various types of genetically modified NSC34 cells have been described in the literature as a means to study neurodegenerative diseases such as SMA and ALS. These include SMN knock-out NSC34($SMN^{-/-}$) cells (Tseng et al., 2016; Custer et al., 2016), NSC34 stably expressing human TDP43 NSC34($hTDP43^{WT}$) (Lu et al., 2012) or human SOD1 NSC34($hSOD1^{WT}$) (Menzies et al., 2002). In order to model aspects of disease pathology, literature reports NSC34 stably expressing mutated forms of human SOD1 transgenes - NSC34($hSOD1^{G93A}$), NSC34($hSOD1^{G37R}$), NSC34($hSOD1^{A4V}$) (Bonafede et al. 2016) and NSC34($hSOD1^{H48Q}$) (Richardson et al., 2013).

1.3.2. Expression of Motor-Neuron Markers by NSC34

NSC34 cells are characterized by motor neuron-specific properties. Specifically, NSC34 cells express the enzyme Choline acetyltransferase (ChAT), which is responsible for the synthesis of the acetylcholine (ACh) neurotransmitter, the major neurotransmitter of neuromuscular junction. Moreover, NSC34 cells are able to generate action potentials that result in the release of stored ACh into the synaptic cleft (Cashman et al., 1992). Receptors involved in such procedures include the Nicotinic acetylcholine receptor (nAChR) that responds to the ACh (Rembach et al., 2004) and the Vesicular acetylcholine transporter (VAChT) that mediates ACh storage by synaptic vesicles (Matusica et al., 2008). During NSC34 differentiation, expression levels of ChAT and acetylcholinesterase (AChE) – an enzyme that hydrolizes ACh and terminates signal transduction at neuromuscular synapses - are significantly upregulated, whereas VAChT levels remain unchanged (Maier et al., 2013). Other properties that model aspects of developmental maturation include the switching from the intermediate filament vimentin to the expression of neurofilament triplet proteins (see next paragraph), and the myotube twitching when co-cultured with mouse myotubes. The latter indicates the capability of NSC34 to generate cholinergic synapses with myotubes (Cashman et al.,1992).

Unlike other neural cell lines, NSC34 cells can adhere to S-laminin (basal lamina glycoprotein), which is found at high density the neuromuscular junctions - a characteristic property of primary motor neurons (Hunter et al., 1991). This adhesion is achieved through S-laminin's leucine-arginine-glutamate (LRE) motif (Hunter et al., 1991). Binding of LRE motif to voltage-gated calcium channels, acts as termination signal for growing axons in the developing neuromuscular junction (Johnson et al., 2013).

NSC34 cells are characterized by motor neuron-specific markers, including the cytoskeletal microtubule-associated protein MAP1a (Cashman et al.,1992) and MAP1b (Benavente et al., 2012), and the neurofilament proteins NF68, NF150 and NF200 (Cashman et al.,1992). The astrocyte-specific intermediate filament GFAP is absent (Cashman et al.,1992). Vimentin is detected in the proliferating fraction of NSC34 cells and is lost after NSC34 maturation (Cashman et al.,1992). Although expression of microtubule-associated protein MAP2 by NSC34 was not reported in an early study (Cashman et al.,1992), it was reported in a later study that revealed the presence of both MAP2 and microtubule-associated protein tau (MAPT), another axonal marker (Maier et al., 2013). MAP2 is a neuronal protein that plays a role in maintaining dendritic structure through its interaction with microtubules. During maturation, the $NSC34_D$ cells increase their expression of MAP2 and MAPT and can be detected by the SMI-32 antibody (non-phosphorylated neurofilaments) (Maier et al., 2013). Additionally, NSC34 cells express β-tubulin III (Rembach et al., 2004), the neuroendocrine tumour marker Chromogranin B (CgB) (Pasternak et al., 1991) and the nervous tissue-specific cytoplasmic protein GAP43 (Pasternak et al., 1989). GAP43 is associated with axonal growth and regeneration state of motor neurons (Skene et al., 1986) and is as well increased during maturation (Maier et al., 2013). CgB, a soluble acidic glycophosphoprotein, is a major component of secretory large dense-core vesicles (LDCV) in neurons and endocrine cells. Urushitani et al., 2006 suggested that both Chromogranin A and B may act as chaperone-like proteins to mutant forms of SOD1 (Urushitani et al., 2006). Moreover, NSC34 cells express neuronal nuclear NeuN (Rembach et al., 2004) and several cell adhesion molecules (CAMs) such as L1, CAM/Bravo, Neurofascin/ABGP and NCAM (Moscoso and Sanes, 1995). Sialic acid-containing glycosphingolipids known as gangliosides are abundant in nervous system and play a role in signalling pathways associated with development and disease pathology (Yu al., 2012). NSC34 express the lipid raft-associated gangliosides GD1a, GM1, GM2 (Matsumoto et al., 1995), GT1b and GQ1b (Matusica et al., 2008). Finally, NSC34 cells express the Hb9 transcription factor, a major motor-neuron specific marker (Matusica et al., 2008).

NSC34 cells express a variety of surface receptors for various growth factors essential for their maturation and development such as Glutamate Receptor Proteins (Eggett et al., 2000), discussed in more detail below and several Growth Factor Receptors discussed in more detail below (Matusica et al., 2008; Turner et al., 2004; Usuki et al., 2001).

Initial studies on NSC34 reported no detectable expression of glutamate sensitivity (Durham et al., 1993), a serious drawback for a cell line mostly used as a tool for toxicological assessments. This problem was solved by Eggett et al. (2000) that were able to obtain mature glutamate-sensitive cells by differentiating NSC34 using growth conditions via serum deprivation. Such differentiated NSC34D cells express several glutamate receptors including the NMDA receptors NR1 (GluN1) and NR2 (GluN2A, GluN2B, GluN2D), the AMPA receptors GluR1 (nearly ubiquitous, known also as GluA1), GluR2 (GluA2), GluR2/3 (GluA2/3), GluR4 (GluA4) and the Kainate receptors GluR6/7(GluK2/3), KA2 (GluK5) (Eggett et al., 2000; Hounoum et al., 2016). This differentiation procedure resulted in half cell population loss after 24-48h of differentiation medium addition, with the remaining cells having long neuron-like projections (Eggett et al., 2000).

Regarding Growth Factor Receptor expression, NSC34 cells express both the low-affinity pan neurotrophin receptor $p75^{NTR}$ and the high affinity tropomyosin-like receptor kinases TrkB, TrkC (Turner et al., 2004; Matusica et al., 2008). However, NSC34 cells are devoid of the high-affinity NGF receptor TrkA (Turner et al., 2004; Matusica et al., 2008). Both truncated (100kDa) and full-length (140kDa) isoforms of Trks were detected using Immunoblotting. Moreover, proteins associated with the $p75^{NTR}$ receptor such as sortilin and the previously mentioned ganglioside GT1b were present (Matusica et al., 2008). Other receptors associated with NSC34 include the ciliary neurotrophic factor receptor CNTFR (Usuki et al., 2001; Matusica et al., 2008), the Gp130 cytokine receptor (Usuki et al., 2001), the vitamin D receptor (VDR) (Almokhtar et al., 2015) and the neurotrophin receptor homolog NRH2 (Turner et al., 2004). Although, the role of NRH2 in neurotrophin signalling remains unclear, it is known that it forms a receptor complex with TrkA to create high-affinity NGF binding sites (Wong et al., 2008). Furthermore, NSC34 cells express the tumor necrosis factor receptors TNFR1 and TNFR2 (He et al., 2002). TNF-α induces neurotoxicity via the TNFR1 receptor (p55), whereas proliferation is mediated through the TNFR2 (p75) (Yang et al., 2002). However, Wen et al., 2006 supported that immature NSC34 possess a limited amount of TNFR1, as direct activation of TNFR1 receptor by an agonist anti-TNFR1 antibody induced a maximum of 30% cell death. This limited amount of TNFR1 could explain why physiological concentrations of recombinant TNFα alone was unable to kill cells (Wen et al., 2006). NSC34 cells also express endocannabinoid receptor CB1 but not CB2 (found in glial cells), along with different enzymes related to endocannabinoid metabolism. A significant 5-fold up-regulation in differentiated NSC34D cells in contrast to undifferentiated NSC34 cells was also observed. The CB1 is suggested to portray a neuroprotective role from excitotoxic damage due to the inhibitory effects on glutamate release (Moreno-Martet et al., 2012). Benavente et al., 2012 provided the first evidence of the role of the Bone morphogenetic proteins (BMPs) on motor neuron differentiation. BMP-2 upon binding to its receptor the BMP type II receptor (BMPRII) - a key protein for synapse assembly that is expressed in NSC34 cells - has the ability to inhibit axonal regeneration, hence, the outgrowth of neural cells. Specifically, through their experiments they showed that Id1 - a negative regulator of tissue-restricted gene expression that inhibits the differentiation of muscle, erythroid, myeloid, and neurogenic precursors - is highly expressed in undifferentiated NCS34 and significantly decreased in NSC34D. Addition of BMP-2 to NSC34D induced the Id1 expression through Smad-1 pathway, leading to the impairment of the NSC34D differentiated morphology (Benavente et al., 2012). Although BMP-2 inhibited differentiation, it increased the expression and localization of BMPRII at growth cone tips, possibly providing cells more BMPRII proteins for a proper formation of synapses (Benavente et al., 2012). Both undifferentiated NSC34 and differentiated $NSC34_D$ cells express BDNF (26 kDa). Only immature NSC34 express pro-BDNF (35 kDa) (Matusica et al., 2008). Both NSC34 and NSC34D

cells do not express NGF, NT3, and NT4 neurotrophins (Matusica et al., 2008). All the previously mentioned motor neuron-specific markers and properties are summarized in Table 1.3.2. below.

Table 1.3.2.: NSC34 cell markers and properties

Marker			Cell		Method	Reference
Class	**Name**	**Gene**	**NSC34**	**NSC34$_D$**		
Cholinergic Markers	ChAT	CHAT	+	++	FA; RT-PCR	Cashman et al.,1992; Maier et al., 2013
	Ach (Acetylcholinesterase)	ACHE	+	+	CH[14]	Cashman et al.,1992
	NAChR		+	+	IHC	Rembach et al., 2004
	VAChT		+	+	FC, WB; RT-PCR	Matusica et al., 2008; Maier et al., 2013
	AChE		+	+	RT-PCR	Maier et al., 2013
Cytoskeletal proteins	Vimentin	VIM	+	-	IHC	Cashman et al.,1992
	NF68 NF150 NF200	NEFL NEFM NEFH	+	+	IHC	Cashman et al.,1992
	SMI-32	-	+	+	WB	Maier et al., 2013
	MAP1a		+	+	IHC	Cashman et al.,1992
	MAP1b		+	+	IF	Benavente et al., 2012
	MAP2a MAP2b		-	++	IHC; RT-PCR,WB	Cashman et al.,1992; Maier et al., 2013
	MART		+	++	RT-PCR, WB	Maier et al., 2013
	GFAP	GFAP	-	-	IHC	Cashman et al.,1992
	b-tubulin III	TUBB3	+	+	WB	Rembach et al., 2004
Neuronal proteins	GAP43	GAP43	-	++	RT-PCR, WB	Pasternak et al., 1989; Maier et al., 2013
	Chromogranin B (CgB)	CHGB	+	ND	RT-PCR	Pasternak et al., 1991
	Hb9	MNX1	+	+	WB	Matusica et al., 2008
	NeuN	RBFOX3	+	+	WB	Rembach et al., 2004
CAMs	L1	L1CAM	+	ND	RT-PCR	Moscoso and Sanes, 1995
	Bravo	NRCAM	+	ND	RT-PCR	Moscoso and Sanes, 1995
	N-CAM	NCAM1	+	ND	RT-PCR	Moscoso and Sanes, 1995
	Neurofascin	NFASC	+	ND	RT-PCR	Moscoso and Sanes, 1995
Gangliosides	GD1a		+	+	IHC	Matsumoto et al., 1995
	GM1		+	+	IHC, CT	Matsumoto et al., 1995

	GM2		+	+	IHC	Matsumoto et al., 1995
	GT1b		+	+	WB, FC	Matusica et al., 2008
	GQ1b		+	+	FC	Matusica et al., 2008
Glutamate receptors	GluNR1	GRIN1	-	+	IHC	Eggett et al., 2000
	GluNR2A/B GluNR2D	GRIN2A GRIN2B GRIN2D	-	+	IHC; RT-PCR	Eggett et al., 2000; Hounoum et al., 2016
	GluR1 GluR2 GluR3 GluR4 GluR6 GluR7	GRIA1 GRIA2 GRIA3 GRIA4 GRIK6 GRIK3	-	+	IHC; RT-PCR	Eggett et al., 2000; Hounoum et al., 2016
	KA2	GRIK5	-	+	IHC	Eggett et al., 2000
Cytokine receptors	TNFR1 TNFR2	TNFRSF1A TNFRSF1B	+	+	WB	He et al., 2002; Wen et al., 2006
	Gp130	IL6ST	+	ND	IF	Usuki et al., 2001
Neurotrophin receptors	TRKA	NTRK1	-	-	WB	Turner et al., 2004
	TRKB	NTRK2	+	+	WB; FC	Turner et al., 2004; Matusica et al., 2008
	TRKC	NTRK3	+	+	WB, FC	Matusica et al., 2008
	P75NTR	NGFR	+	+	WB; FC	Turner et al., 2004; Matusica et al., 2008
	SORTILIN	SORT1	+	+	WB, FC	Matusica et al., 2008
	NRH2		+	+	WB	Turner et al., 2004
	CNTFR	CNTFR	+	+	IF; FC	Usuki et al., 2001; Matusica et al., 2008
	c-Ret	RET	+	ND	WB, RT-PCR	Ryu et al., 2011
Neurotrophins	NGF	NGF	-	-	WB	Matusica et al., 2008
	BDNF	BDNF	+	+	WB	Matusica et al., 2008
	NT3 NT4	NTF3 NTF4	-	-	WB	Matusica et al., 2008
	PRO-BDNF	BDNF	+	-	WB	Matusica et al., 2008
Transcription Factor	Inhibitor of DNA Binding 1	Id1	++	+	WB	Benavente et al., 2012
Other Receptors	GLUT3 Glucose Transporter	SLC2A3		+	WB	Daniel et al., 2013
	BMPR2	BMPR2	+	++	RT-PCR, WB	Benavente et al., 2012
	Vitamin D receptor	VDR	+	ND	RT-PCR	Almokhtar et al., 2015
	Endocannabinoid receptor CB1	CNR1	+	+	RT-PCR, WB, IF	Moreno-Martet et al., 2012
	Endocannabinoid receptor CB2	CNR2	-	-	RT-PCR, WB, IF	Moreno-Martet et al., 2012
Kynurenine pathway (KP) enzymes	TDO IDO KMO		ND	+	RT-PCR	Chen et al., 2011

	HYNU KAT-I 3HAO ACMSD QPRT					
	Kynurenine amino transferase-II	KAT-II	ND	-	RT-PCR	Chen et al., 2011

*ND: not determined, IF: Immunofluorescence, IHC: Immunohistochemistry, WB: Western Blot, FC: Flow Cytometry, FA: Fonnum Assay, CH^{14}: [14C] Choline. * ++: Increase of expression, +: Expression, -: No expression

1.3.3. Two-dimensional NSC34 ALS models

In order to study a variety of neuroprotective and neurotoxic factors associated with ALS pathophysiology, several two-dimensional (2D) monolayer motor neuron culture models have been utilized, including the NSC34 cell line. Studies focus on the *in vitro* simulation of the oxidative stress, excitotoxicity, neuroinflammation and protein aggregation implicated in ALS pathophysiology further discussed in the following section.

1.3.3.1. 2D NSC34 Models of Oxidative Stress

Both aetiology and progression of ALS have been associated with oxidative stress, where free radicals and reactive oxygen species (ROS) accumulate. Accordingly, many cellular models tried to probe the neurotoxic effects of H_2O_2. H_2O_2 oxidative insult leads to cytochrome c release from mitochondria, activation of the caspase cascade and apoptotic cell death (Hsu et al., 2012). Several published studies have modelled oxidative stress effects in ALS by exposing NSC34 or NSC34(SOD1) cells to H_2O_2 solutions. Experimental protocols vary in terms of H_2O_2 concentration and duration of exposure.

Cookson et al. 1998 studied biochemical changes in motor neurons after oxidative insult, exposed NSC34 cells for 30 minutes to 50 μM-1 mM peroxynitrite (ONOO-) or H_2O_2 and quantified cell viability and DNA breakdown at several time points (0-6h). Delayed cell death was observed in both treatments. Several morphological changes including extensive membrane blebbing, shrunken morphology and distinct nuclear condensation were observed after 4 hours of exposure. However, under those conditions some cells remained unaffected (Cookson et al. 1998).

Bonafede et al. 2016 tested the hypothesis that adipose-derived stromal cells (ASCs) can promote neuroprotection and neurogeneration in ALS motoneuron models through the release of exosomes. Using murine ASC-derived exosomes on NSC34 and NSC34 transgenes including $hSOD1^{G93A}$, $hSOD1^{G37R}$ and $hSOD1^{A4V}$ they showed for the first time that exosomes could rescue NSC34 cells from oxidative damage. To establish the optimal concentration of H_2O_2 they treated NSC34 cells with 50 μM and 10 0μM H_2O_2 and tested the neuroprotective effect of ASCs-exosomes (concentration 0.2 mg/ml or 0.4 mg/ml). Viability and apoptosis were evaluated by acridine orange/propidium iodide double staining after 2h, 4h, 6h, 8h and 18h of H_2O_2 treatment with or without exosomes, as well as, by ATP assay. Results showed a dose-dependent effect of H_2O_2 on NSC34 viability. Different hSOD1 transgenes displayed different susceptibility to H_2O_2. Exosomes showed a significant protective effect against H_2O_2-induced damage in an inverse dose-depended manner, with the lower concentration (0.2 mg/ml) exerting more beneficial effect than the higher concentration (0.4 mg/ml). It was implicated that the beneficial effect of exosomes is due to the secretion of neuroprotective miRNAs such as miRNA21, miRNA222 and miRNAlet7a (Bonafede et al. 2016).

Maier et al. 2013 used $NSC34_D$ cells to investigate early degeneration after 24h exposure to 0-100 μM H_2O_2, 0-100 ng/ml TNFα and 0-10 mM Glutamate. High doses of neurotoxins resulted in significant cell loss, whereas lower doses were sufficient to induce significant up-regulation of BAX expression. Low concentration

of neurotoxins increased cell death in undifferentiated NSC34 cells in contrast to differentiated $NSC34_D$, where no obvious adverse effects were observed. This repressed responsiveness of $NSC34_D$ was attributed to atRA-induced differentiation which leads to Bcl2 overexpression and hence reduction of apoptotic responsiveness to pro-apoptotic signals *in vitro* (Maier et al. 2013).

Hemendinger et al. 2012 investigated the effect of the FDA-approved ALS drug Riluzole in $NSC34_D$ cells that were exposed to 0-100 μM H_2O_2 and reported limited effects on cell survival, though not providing information on the molecular basis (Hemendinger et al. 2012). The same study (Hemendinger et al. 2012) investigated the effect of other neurotoxic injury pathways by exposing $NSC34_D$ cells to toxins associated with calcium dysregulation and protein aggregation including staurosporine (STS), thapsigargin (Thaps) and homocysteine (HCy). STS has the ability to increase intracellular Ca^{+2} levels independent of endoplasmic reticulum (ER) stress at very low concentrations, while Thaps does that via ER stress - by inhibiting the Ca^{2+}-ATPase of ER- at higher concentrations. On the other hand, HCy is involved in excitotoxicity, ROS generation through activation of microglia, regulation of potassium and ER stress. High content imaging was used to assess toxicity. The strongest neurotoxin for $NSC34_D$ cells was STS (TC_{50} = 0.01 μM), followed by Thaps (TC_{50} = 0.9 μM) and HCy (TC_{50} = 2200 μM) to kill at the same level as H_2O_2 (TC_{50} = 15 μM). *TC_{50} value* is the concentration that achieves 50% of the maximal cell death response. Riluzole co-treatment of cells affected only $NSC34_D$ stressed by Thraps, but had no significant effect on other stress factors (Hemendinger et al. 2012).

In another work, Hemendinger et al. 2011, used 2.2 mM of HCy on NSC34D cells and evaluated the effect of B12 vitamin to protect against HCy-mediated motor neuron cell death. 2 h pre-treatment with 0.6 μM and 0.4 μM B12 prior to HCy was able to inhibit caspase 3/7 activation and reverse cell death as evaluated with Hoechst/PI and H2DCFH-DA staining (Hemendinger et al. 2011).

Acsadi et al. 2009 utilized NSC34($SMN^{-/-}$) cells to model mitochondrial dysfunction in Spinal Muscular Atrophy. NSC34 and NSC34($SMN^{-/-}$) were starved for 10 hours and incubated for 20 minutes with 7.5 μM H2DCFDA. As a positive control to measure the ROS production in NSC34($SMN^{-/-}$), NSC34 treated with 100μM H_2O_2 were used. Cells analysed at 48 and 72 hr after SMN knock-down showed a 12% and 29% increase in H2DCFDA fluorescence emission, indicating increased generation of free radicals (Acsadi et al. 2009).

Ryu et al., 2011 showed altered expression of non-phosphorylated and phosphorylated forms (Tyr 905, 1016, and 1062) of c-Ret receptor in both motor neurons of the lumbar spinal cord in ALS transgenic (G93A) mice and NSC34($hSOD1^{G93A}$). *In vitro* treatment of NSC34($SOD1^{WT}$) and NSC34($SOD1^{G93A}$) cells with 50-100 μM H_2O_2 for 6h resulted in altered cell morphology with membrane blebbing or shrunken and distinct nuclear condensation, and well as reduction in the non-phosphorylated and phosphorylated c-Ret (Tyr 905, 1016, and 1062) in a dose-dependent manner. To check if the GDNF signalling pathway was impaired, Ryu et al., 2011 treated both NSC34($SOD1^{WT}$) and NSC34($SOD1^{G93A}$) with 100 ng/ml GDNF for 0, 10, 20, 30 and 60 min after a 6h treatment with 100 μM H_2O_2. Data indicated that GDNF signalling was impaired in NSC34($hSOD1^{G93A}$), as c-Ret phosphorylation was reduced. siRNA against c-Ret led to increased expression of pro-apoptotic protein Bax upon oxidative stress induction (Ryu et al., 2011).

1.3.3.2. 2D NSC34 Models of Excitotoxicity

Glutamate is the most abundant excitatory neurotransmitter in the Central Neuronal System. Disruption of physiological glutamate receptor activation can lead to neuronal injury and death. It is implied that glutamate excitation disrupts AMP:ATP homeostasis and activates AMPK that increases glucose uptake and ATP production. This increases the sensitivity of primary motor neurons to glucose availability and their vulnerability to excitotoxicity. Daniel et al., 2013 showed that Riluzole increased the rate of glucose influx in $NSC34_D$ cells by directly activating AMPK and inducing the intracellular translocation of the nearly ubiquitous GLUT1 and the

motor neuron-specific GLUT3 glucose transporter. Consequently, glucose uptake and energy production were increased and NSC34 cells could withstand oxidative and ER stress and glutamate excitation (Daniel et al., 2013).

Hounoum et al., 2016 in their study on $NSC34_D$ cells assessed the cell death induced by glutamate excitotoxicity. 0.1 to 5 mM of glutamate on $NSC34_D$ for 48h induced no change in cell viability, whereas 10 mM led to a significant 30% decrease. This concentration was 100-fold higher compared to the one (0.1 mM) that induced 50% cell death in primary motor neurons. Furthermore, using Ca^{2+} measurements via the dye Fura-2AM, they checked how glutamate affected Ca^{2+} transients in $NSC34_D$. Acute application of glutamate immediately induced cytosolic Ca^{2+} influx that increased Fura-2AM intensity. While 0.1 mM glutamate was able to induce high and sustainable Ca^{2+} entry in motor neurons, it induced just a small transient Ca^{2+} influx in $NSC34_D$. Considering that $NSC34_D$ express only some of the glutamate receptor subunits, in contrast to motor neurons, Hounoum et al., 2016 concluded that $NSC34_D$ cells are inappropriate experimental model for glutamate-mediated excitotoxicity (Hounoum et al., 2016). Another study on $NSC34_D$ reported also that 1 mM failed to induce vacuolation of cells and showed no electrophysiological evidence of synaptic connections (Durham et al., 1993).

On the other hand, several studies on excitotoxicity support the exact opposite view, that is that $NSC34_D$ are suitable for excitotoxicity studies. Maier et al., 2013 reported that 2-10 mM of glutamate were able to induce a significant increase in LDH release and Bax/Bcl-2 ratio in $NSC34_D$ cells. However, authors noted that only highest concentration of glutamate (10 mM) led to significant cell loss, and hence, proposed that the important mechanism for cell death in $NSC34_D$ is oxidative stress and not GluR signalling (Maier et al., 2013). In another study, $NSC34_D$ cell line was reported as an appropriate in vitro cell model for drug screening against VX, as it showed sensitivity to both VX and glutamate (Kanjilal et al., 2014). VX is an organophosphate nerve agent that inhibits AChE activity causing the accumulation of ACh, which correspondingly leads to a cholinergic crisis that triggers glutamergic response (McDonough & Shih, 1997). Upon glutamate induction, caspase-3 activity was elevated with the highest increase at 5mM. Further increase in glutamate concentration (10-20 mM) resulted in decrease of caspase-3 activity. This effect was attributed to the activation of other cell death mechanisms caused by glutamate incubation such as necrosis and caspase-independent cell death that do not activate caspase-3. Upon VX induction, caspase-3 activity was elevated in both dose (10-100 nM) and time (17-23h post-exposure) dependent manner, with 20h post-exposure having the maximal increase. Moreover, VX increased Caspase-9 activity at all concentrations. Cell death was measured via flow cytometry using annexin V/propidium iodide staining. Cell treatment of with therapeutics against neurotoxic agents – 600 µM pralidoxime (2-PAM) and 1 µM dizocilpine (MK-801) – just prior to VX, reduced caspase-3 or -9 activation. However, authors mentioned that the direct involvement of glutamate in the VX effect is still under investigation (Kanjilal et al., 2014).

To investigate the role of astrocytes in the function and survival of motor neurons, Benkler et al., 2013 conducted experiments using a co-culture of murine primary cortical astrocytes and $NSC34_D$ cells. 48 h prior to co-culturing, WT and $hSOD1^{G93A}$ astrocytes were activated with the bacterial endotoxin lipopolysaccharide (1 µg/mL LPS), a cocktail of growth factors (1:100 G5 supplement) or the b-lactam antibiotic ceftriaxone (1 µM CEF). Astrocytic activation of WT cells resulted in upregulation of neurotrophic factor mRNA levels and overexpression of the two GLT-1 and GLAST astrocytic glutamate transporters, which subsequently promoted glutamate clearance. Conversely, as in $hSOD1^{G93A}$ astrocytes GLT-1 and GLAST expression remained stable, glutamate clearance was no further altered. Importantly, the untreated $hSOD1^{G93A}$ astrocytes have reduced glutamate uptake capacities. After activation, transwells with astrocytes were inserted into 12-well plates where $NSC34_D$ cells were seeded and exposed 4 mM glutamate for 24 h. $NSC34_D$ viability was evaluated using alamar BlueÒ, after astrocyte transwells removal. Results showed that only the WT astrocytes promoted neuroprotection from glutamate-induced excitotoxicity (Benkler et al., 2013).

1.3.3.3. 2D NSC34 Models of Neuroinflammation

Maier et al. 2013 demonstrated that 24h treatment of $NSC34_D$ with 50-100 ng/ml TNFα induced significant LDH release (Maier et al. 2013). Additionally, Correia et al., 2015 demonstrated an increase in the TDP-43 cytoplasmic levels after 10 ng/ml TNFα exposure on NSC34 and NSC34(hTDP- 43 $^{WT-HA}$) for 6h. Both transfected and non-transfected cells showed a translocation of TDP-43 from the nucleus into the cytoplasm, indicating that TNFα exposure activated the TNFα/NF-κB signalling pathway that can result in abnormal cytoplasmic TDP-43 localization and aggregation (Correia et al., 2015).

Other studies suggest that TNFα alone is unable to induce neurotoxicity. Such studies include the D'Ambrosi et al., 2009 study where both NSC34(hSOD1^{G93A}) and NSC34(hSOD1^{WT}) cells were treated for 3 days with supernatant obtained from 48h BzATP-activated- hSOD1^{G93A} microglia (BzATP: microglial activator). This activated microglial supernatant was able to induce statistically significant NSC34(hSOD1^{G93A}) and NSC34(hSOD1^{WT}) death that could not be reversed by the addition of 0.5 ng/ml anti-TNFα antibody. Consistently, 5 ng/ml murine TNFα was unable to promote cell death, indicating that TNFα alone is incapable for neurotoxicity generation (D'Ambrosi et al., 2009).

He et al., 2002 investigated the interplay between activated microglia and injured motor neurons using the murine microglial BV-2 and motor-neuron NSC34 cell lines. BV-2 cells were firstly activated by two stimuli: the LPS (an effective stimulator of microglia; Zielasek and Hartung, 1996), or the 48h serum-deprived NSC34. Serum deprivation for 48h in NSC34 causes cell death and release of factors that attract BV-2 cells, upregulate their phagocytotic function and produce excess of NO in BV-2 cells. Supernatants of activated BV-2 cells were further added into NSC34 cultures. Supernatants of BV-2 activated by both ways led to the production of NO, but only LPS-activated BV-2 supernatant was neurotoxic to NSC34 in a dose-dependent pattern. Direct induction of NOC-12 (a nitric oxide donor) on NSC34 did not alter cell viability. In contrast, addition of anti-TNFα antibodies to the LPS-activated BV-2 supernatant reduced cell death and inhibited NO generation. Despite the fact that 1 μg/ml LPS in BV-2 cells produced only 0.3 ng/ml of TNFα in supernatant, this low amount was still able to induce NSC34 cell death. Such effect could not be reproduced by the use of recombinant TNFα, where 20-fold TNFα increase was required in order to kill NSC34 cells. Consequently, authors concluded that the released microglial TNFα is essential for generating NSC34 neurotoxicity and implicated that other TNFα-independent secreted microglial factor(s) induce NOS expression and facilitate this procedure (He et al., 2002).

The same group (Wen et al., 2006) elucidated that NSC34 neurotoxicity was mediated through TNFR1, but no TNFR2 receptor. Specifically, they demonstrated that LPS-activated BV-2 supernatant supplementation of NSC34 resulted in 1.8-fold up-regulation of TNFR1 expression in a paracrine fashion. 2h pre-treatment of BV-2 supernatant with 4 μg/ ml anti-TNFα antibody or 10 μg/ml soluble TNFR1 receptor prior to the 24h LPS stimulation and the 48h LPS-activated BV-2 supernatant induction of NSC34, was able to reverse cell death. This action could not be reproduced by direct recombinant TNFα application or anti-TNFR2 antibody on NSC34. Moreover, when LPS-activated BV-2 supernatant was pre-treated with 100 μM L-NIL (iNOS inhibitor), cell viability was partially restored. In contrast, direct supplementation of L-NIL on unstimulated BV-2 or NOC12 pre-treatment displayed no change in cell death. Consistent with their previous study, addition of recombinant TNFα (in DMEM medium) to NSC34 for 48 h led to dose-dependent cell death only at non-physiological concentrations (5 ng/ml vs 0.3 ng/ml). Combination of TNFα and NO directly to NSC-34 cells in DMEM or unstimulated BV-2 supernatant - although showed some synergistic effect when applied with non-physiological concentrations of TNFα - could not as well generate cell death at physiological concentrations. Consequently, data support that along with TNFα release by microglia, iNOS activation-related synergistic factor is the necessary agent to facilitate NSC34 cell death (Wen et al., 2006).

Li et al., 2007 used the same NSC34 stress stimuli as He et al., 2002 in order to elucidate the opposing roles of microglia (neuroprotective and neurotoxic). Treatment of NSC34 cells with low concentrations of LPS-

stimulated BV2 medium for 36h resulted in inhibition of 2,5-hexanedione-induced aggregates and increase neuronal processes. The 2,5-hexanedione (2,5-HD) is a toxin that promotes a phenotype resembling neuropathy with large axonal swelling due to neurofilament multifocal aggregates. On the contrary, 36h treatment with high concentrations of LPS-stimulated BV2 medium reduced NSC34 viability, apoptosis and inhibition of neuronal processes. Consequently, neuronal survival was dependent on the applied concentration of LPS-activated microglial supernatant. Further analysis of LPS-stimulated BV2 supernatant revealed overexpression of TNFα, IL-1β and IL-6 varied both temporally and quantitatively. In conclusion, they proposed that the balance between co- and counter- effects of various microglial factors directs fate (Li et al., 2007).

Bonafede et al. 2016 introduced for the first time the concept of exosomes protecting NSC34 cells from oxidative insult - an action promoted by secretion of neuroprotective miRNAs (Bonafede et al. 2016). However, exosomes of activated cells may as well contain inflammatory-related microRNAs, known as inflamma-miRNAs (Brites & Fernandes, 2015). These toxic exosomes are able to transfer from mSOD1 astrocytes to MNs (Basso et al., 2013). Pinto et al., 2017, investigated how NSC34-derived exosomes affect other cell types, especially the retroviral-immortalized cell line N9. Exosomes secreted by both NSC34$_D$ (hSOD1^{WT})- and NSC34$_D$ (hSOD1^{G93A})- were incorporated into a 1:1 co-culture of NSC34$_D$ and N9 microglial cell line for 24h. Results showed that mutant SOD1 exosomes were rich in miR-124 and had a preference in entering N9 over NSC34$_D$ cells. Exosomal internalization into N9, reduced the phagocytic ability of N9 by 50%, increased the number of senescent N9 cells, overstimulated the NF-kB pathway, produced NO, activated metalloproteinases MMP-2, and MMP-9, upregulated microglial receptors TREM2, RAGE and TLR4 and generated inflammatory response (IL-10, and IL-1β, TNFα, iNOS and MHC- II). Such alterations indicate microglial switch to mixed M1 and M2 subpopulations after the exosome treatment (Pinto et al., 2017).

Mishra et al., 2016, in order to elucidate the role of glia in non-cell autonomous toxicity in ALS studied astroglial inflammatory response after exposure to ALS patients' cerebrospinal fluid (ALS-CSF). Specifically, supernatant of ALS-CSF treated astroglia were added into NSC34 culture for 48h, followed by a cell viability assay (MTT assay). ALS-CSF supplementation in astroglia lead to upregulation and generation of TNFα and IL-6 cytokines, and prostaglandin E2 (PGE-2) and cyclo-oxygenase 2 (COX- 2) inflammation/toxicity mediators. VEGF and GDNF growth factors as well as IL-10 anti-inflammatory cytokine were down-regulated, while glutamate, NO, and ROS were impaired. NSC34 cells treated with ALS-CSF astroglial supernatant demonstrated a 25% decrease in their cell viability, as well as, several morphological alterations including vacuolation, clumping, neurite beading and decrease in the number of cells maintaining axons (Mishra et al., 2016).

1.3.3.4. Other 2D NSC34 Neurotoxic Models

The neuroprotective effect of cerebrolysin was evaluated using the NSC34 cell model (Keilhoff et al., 2014). Cerebrolysin is a proteolytic peptide fraction with a 75% free amino acid and a 25% low-molecular-weight, biologically active peptide concentration. These peptides are able to react with antibodies against GDNF, CNTF and insulin-like growth factors IGF-1 and IGF-2. In this study, Keilhoff et al., 2014 induced on NSC34 cells mechanical stress by media change and metabolic stress by oxygen glucose deprivation (OGD). OGD conditions were reached using nitrogen gas to displace ambient air in incubator, therefore generating a 5% CO_2 and 1% O_2 atmosphere. OGD reduced the metabolic activity by approximately more than half. 0.5 - 5.0 mg/ml of cerebrolysin were added 24 h before (Pre-CL group), in parallel (Para-CL group) or 8 h after (Post-CL group) OGD induction with the respective medium change, following cell survival and proliferation assays (MTT and BrdU-labeling). Results showed a temporary anti-proliferative but initially neuroprotective effect of cerebrolysin on OGD-induced NSC34 cells, with higher doses leading to cell death. Post cerebrolysin application demonstrated the best improvement in metabolic activity, however that effect was only temporal (Keilhoff et al., 2014). In another study, Keilhoff et al., 2016 showed that after 24h only OGD, but not LPS treatment could induce toxicity

to NSC34 cells. This toxicity was reduced insignificantly by 100 μM minocycline treatment, with minocycline being unable to alter the expression of Bax and caspase-3 proteins (Keilhoff et al., 2016).

The role of kynurenine pathway in ALS pathophysiology was also investigated in NSC34 model (Chen et al., 2011). This pathway catabolises tryptophan to generate NAD+. During neuroinflammation, the kynurenine pathway may produce both neurotoxic and neuroprotective molecules. Quinolinic acid (QUIN) - a potent excitotoxin (Stone and Perkins 1982) toxicity on $NSC34_D$ was evaluated via the LDH assay. Results demonstrated that QUIN induced a time and doze dependent toxicity, which was partially reduced in the presence of the NMDA receptor antagonists (2-amino-5-phosphonopentanoic acid (APV), MK-801 and memantine). Kynurenic and picolinic acids known for their neuroprotective effect (Perkins and Stone 1982; Hilmas et al. 2001 and Kalisch et al. 1994; Jhamandas et al. 2000), were also able to reverse the toxic effect. Moreover, INFγ-activated BV-2 cells medium (100IU/μl INFγ for 48h is known to generate QUIN) was transferred onto $NSC34_D$ cells and incubated for 48 h. 30 min pre-treatment of BV-2 with an inhibitor of kynurenine pathway (1-methyl-DL- tryptophan; 1-MT) before activation decreased QUIN release in BV-2 and cell death in NSC34 (Chen et al., 2011).

NSC34 cells were also utilized to study misfolded proteins such as Sigma receptor 1 protein (Prause et al., 2013), mitochondrial dysfunction with activation of the unfolded protein response (Prell et al., 2012), hypoxia (Xu et al., 2011) and as tool for antioxidant screening (Barber et al., 2010). All the previously mentioned 2D NSC34 studies are reported in Table 1.3.3. below.

Table 1.3.3.: 2D NSC34 cell model neurotoxic studies

Cell type	Stimuli			Drug		Method	Result	Reference
	Name	Conc.	Dur.	Name	Conc			
NSC34	ONOO-, H_2O_2	0.05-1mM	30'	-	-	MTT, LDH	~10% and 30% cell death at 100μM and 500μM	Cookson et al. 1998
NSC34 NSC34(hSOD1^{G93A})	H_2O_2	50-100 μM	2-18h	Exosomes	0.2-0.4 mg/ml	AO/PI staining ATP assay	~100% cell death after 6h	Bonafede et al. 2016
NSC34D	H_2O_2 TNFα L-glut	0-100 μM 0-100 ng/ml 0-10 mM	24h	-	-	LDH	Significant cell loss at higher concentration Significant LDH release at 2-10mM of Glut.	Maier et al., 2013
NSC34D	H_2O_2 STS Thaps HCy	0-100 μM 0-0.1 μM 0-1 μM 0-1000 mM	24h	Riluzole	10Mm	HCM	Neuro-rescue only against Thaps	Hemendinger et al. 2011
NSC34D	HCy	2.2 mM	24h	B12	0.4-0.6 μM	Hoechst/PI H2DCFH-DA	Inhibition of caspase 3/7 activation Reverse cell death	Hemendinger et al. 2011
NSC34 NSC34(SMN-/-)	H_2O_2	100 μM	20'	-	-	H2DCFH-DA	ROS production in SMN Knock down	Acsadi et al. 2009
NSC34(SOD1^{WT}) and NSC34(SOD1^{G93A})	H_2O_2	100 μM	6h	GDNF	100 ng/ml	IF, WB	Altered cell morphology, c-Ret decrease	Ryu et al., 2011
NSC34(SOD1^{WT}) and NSC34(SOD1^{G93A})	-	-	5h	Riluzole	0-150 μM	WB, dGlc. uptake	Significant increase in glucose uptake at 25 μM	Daniel et al., 2013
NSC34D	L-glut	0.1-10 mM	48h	-	-	Ca^{2+} Imaging Trypan blue	10mM caused 30% cell death Small transient Ca^{2+} influx	Hounoum et al., 2016
NSC34D	L-glut	1 mM		-	-		No effect on cell morphology No action potential production	Durham et al., 1993
NSC34D	VX, L-glut	10–100nM 0.1–20 mM	17-23h	2-PAM, MK-801	600 μM 1 μM	Annexin V/PI. Caspase 3/7,9 assays. Acetylcholine/Acetylcholinesterase Assay	VX caused time/dose-dependent caspase 3 increase and elevation of Caspase 9 Up to 5mM of Glutamate	Kanjilal et al., 2014

NSC34D	L-glutamic acid	4 mM	24h	Activated WT/hSOD 1^{G93A} astrocytes *		Alamar Blue	WT astrocytes exert neuroprotection	Benkler et al., 2013
NSC34	BV-2 supern. * TNFα NOC-12	- 2-40 ng/ml 0-200 µM	48h 24h 24 h	2h pre - incubation anti-TNFα	4 µg/ml	MTT, L929 assay, NO colorimetric assay, Griess reaction, DAF-2DA staining, Microglial phagocytosis and migration.	NOC-12 no alteration of cell viability BV-2 supernatants produced NO, but only LPS one caused cell death	He et al., 2002
NSC34	BV-2 supern. * TNFα NOC-12	- 0.078 - 20 ng/ml 50 µM	48h 48h 48h	Anti-TNFα Soluble TNFR1	4 µg/ml 10 µg/ml	MTT, L929 bioassay Griess reaction RT-PCR	1.8-fold up-regulation of TNFR1	Wen et al., 2006
NSC34	BV-2 supernatant * 2,5-HD	- 7 mM	36h 7 days	-	-	Annexin-V/PI staining, ICC	High dose neurotoxic, low dose neuroprotective 2,5-HD caused NFH positive aggregates in 70% of NSC34	Li et al., 2007
NSC34($SOD1^{WT}$) NSC34($SOD1^{G93A}$)	mSOD1 Exosomes		2-24h	-	-	qRT-PCR, Gelatin zymography assay, Griess reaction, WB, ICC	50% Reduction of N9 phagocytic ability, increase senescent N9 cells, NF-kB overstimulation, NO and inflammatory response generation, MMP activation	Pinto et al.,2017
NSC34($SOD1^{WT}$) NSC34($SOD1^{G93A}$)	Microglia supern. TNFα	 5 ng/ml	48h 48h	Anti-TNFα	0.5 ng/ml	Cell Titer Blue Viability fluorometric assay	BzATP-activated Microglia supernatant induced cell death in contrast to TNFα	D'Ambrosi et al., 2009
NSC34	ODG	-	24-48h	Cerebrolysin	0.5 - 5.0 mg/ml	MTT, FACS	50% reduction after OGD induction	Keilhoff et al., 2014
NSC34	ODG LPS	- 2 mg/ml	24-48h	Minocycline	100 µM	MTT, FD/PI staining, RT-PCR	LPS induced no toxicity Minocycline led to insignificant cell death reduction	Keilhoff et al., 2016
NSC34	ALS-CSF astroglial medium	-	48h	-	-	MTT	25% decrease in their cell viability	Mishra et al., 2016
NSC34 NSC34(hTDP- 43) WT-HA	TNFα	10 ng/mL	6h	-	-	WB, ICC	TDP-43 mis-localization and aggregation	Correia et al., 2015
NSC34D	QUIN INFγ-activated BV-2 medium*	0-4 µM -	24-72h 48h	APV, MK-801, memantine, Kynurenines 1-MT	0-4 µM 0-2 µM	LDH, ICC, RT-PCR	Time and doze dependent QUIN toxicity, reversed upon NMDA agonists or kynurenines	Chen et al., 2011

1.4. Three-dimensional neuronal Cell culture and Co-culture models

1.4.1. Introduction to three-dimensional (3D) models

Although being convenient, the traditional two-dimensional (2D) monolayer culture is unable to recapitulate the *in vivo* cellular physiology in terms of cellular organization and interaction (Simian & Bissell, 2016). Cells grown in 2D environment - on glass or polystyrene substrate – differ morphologically and physiologically from those of the native tissue (Edmondson et al., 2014). 2D culture affects the spatial organization of cell surface receptors leads to a subsequent alteration of signalling transduction and gene expression (Edmondson et al., 2014). The flatter and more stretched appearance of these cells compared to native tissue (Gupta et al., 2016) results in alterations of key cellular biological responses, including cell proliferation, differentiation, migration, apoptosis, and protein expression. Thus, data collected from such 2D monolayer culture experiments can often be misleading and nonpredictive for the native tissue responses, which partially explains the low percentage of drug candidates succeeding in clinical trials (Edmondson et al., 2014). On the contrary, the three-dimensional (3D) environment that resembles the Extracellular matrix (ECM) enables the development of both cell-cell and cell-ECM interactions that support intracellular communication, reflecting more accurately *in vivo* conditions. Bissell's lab provided the first evidence on the importance of 3D microenvironment for an accurate cell physiology. Specifically, 2D culture of human breast epithelial cells lead to the formation of tumour-like cells, while the incorporation of those cells into a 3D analogs resembling their native microenvironment restored normal growth behaviour (Petersen et al., 1992). Smith et al. compared a conventional monolayer culture of mixed primary mouse neuron and glial cells to 3D Alvetex scaffold cultures. The glial morphology in 3D culture resembled more the one found *in vivo*. Moreover, it was found that cells in 3D cultures formed functional neuronal networks and were able to exhibit spontaneous local field potentials (Smith, et al., 2015). Additionally, 3D cell culture allows the co-culture of multiple cell types, and hence, favours the interplay between cells (Haycock, 2010). Nevertheless, 3D cell culture is more advanced in terms of predicting cellular differentiation and maintain properties of differentiated cells (Huh et al., 2011). For instance, Farrell et al. 2007 in their work on the osteogenic potential of adult rat mesenchymal stem cells (MSCs), cultured MSCs in both 2D and inside 3D collagen glycosaminoglycan scaffolds. Results showed that the expression of collagen type I – marker of osteogenesis - was only present in 3D culture of adult rat mesenchymal stem cells (Farrell et al. 2007).

A variety of 3D cell culture technologies have been developed, including multicellular spheroids, organoids, scaffolds, hydrogels, organs-on-chips and 3D bioprinting, whose strengths and weaknesses are summarized in recent review (Fang & Eglen, 2017). Porous biocompatible scaffolds can be designed utilizing natural-occurring biopolymers, such as collagen, or synthetic materials such as Poly glycolic (PGA) and Poly lactic (PLA) acids (Haycock, 2010). Techniques such as electrospinning, wet spinning and sponge-like fabrication method (freeze drying and gas foaming) enable their fabrication with micro scale control (Haycock, 2010). Cellular spheroids are self-assembled spherical clusters of cell colonies originated either from single or multiple cells. Exploiting the tendency of adherent cells to form aggregates, various techniques to generate spheroids were developed (Haycock, 2010), including the hanging drop, rotating culture, or concave plate techniques (Haycock, 2010). Characterized by cellular heterogeneity, 3D spheroids cultures closely resemble *in vivo* tissues. Specifically, cells that form a spheroid can be distinguished into viable/ highly proliferating cells - mainly found in the outer layers of a spheroid that is exposed to the medium - and into quiescent, apoptotic, hypoxic, and necrotic cells - found in the core that receive less oxygen, growth factors, and nutrients (Edmondson et al., 2014).

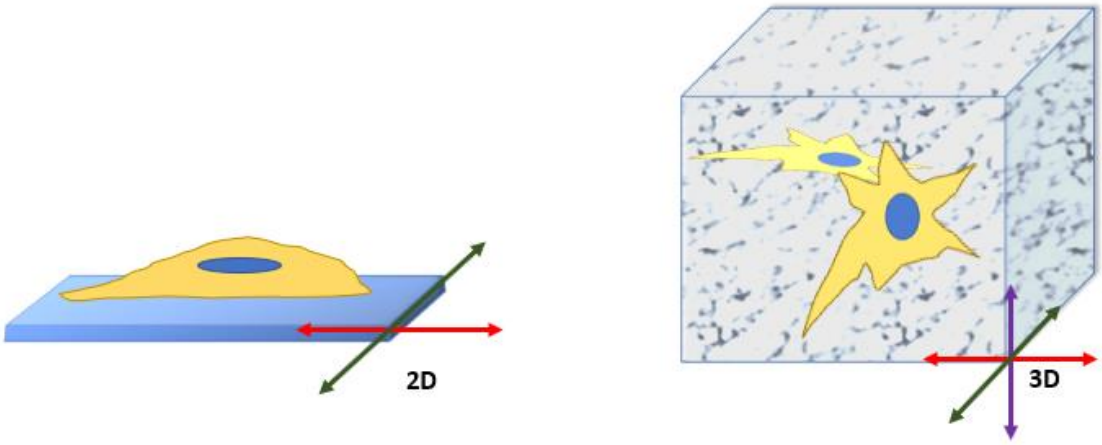

***Figure 1.4.1:* Comparison of 2D and 3D cell culture**. *In 2D culture cell grow covering x-y plane and maintain a flattened morphology, while 3D culture cell cover x-y-z plane obtaining more cuboidal morphology.*

1.4.2. Three-dimensional (3D) neuronal co-culture models

The work of Smith, et al., 2015, is an example of a three-dimensional (3D) neuronal co-culture model (Smith, et al., 2015). Another example is the work of Haycock and his co-workers, where a 3D *in vitro* peripheral nerve model using aligned electrospun-polycaprolactone-fibre scaffolds of various diameter was designed. On those scaffolds, they cultured neuronal cells or primary Schwann cells alone or in co-culture, and as well as, dorsal root ganglions that contained both types of cells. Results showed a direct relationship between fibre diameter, neurite outgrowth and Schwann cell morphology (Daud et al., 2012). Furthermore, Ren et al. 2016 provided the first example of an *in vitro* biologically relevant cortical plate assembly. Utilizing 3D silk scaffolds, they designed a biofidelic neurobiology platform where fetal rat cerebral cortical cells were differentiated into distinct populations of neuroglial stem/progenitor cells, mature neurons or epithelial-mesenchymal cells, (Ren et al., 2016). Additionally, Choi et al., 2013 using cerebral cortical neuronal cells, designed a size-controllable networked neurosphere model that resembled the cytoarchitecture of the brain's cortical region and enabled the quantitative and qualitative assessment of amyloid beta (Aβ) toxicity. Hence, they developed a potential *in vitro* model for Alzheimer's disease studies (Choi et al., 2013). In another potential in vitro for Alzheimer's disease (AD) model, Kim et al. 2015, using human neural progenitor cells (hNPCs) that were mutant for familial AD, designed a Matrigel-based 3D culture system that favoured Aβ deposition (Kim, et al., 2015).

As far as motor neurons are concerned, several published works focus on the formation of functional neuromuscular junctions (NMJ). However, no 3D models dedicated to NSC34 cells were found in literature. Most of studies use primary motor-neurons in co-cultures with other types of cells. The bi-directional communication between motor neurons and muscle cells that is essential for the formation and healthy maintenance of neuromuscular junction, was demonstrated by Zahavi et al., 2015. In this compartmentalized microfluidic platform, motor neurons communicated with muscle cells by expanding their axons through microgrooves. With this platform, the proximal and distal effects of oxidative stress as well as glial-derived neurotrophic factor (GDNF) treatment of cells were investigated. Results demonstrated that axonal growth and innervation was promoted only when GDNF added directly to axons but not to soma. Furthermore, this team was able to track for the first time the retrograde transport of secreted GDNF from a muscle cell to motor neuron (Zahavi, et al., 2015). Vilmont et al. designed a Matrigel-based 3D neuron-muscle co-culture system that can be easily integrated with microfluidic devices. Co-culture of dorsal root ganglia from rat spinal cord explants with murine primary myoblasts, led to a long-term survival of myofibers, motor neurons and supporting glial cells, as well as promoted the formation of functional neuromuscular junctions with post-synaptic specialization (Vilmont et al.,

2016). Additionally, Cvetkovic et al., 2017 developed a modular cellular system comprised of multi-layered tissue rings stacked on 3D printed hydrogel structure that mimicked anatomical muscle–tendon–bone organization. The multi-layered rings contained differentiated skeletal muscle cells (C2C12) and mouse embryonic stem cell-derived motor neurons (MNs) inside an extracellular matrix (Fibrin and Matrigel). Upon chemical stimulation, the site-specific muscle contraction was observed or inhibited (Cvetkovic et al., 2017). Happe et al. 2017 improved the current NMJ models by using mouse and human myoblast and aligning them to mechanically patterned extracellular matrix with alternating soft and stiff stripes (Happe et al., 2017). Demestre et al. 2015 optimized the generation of hiPSCs-derived myogenic cells that could form multinucleated striated myotubes and were able to contract and generate action potentials upon electrical and acetylcholine stimulation. Those cells were incorporated in co-cultures systems comprised of hiPSCs-derived MNs (Demestre, et al., 2015).

Additionally, Uzel et al. 2016 used optically excitable mouse embryonic stem cell-derived MNs and the C2C12 cells to design a compartmentalized microfluidic platform that resembled the *in vivo* physical cell distribution (Uzel et al., 2016). More recently, Osaki et al., 2018 developed a 3D model of ALS using hiPS-derived muscle cells and optogenetic motor neurons (Osaki et al., 2018). Finally, Blizzard et al. 2015 developed a compartmentalized microfluidic device for site-specific excitotoxin exposure (associated with degeneration in ALS), revealed the effect of neuron, astrocyte and muscle cells on each other (Blizzard, et al., 2015).

Gao et al. 2016 in their experiments, integrated for the first time three technologies: A) micropatterning, B) genetically encoded calcium indicators (GCaM: R-GECO) and C) microfluidics in order to position neurons and astrocytes in defined locations. Surface patterning and compartmentalized microfluidics enabled guided interactions between cells grown in distinct and fluidically separated culture chambers, and allowed both drug or viral vector delivery. While, GCaM (green) and R-GECO (red) calcium indicators - emit fluorescence upon calcium influx- enabled a real-time imaging of calcium dynamics within cell populations. Genes of calcium indicators were subcloned into viral vectors under pan-neuronal human synapsin-1 or the astrocyte-specific GfaABC1D promoters. Transduction of cells was performed after 4-5 days of seeding, where virus reached cells through the microfluidic flow. The flow was achieved by difference in volume between the two connected reservoirs of microfluidic device (400µl loading and 100µl waste reservoir). Both neuron-neuron and neuron-astrocyte interactions in normal and pathophysiological conditions were evaluated. Such pathological conditions were induced by glutamate on cells. 50 µM of glutamate was applied to acutely stimulate cultures in order to model longer-term effects of excitotoxicity and record the patterns of calcium signalling. Neurons and astrocytes were cultured either as monoculture or co-cultured in the same or adjacent microfluidic compartment. Co-cultured astrocytes and neurons in the same compartment had spatially restricted microdomain calcium activity with higher frequency compared with astrocytes in monocultures. The same result was observed when cells were located in adjacent compartments, as neurons extended their axons into the astrocyte compartment and formed functional interconnections with astrocytes (Gao et al., 2016).

Kunze et al., 2013, conducted experiments with astrocyte-neuron co-cultures to understand non-cell autonomous mechanisms in ALS. Briefly, utilizing $hSOD1^{WT}$ or $hSOD1^{G93A}$ astrocytes with cortical neurons in cell co-culture inside a compartmentalised microfluidic platform (no direct cell-cell contact), they studied the neural cell response for up to two weeks. Results showed a 45% neuronal cell density reduction when neurons were co-cultured with $hSOD1^{G93A}$ astrocytes, as well as, loss of synapsin protein expression when glutamate (2.6-9 µM) was applied. On the other hand, a reduction of glutamate-induced stress was observed when neurons were in close metabolic contact (indirect cell-cell contact) with $hSOD1^{WT}$ astrocytes (Kunze et al., 2013).

1.5 ALS treatments

1.5.1. Antioxidant Therapies and ALS Drugs

So far, only no therapy with substantial clinical benefits exist for ALS patients (Petrov et al., 2017, Brown & Al-Chalabi, 2017). Only two FDA-approved drugs for ALS have been developed with limited effect on life expectancy. The first one is Riluzole (benzothiazole) (Bensimon et al., 1994) that was approved in 1995 extends survival for approximately 3 months (Clerc et al., 2016). Protective effects of Riluzole are mediated by the inhibition of voltage-gated sodium channels, with a consequent decrease in the pre-synaptic release of glutamate targeting in that way the excitotoxicity (Doble et al., 1996). The clinical utility of Riluzole is in doubt due to its high cost and modest efficacy (Musaro et al., 2013). After 22 years of Riluzole FDA-approval, another drug known as Edaravone was approved in 2017. Edaravone is free radical scavenger that eliminates lipid peroxides and hydroxyl radicals, targeting oxidative stress. The mechanism of action of this drug remains unknown according to official drug company (Rothstein, 2017).

Through years different type of agents have been tested for potent therapeutics for ALS disease (Barber et al., 2010; Pandya et al., 2013). Such agents are antioxidants that target the oxidative stress observed in ALS pathophysiology. Although many patients take dietary supplements of antioxidants on the advice, antioxidant treatment studies showed no significant effect (Orrell et al., 2008). However, this may be attributed to the lack of chemical properties necessary to penetrate the blood–brain barrier (BBB) and reach central nervous system (De Boer et al., 2007). Thus, trials of antioxidant therapies are still ongoing as may prove to be effective (Barber & Shaw, 2010).

Therefore, the standard treatment for ALS remains the multidisciplinary care, including nutritional (nasogastric feeding) and ventilatory support and symptom management (Brown & Al-Chalabi, 2017). Several novel approaches have been proposed. Such approaches include RNA-targeted therapies to silence ALS associated genes with the use of adeno-associated viruses (AAV) (Brown & Al-Chalabi, 2017). Utilizing advanced technologies (genomics, transcriptomics, metabolomics and imaging) more personalized therapeutics based on biomarkers and individual's disease subtype are in process to be developed in future (Hardiman et al., 2017).

1.5.2. Neurotrophins/ Microneurotrophins

Polypeptidic neurotrophic growth factors (NTs; neurotrophins) impairment is clearly involved in ALS progression, as it causes selective motor neuron death. Both experimental animal models and neuronal organotypic cell cultures demonstrated that supplementation of neurotrophic factors can rescue motor neurons cells from death (Ekestern et al, 2004). Despite this success, the administration of neurotrophic factors to ALS patients had a debatable therapeutic efficacy (Ekestern et al, 2004), mostly due to the fact that most neurotrophins are unable to cross the blood-brain barrier (BBB) and reach CNS (Glajch et al., 2016).

Neurotrophins play a significant role in neural survival, development, function and plasticity (Chao, 2003). In mammals four neurotrophins with similar sequence and structure homology are present: Nerve Growth Factor (NGF), Brain-Derived Neurotrophic Factor (BDNF), Neurotrophin-3 (NT-3), and Neurotrophin-4 (NT-4) (Hallbook, 1999). Mature neurotrophins activate tyrosine kinase receptors of the tropomyosin-related kinase family, known as Trks (TrkA, TrkB and TrkC) with high affinity, and p75 neurotrophin receptor ($p75^{NTR}$) - a member of the tumour necrosis factor receptor superfamily - with lower affinity. Specifically, NGF and NT3 bind to TrkA receptor, BDNF and NT-4/5 activate TrkB receptor, while NT-3 recognizes TrkC (Bothwell, 2016). Immature-unprocessed neurotrophins (known as pro-neurotrophins) selectively bind to $p75^{NTR}$ (Reichardt, 2006) with the help of the co-receptor sortilin (Skeldal et al., 2012). $p75^{NTR}$ and Trk receptors can function synergistically, antagonistically or independently (Vicario et al., 2015). When a ligand binds to a Trk receptor, the receptor is homodimerized causing autophosphorylation of tyrosine residues in the Src homology 1 (SH1) domain that subsequently promotes a cascade of phosphorylation events that activate specific downstream

intracellular pathways (Chao, 2003). Such pathways include the Ras-Raf-MEK1/2-ERK1/2 pathway, the phospholipase C-γ (PLC-γ) pathway and the phosphatidyl inositol-3 kinase (PI3K)/Akt pathway (Chao, 2003). These pathways promote cell survival and differentiation by activating the pro-survival transcription factor CREB or the nuclear factor-kB (NF-κB) pathway that regulate the expression of anti-apoptotic Bcl-2 protein (Chao 2003; Reichardt, 2006). On the other hand, $p75^{NTR}$ activates both NF-kB(survival) and cJun/JNK kinase pathways (cell death) and modulates RhoA activity (Chao, 2003; Bhakar et al., 2003; Reichardt, 2006). Downstream effects of $p75^{NTR}$ activation depend upon ligand and other interacting with $p75^{NTR}$ receptors co-expression (DeFreitas et al., 2001; Nykjaer et al., 2004). These signalling pathways are illustrated in Figure 1.5.2.

The study of neurotrophin effects to motor neurons is limited (Deinhardt & Schiavo, 2005) due to lack of existing well-characterized motor neuron-like cell lines, equivalent to the rat PC12 pheochromocytoma cell line that is utilized for TrkA studies (Matusica et al, 2008).

The neuro-steroid dehydroepiandrosterone (DHEA) is an estrogen and androgen intermediate that is naturally produced in brain and adrenal glands. DHEA binds to both Trks and $p75^{NTR}$ receptors with K_D at nanomolar concentrations (Lazaridis et al., 2011; Pediaditakis et al., 2015), thereby promoting cell survival (Charalampopoulos et al., 2008). Although DHEA can easily cross BBB, as a neurosteroid it may affect the endocrine system and promote cancer. The removal of the estrogenic or androgenic properties of DHEA, led to the synthesis of 17-spiro DHEA analogs that could bind and activate Trk receptors, known as Microneurotrophins. Microneurotrophins can penetrate the BBB and have the potential to be used as therapeutics in neurodegenerative diseases and brain trauma. For example, BNN27 binds and activates only the NGF-receptor TrkA, penetrates BBB and does not interact with estrogens and androgens (Pediaditakis et al., 2016). Moreover, in mouse Cerebellar Granule Neurons (CGNs) that express $p75^{NTR}$, but not TrkA receptors was shown that BNN27 interacts and activates $p75^{NTR}$ receptors, reversing the serum deprivation-induced apoptosis of cells (Pediaditakis et al., 2016). In motor neuron-astrocyte co-cultures BNN27 was able to improve cell survival (Glajch et al., 2016). Recently, it was demonstrated that another microneurotrophin the BNN-20 can mimic the action of the endogenous BDNF by acting through the TrkB neurotrophin receptor pathway, and hence, serve as neuroprotective agent (Botsakis et al., 2017).

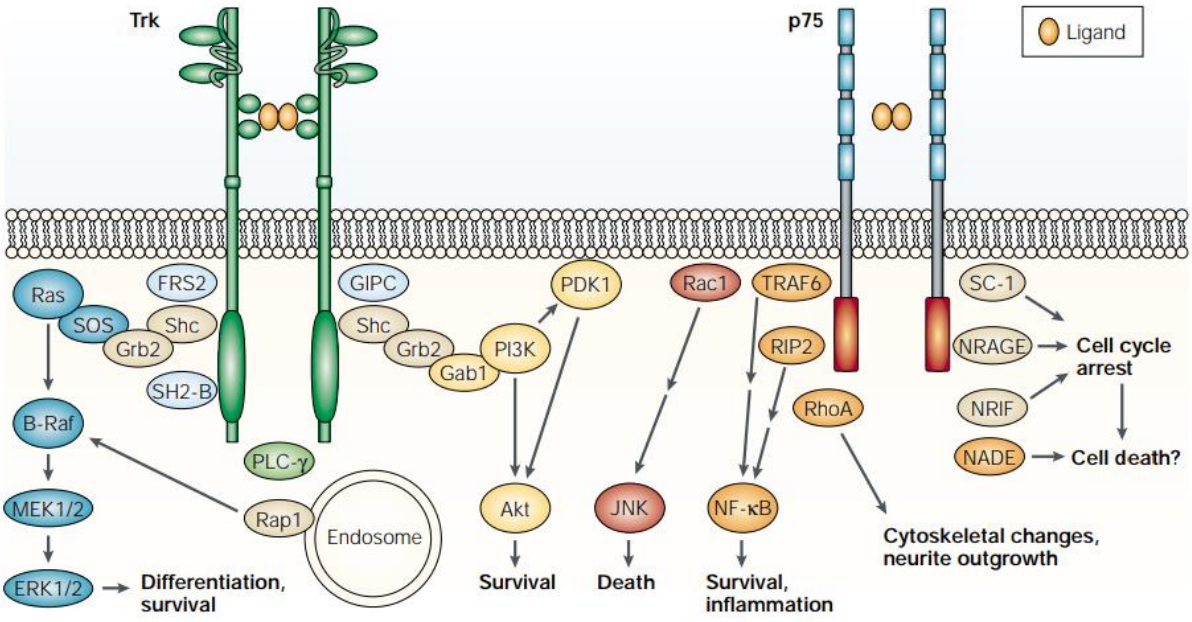

***Figure 1.5.2:* Trks and $p75^{NTR}$ mediated Signalling Pathways**. *Trks activation promotes differentiation and survival, while may induce both apoptosis and survival. (Chao, Nature Reviews Neuroscience, 2003)*

1.6 Thesis Objectives and Outline

This thesis focused on three main objectives:

1. Characterize the expression and response of neurotrophin receptors in NSC34 cells grown in a Matrigel Sandwich culture. This study aimed to provide a novel cell line-based experimental platform for studying TrkB-mediated signaling that would potentially enable the evaluation of neuroprotective drugs, as the PC12 model for TrkA studies. Activation of signaling pathways Erk1/2, JNK, AKT was investigated upon Pro-NGF, NGF, BNN20 and BDNF treatment.
2. Quantify the response of NSC34(-) and NSC34(hSOD1^{G93A}) cells to various ALS-related stimuli that stress cells. Also, evaluate the ability of various compounds or drugs to reverse adverse effects of effective stress stimuli. This was based on the *in vitro* NSC34 model for ALS systemic studies that was previously developed in the IMBB Neural Tissue Engineering lab (Ioanna Lapi, Dr. D. Tzeranis). Specifically, the work of Ioanna Lapi introduced a novel method to bypass several challenges of NSC34 culture (including poor cell detachment) by developing a Matrigel sandwich culture (Durham et al., 1993) and uniformly distributing cells without aggregates. This model has two main features: a) an appropriate cell player that expresses neurotrophin receptors and several key motor neurons characteristics and b) a cell culture procedure that enables high-throughput quantification by state-of-the art tools including automated imaging (High content microscopy) and proteomics. By exploiting such tools, various compounds – potential stress inducers: H_2O_2, NMDA, AMPA, IL1α, INFγ, TNFα, Pro-NGF or potential neuroprotective agents: NGF, BDNF, CTNF, GDNF were evaluated in a controlled environment in order to investigate of pathogenic aspects of ALS. This system aimed to determine any difference between WT and ALS disease cells in response to a stimulus and predict the efficacy of candidate ALS treatments (BNN20) and FDA-approved drugs (Edaravone, Riluzole).
3. Develop a novel 3D NSC34 ALS model based on porous Collagen-I scaffolds that would recapitulate more accurately the *in vivo* conditions and be further modified to utilize other cell types such as Embryonic-derived motor neurons or iPSCs. This model was based on co-culture system of C2C12 and NSC34. The work described in this thesis describes the optimization of several cell culture features including cell state (differentiated or undifferentiated), number, ratio and morphology (spheres or single cells). An attempt to generate genetically engineered C2C12 cells has been as well made. Future objective is to compare its functionality to corresponding 2D NSC34 model.

The two first objectives were performed in collaboration with Kelly Iordanidou. Successful development of such models is of high importance, as these models serve in improved *in vitro* compound screening prior to laboratory animals use, reducing the need for animals in the first stages of a pharmacological studies.

Chapter 2: Materials and Methods

2.1. Eukaryotic Cell Cultures

2.1.1. NSC34 Cell Culture and Differentiation

NSC34 cells were a kind gift of Prof. P. Shaw (Sheffield Institute of Translational Neuroscience, U.K.). The provided cells were transfected with normal or mutant forms of human SOD1 ($hSOD1^{WT}$, $hSOD1^{G93A}$, Sham Control). NSC34 cells were seeded at a concentration of ~$15x10^4$ cells per 6 well plate (Thermo Scientific™ Nunc™ Cell-Culture Treated multi-well plates) and cultured under normal growth conditions at 37°C and 5% CO_2. NSC34 were maintained in proliferation medium consisted of High-glucose DMEM (Sigma), 10% FBS (Biosera), 1% penicillin/streptomycin (Sigma) and 0.25 mg/ml Geneticin (G418, Sigma) as selection marker for transfected cells (Cashman et al., 1992). Every 2-3 days, 60% of the medium was replaced with fresh proliferation medium. Upon 70-80% confluency, NSC34 cells were sub-cultured: every 4 days for NSC34(-) and every 6 days for NSC34($hSOD1^{G93A}$). No dissociation reagent (Trypsin, Accutase) was required, as cells could be dissociated by gentle pipetting.

NSC34 were differentiated using the following protocol: Once NSC-34 cells reached 70-80% confluency, 1 μM Ara-C (Sigma) was added in the proliferation medium to eliminate the fraction of highly proliferating cells. The following day, medium was switched into differentiation medium as described in (Eggett et al., 2000). Differentiation medium consisted of 1:1 DMEM/F12 (Sigma), supplemented with 1% FBS (Biosera), Eagle's medium nonessential amino acids (Thermo), 0.25 mg/ml G418 (Sigma), 1% Penicillin/Streptomycin (Thermo). 24 h later, a considerable amount of cell death was observed and the medium was replaced with fresh differentiation medium without Ara-C. The remaining population of cells was let to proliferate for 2-3 days and was denoted as $NSC34_D$. Figure 2.1.1. displays images of undifferentiated NSC34 and differentiated $NSC34_D$.

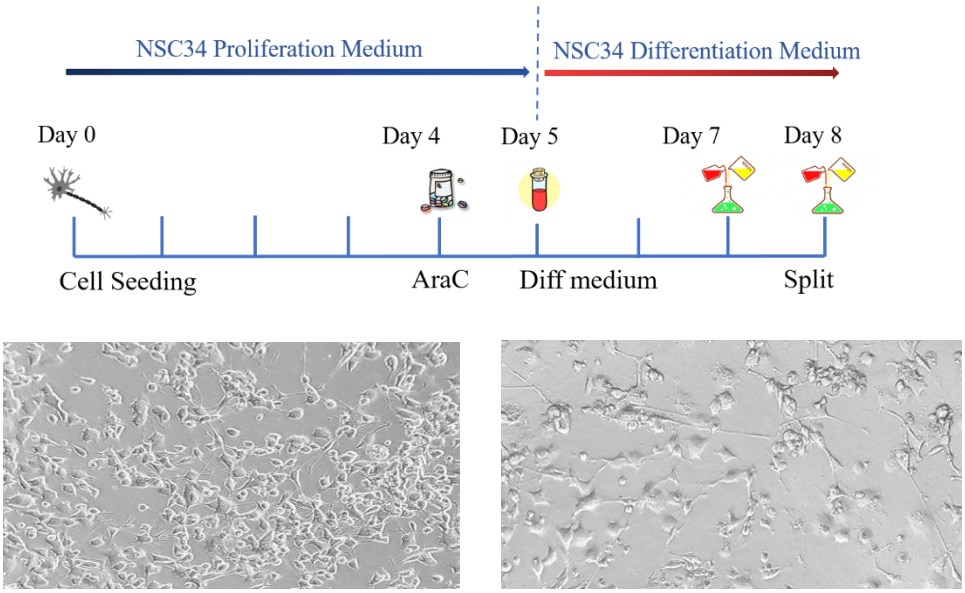

***Figure 2.1.1.*: NSC34 Differentiation Protocol.** *Above: NSC34 differentiation scheme. Left: Undifferentiated NSC34 culture after Ara-C supplementation. Right: Differentiated $NSC34_D$ culture, with visible neuronal axons. Images acquired by a 10x lens.*

2.1.2. C2C12 Cell culture and Differentiation

C2C12 cell line is an immortal skeletal myoblast line originated from thigh muscle satellite cells of female C3H mouse donor (Yaffe and Saxel, 1977). Proliferation of C2C12 occurs in growth medium consisting of High-glucose DMEM (Sigma), 20% FBS (Gibco) and 1% penicillin/streptomycin (Sigma). C2C12 were plated ~$4x10^4$ in 6 well plate (Thermo Scientific™ Nunc™ Cell-Culture Treated multi-well plates) and cells are cultured under normal growth conditions at 37°C and 5% CO_2. Every other day, the medium was replaced with fresh growth medium. Upon 50-60% confluency, C2C12 cells were sub-cultured (every 2-3 days). Higher confluency may result in C2C12 spontaneous differentiation, and thus continued passaging of the cells will propagate cells with limited differentiation capacity.

Under appropriate culture conditions, C2C12 cells differentiate into myotubes (insulin supplementation, reduction of FBS amount in the culture medium, 2% Adult Horse Serum that contains insulin (HS), insulin-transferrin-selenium). Here, ITS (Thermo Scientific™) was used as a basal medium supplement used. Specifically, the 100× ITS mixture (insulin-transferrin-selenium) contains 1.0 mg/ml recombinant human insulin, 0.55 mg/ml human transferrin (substantially iron-free), and 0.5 µg/ml sodium selenite. Insulin plays a significant role in glucose and amino acid influx, protein, lipid and nucleic acid synthesis, as also in intracellular transport. Studies showed that it promotes myogenesis by inducing the NF-kB through an AKT/P70S6 kinase/p38-mitogen-activated protein kinase (MAPK) and downregulating the p42/p44-MAPK (Conejo et al., 2001,2002), as well as reducing the activating protein-1 (AP-1) DNA binding activity (Conejo et al., 2000). Transferrin provides a physiologically appropriate method to supplement the culture with iron. Having the ability to tightly bind free iron under physiological conditions and facilitating its storage and transport to the cells, transferrin acts as an important extracellular antioxidant. Free iron is bound to transferrin and then in a controlled receptor-mediated manner is delivered to cells, thereby, no free iron exists to catalyze the production of peroxide and oxygen radicals that may lead to cytotoxicity. Last but not least, selenium is an essential metal for cell culture that is incorporated into enzymes with various antioxidant functions, called seleno-enzymes. Furthermore, selenium acts as a co-factor for glutathione peroxidase, an enzyme that protects cells from the deleterious effects of peroxides and hydroperoxides.

To differentiate cells, C2C12 were allowed to reach 90% confluency. Prior to switch from growth medium to differentiation medium, cells are wash once with PBS (Gibco). C2C12 differentiation medium consist of High-glucose DMEM (Sigma), 0.5% FBS (Gibco),1% penicillin/streptomycin (Sigma) and 1% ITS (Thermo Scientific™). Ara-C Myogenesis is initiated 24-48h later, whereas fusion into myotubes takes 4-6 days. Two days after the switch to differentiation medium, medium was supplemented with 1 µM Ara-C (Sigma) to eliminate non-fused myotubes. Two days later, medium was replaced with fresh medium with no Ara-C and cells were considered as differentiated $C2C12_D$. Figure 2.1.2. displays the undifferentiated and differentiated C2C12 culture and illustrates the C2C12 differentiation protocol.

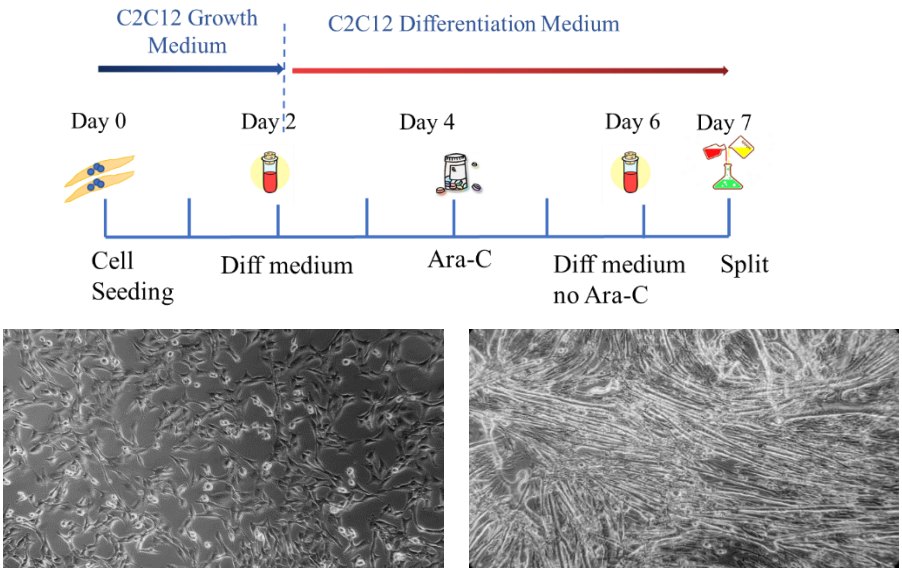

Figure 2.1.2.: C2C12 differentiation protocol and culture. *Previous page illustrates C2C12 differentiation protocol from seeding (Day 0) and 1 μM Ara-C supplementation (Day 4) to $C2C12_D$ generation (Day 6). Left: Undifferentiated (day 1) C2C12. Right: Differentiated (day 6 of differentiation) C2C12 ($C2C12_D$).*

2.1.3. HEK293T, NIH/3T3 and CHO Cell culture

HEK293T, NIH/3T3 and CHO cell lines were cultured in growth medium (High-glucose DMEM (Sigma), 10% FBS(Gibco), 1% penicillin/streptomycin (Thermo). Cells were passaged every 2-3 days, when they reached 80-90% confluence.

2.2. Matrigel Sandwich Culture

Cells were cultured following the protocol developed by Ioanna Lapi, illustrated in Figure 2.2. 10^4 $NSC34_D$ cells were seeded in 120 μl of differentiation medium in each well of a collagen I-coated 96-well plate (Thermo Scientific™). Each well had been coated by incubating 100 μl 50 μg/m rat-tail collagen I solution (BD) in 50 mM acetic acid overnight at 37°C/5% CO_2, followed by two dH_2O washes (150 μl) and one sterile PBS wash (100 μl). To reduce evaporation, the perimetry of the 96-well plate was filled with dH_2O. Gentle pipetting during the whole procedure and very slow steps were essential to avoid cell detachment. Additionally, after $NSC34_D$ seeding a small amount of medium (approximately 40 μl) always remained in each well of the 96-well plate in order to keep the bottom surface of the well always fully covered. This step was crucial to prevent cell detachment and was applied in all steps after cell seeding in 96-well plate. Two days later, cells were rinsed once with 150 μl sterile PBS to remove dead cells, and then 70 μl ice-cold 0.25 μg/ml Matrigel (Corning) solution in differentiation medium was added to each well. This 70μl was diluted by the remaining 40μl medium resulting in a final 0.16 μg/ml concentration inside the well. After Matrigel addition, cells were incubated at 37°C/5% CO_2 for 90 min in order to allow Matrigel to jellify. Then, 80 μl extra pre-warmed differentiation medium were added per well. Two days after adding this Matrigel layer, cells were ready for experimental procedures.

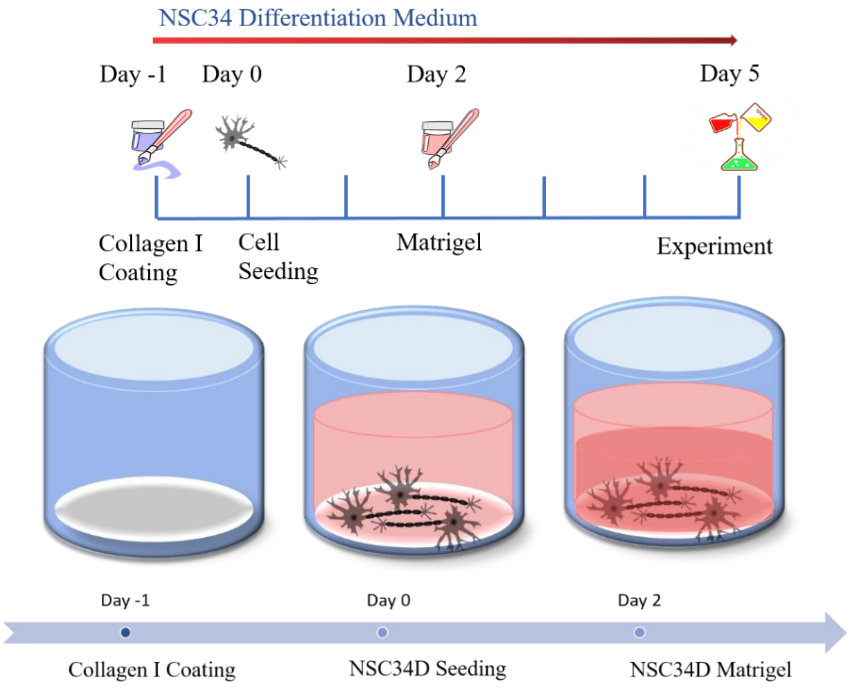

***Figure 2.2.*: NSC34$_D$ Sandwich Matrigel Culture Protocol.** *Above: Time outline for the preparation of the NSC34 sandwich culture. Below: 96 Well plate well where NSC34$_D$ were firstly seeded on collagen I-coated surface (Day 0) and supplemented with Matrigel (Day 2). On Day 4 cells were ready for Live-or-Dead or Signalling experiment.*

2.3. NSC34$_D$ stimulation and drug treatment

In order to model mechanisms associated with ALS pathogenesis, various compounds – potential stress inducers and potential neuroprotective agents were evaluated in a controlled environment of Matrigel Sandwich culture. The experiments were performed after two days of Matrigel coating of the cell culture (Day 4). First of all, NSC34$_D$ were washed 3 times with 150 µl of PBS and then subjected to 4h serum deprivation for synchronization. In each well 120 µl FBS-depleted differentiation medium was added and then the plate was left in incubator for 4h. Various concentrations of potential neuroprotective and neurotoxic agents were prepared through serial dilutions in differentiation medium and added to cell culture after the 4h serum deprivation and serum free medium removal (120 µl). 80 µl of stress stimuli were added in each well that contained the extra 40 µl to form 120 µl final volume in each well. Table 2.4. summarizes all the used components and their final concentration inside the wells.

Table 2.3.1. Compounds used in NSC34 treatment

Mechanism	Compound	Concentration	Vendor
Oxidative stress	H_2O_2	0 - 400 µM	Sigma
Neuroinflammation	Human IL1α	0 - 10 ng/ml	Minotech
	Human TNFα	0 -100 ng/ml	Minotech
	Human INFγ	0 - 25 ng/ml	Minotech
Excitotoxicity	NMDA	0.5 -100 µM	
	AMPA	50 - 500 µM	
Neurotrophin activity	NGF	0 - 1000 ng/ml	Millipore
	Pro-NGF	0 - 1000 ng/ml	
	BDNF	0 – 100 ng/ml	Peprotech

	BNN2O (dissolved in DMSO)	0 – 100 nM	
FDA-approved drugs	Edaravone (dissolved in DMSO)	0 - 400 µM	Santa Cruz Biotechnology

$NSC34_D$ cells were serum starved for 4h (differentiation medium without FBS) for 4h and then they were exposed to various stress stimuli for 1 days (16-20h) or 2 days (44h) and the resulting cell viability was quantified via fluorescence imaging. Kill curves for each stimulus were performed. For stimuli that induced apoptosis, potential neuroprotective factors or drugs were as well added together with the stress stimuli to determine if the treatment with this factor could reduce the apoptosis observed. After the cell stimulation period, cells were subjected to 2h post-treatment in fresh differentiation medium. Finally, $NSC34_D$ cells were stained and imaged as described in detail below. Experiments were performed in technical triplicates or duplicates. Overview of the all conducted experiments is provided in Appendix. Some of the performed experiments were excluded from further analysis due to wrong dilution and cell handling. Table 2.3.2. provides a list with the experiments that are included in this thesis.

Table 2.3.2. List of all experiment included in this thesis.

Experiment	Included	Comments
3	yes	conducted by IL. Miss live cell classification
4	maybe	% low healthy live cells in medium
5	maybe	exlude H2O2 treatments. Tnfa seems ok
6	no	staining test
7	yes	live healthy more than average.
8	yes	exclude no treatment
9	yes	
10	no	ROS staining
11	yes	
12	yes	exclude certain wells. Higher % healthy live cells in control
13	yes	
14	no	experimental error
15	no	massive death due to some error
16	no	no "medium". H2O2 induces no death. Weird effect of BNN20
17	maybe	low dead fraction in medium only
18	yes	
19	yes	
20	yes	
21	yes	
22	yes	
23	yes	
24	yes	low dead fraction in medium only
25	yes	
26	maybe	low dead fraction in medium only
27	yes	
28	yes	

2.4. Quantifying Induced Cell Apoptosis by Automated Fluorescence Imaging

2.4.1. Live-or-Dead staining

$NSC34_D$ cells were stained for 1h with Live-or-Dead staining at 37°C/5% CO2 in the dark. Live-or-Dead staining consist of 3 µg/ml Hoechst (blue), 1µM CalceinAM (green) and 1 µM propidium iodide (red). After staining, cells were washed once with 150 µl of PBS. Fluorescence was detected with high content microscopy (operetta).

2.4.2. ROS staining

$NSC34_D$ cells were stained for 1h with 2µM H2DCFH-DA staining (green) and 3 µg/ml Hoechst (blue) at 37°C/5% CO2 in the dark. After staining, cells were washed once with 150 µl of PBS. Fluorescence was detected with high content microscopy (operetta). Data not shown.

2.4.3. Image Processing

The quantification of the cell response was assessed by automated high content microscopy via counting the fraction of dead cells. Cells were classified as dead or live through the supervised classification algorithm (Table 2.4.3.1., Figure 2.4.3.1.).

Table 2.4.3.1. Supervised classification algorithm

Step	Description
Input image	Load Data
Find Nuclei	Read Hoechst channel Threshold images Identify objects whose area >30 µm^2 Define “nuclei” object population
Process Nuclei	Identify borders of each nucleus Calculate mean Hoechst33342 channel intensity per nucleus Calculate mean PI channel intensity per nucleus
Identify cell cytoplasm	Use proprietary algorithm (algorithm C)
Calculate cell morphology features	Calculate cell cytoplasm area and roundness Calculate mean Calcein channel intensity per cell cytoplasm
Identify live cells	Consider cells where: Cell Area > 250 µm² Nucleus Mean PI Intensity < 410 Cytoplasm Mean Calcein Intensity > 200
Identify healthy live cells	Consider cells where: Cell Area > 500 µm² Cell roundness < 0.98 Cytoplasm Mean Calcein Intensity > 200
Identify stress live cells	Live cells not identified as healthy
Identify dead cells	Consider cells where: Nucleus mean PI intensity > 410

Nuclear Segmentation

Cell Segmentation

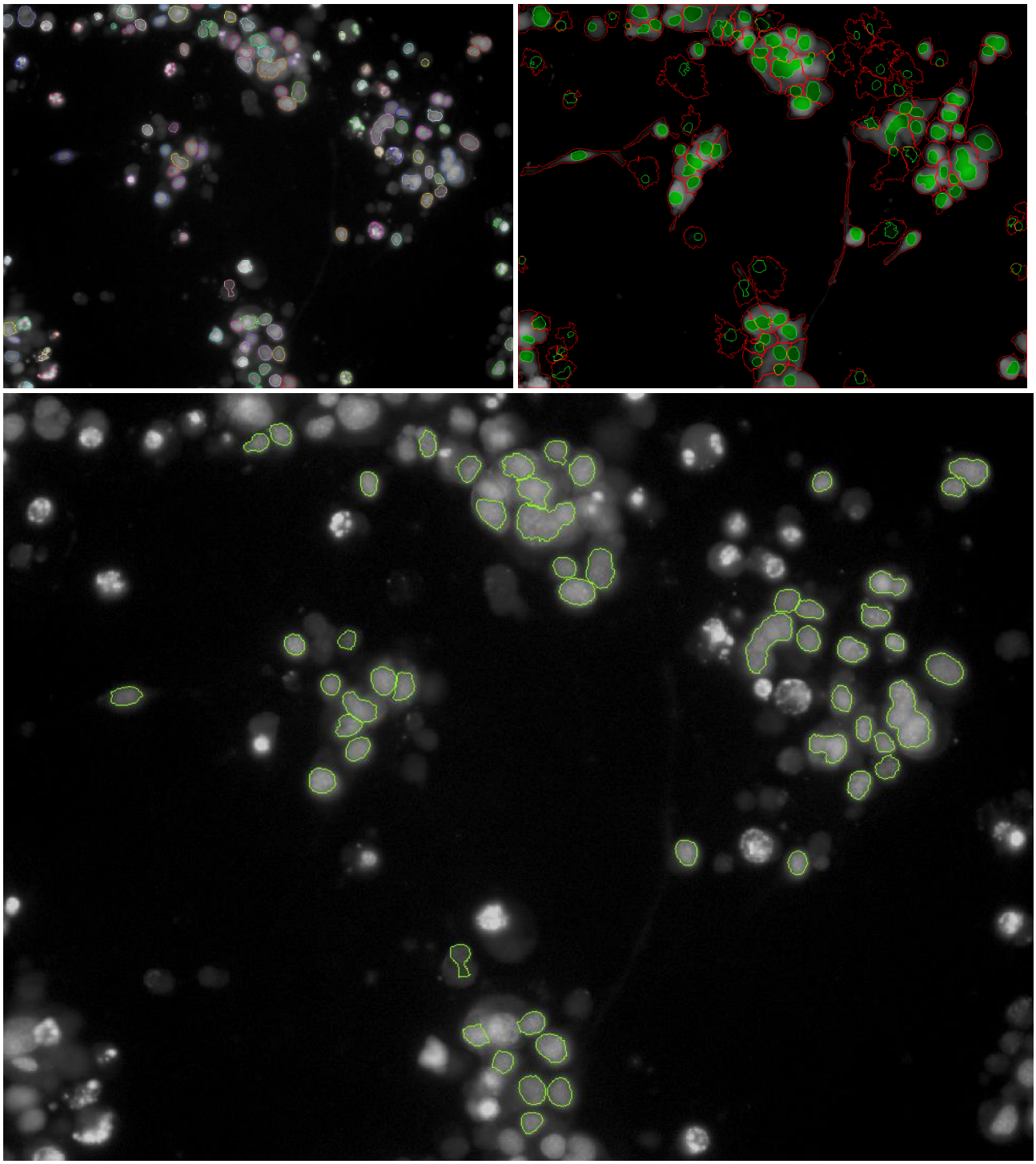

***Figure 2.4.3.1.*: Quantification of NSC34 cell apoptosis via Operetta HCS Microscopy.** *Dead-or-live cells are distinguished through the supervised classification algorithm. This procedure comprises of two major steps: The nuclear segmentation step were all stained nuclei are selected and the cell segmentation step were cell cytoplasm is selected.*

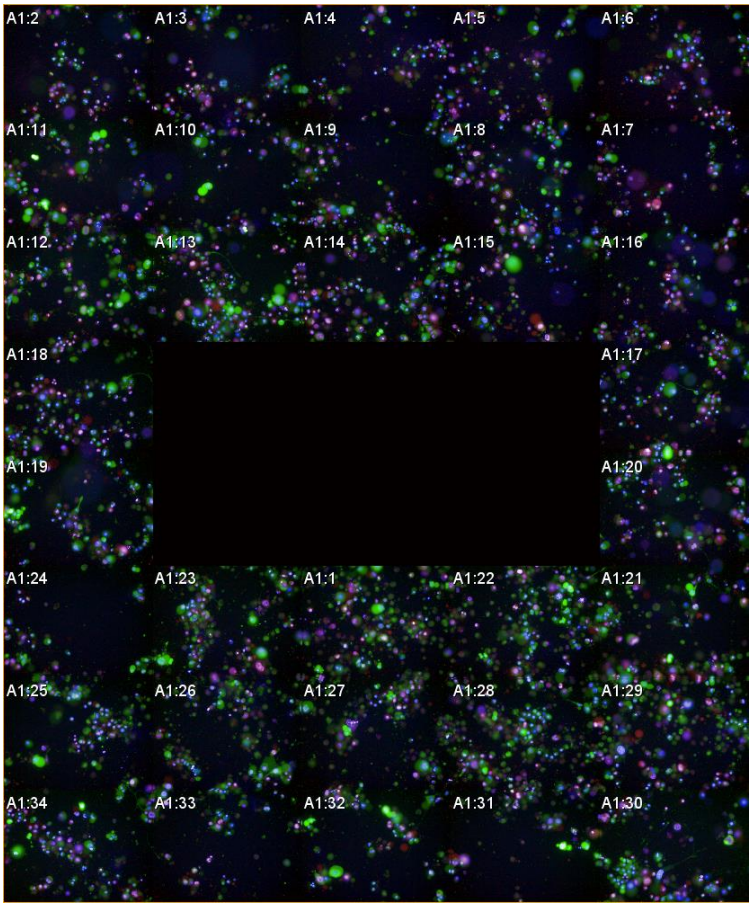

***Figure 2.4.3.2.*: Total surface of a 96-well plate with seeded cells analysed via Operetta HCS Microscopy.** *Cells in the middle of the well are excluded from analysis due to cell aggregates and dead cells that are usually found in there.*

It is worth mentioning that 90% of the well triplicates in each experimental condition had a low coefficient of variation <10% (standard dev/mean) thus there is homogeneity and experimental data is reproducible. Such homogeneity is proved by cell culture medium CV in $NSC34_D$ blank cells (Table 2.4.3.2). NSC34(hSOD1^{G93A}) show a small variance, probably due to classification analysis that is based on simple classification without incorporating more advance cell features.

Table 2.4.3.2. Coefficient of variation

	MEAN				SEM				CV	
	blank		G93A		blank		G93A		blank	G93A
	% Live Healthy	% Dead	% Live Healthy	% Dead	% Live Healthy	% Dead	% Live Healthy	% Dead		
1 DAY MEDIUM	35,3	24,3	49,6	25,9	2,5	1,2	3,3	4,1	0,049383	0,158301
2 DAYS MEDIUM	33,8	24,7	38	23,1	2,7	1	4,6	12,5	0,040486	0,541126
1 DAY DMSO	35,7	23,8	45,6	20,3	1,5	2,9	7,5	8,2	0,121849	0,403941

2.5. Immunoblotting

2.5.1. Receptor detection

Western blot for detecting $p75^{NTR}$ receptor and TrkB were performed. NSC34 (-), $NSC34_D$ (-), NSC34 ($hSOD1^{G93A}$) and NSC34 ($hSOD1^{G93A}$) $_D$, NIH/3T3 (negative control), C2C12, $C2C12_D$ cells were harvested in lysis buffer containing 1:100 Proteinase Inhibitor and 1:50 PMSF. 10% Tris-Glycine sodium dodecyl sulfate–PAGE was used for protein separation. Protein content was determined by Bicinchoninic Protein Assay (BCA method) using the manufacturer's protocol (Thermo Scientific™ Pierce™ BCA™ Protein Assay). Equal amounts of protein (~25 μg/ml) were resolved on SDS-polyacrylamide gels, transferred onto a nitrocellulose membrane (1h) and blocked in 5% BSA solution diluted in 0.1% Tween-20 TBS (TBS-T) for 1h, followed by incubation with the primary antibody. Antibodies against $p75^{NTR}$ (Promega, G3231), TrkB (Abcam, ab33655), GAPDH (Sigma, a8795) diluted 1:1000 in 1% BSA in TBS-T were incubated at 4°C on a shaker overnight. Bound antibodies were visualized using 1:5000 horseradish peroxidase-coupled anti-rabbit IgG secondary antibodies (Invitrogen, 656120) in 1% BSA in TBS-T. GAPDH primary antibody was visualized using 1:5000 horseradish peroxidase-coupled anti-mouse IgG secondary antibody (Merck, AP124P) in 1% BSA in TBS-T. Membranes were developed under ECL chemiluminescence Western Blotting Kit (Thermo Scientific™).

2.5.2. $NSC34_D$ stimulation for signaling studies

Matrigel sandwich cultures containing $1x10^4$ $NSC34_D$ cells were subjected to stress-induction at Day 3 - Day 4. First of all, $NSC34_D$ were washed 3 times with 150 μl of PBS and then subjected to 2h serum deprivation for synchronization. In each well 120 μl FBS-depleted differentiation medium was added and then the plate was left in incubator for 2h. Final concentrations of 100 ng/ml NGF, 100 ng/ml Pro-NGF, 100 ng/ml BDNF and 100nM BNN20 were prepared through serial dilutions in serum depleted medium and added to cell culture after the 2h serum deprivation and serum free medium removal (120 μl). 60 μl of stress stimuli were added in each well that contained the extra 40 μl to form 100 μl final volume in each well. Serum free treated cells with no exposure to any compound served as controls. Stressed for 30' and 60' cells with their controls were lysed simultaneously. DMSO 1% final concentration was used as control (vehicle) for BNN20.

For western blot analysis, $2x10^4$ $NSC34_D$ cells from two 96-wells in duplicates were harvested in lysis buffer containing 1:100 Proteinase Inhibitor and 1:50 PMSF for every condition. Due to high content of proteins in Matrigel, BCA method was not useful. Although, due to the same number of cells in each well of 96-well plate, obtaining equal amount of protein was feasible. Every two wells were lysed using the same 40 μl of lysis buffer. Protein were loaded and run on 12% SDS-PAGE. Then, the proteins were transferred to a nitrocellulose membrane and blocked in a solution of 5% BSA and 0.1% Tween-20 in TBS (TBS-T) for 1h followed by incubation with the primary antibody of 1:1000 total and phospho-p44/42 MAPK (Erk1/2) (Thr202/Tyr204) (Cell Signaling), the total and phospho-SAPK/JNK (Thr183/Tyr185) (Cell Signaling), the total and phospho-Akt (Thr308) (Cell Signaling) and GAPDH (Sigma, a8795) in 1% BSA in TBS-T on shaker at 4 °C, overnight. Anti-rabbit and anti-mouse secondary antibody conjugated to horseradish peroxidase (1:5000) in 1% BSA in TBS-T were incubated for 1h at RT prior to development with the ECL Western Blotting Kit (Thermo Scientific™). Stripping of the membranes after the phospho-Ab detection was performed, prior to probing membranes with the total protein.

2.6. Spheroid cell formation

Spheres were generated by the hanging droplet method (Laib et al., 2009). Briefly, cells were counted and suspended in 1:4 methyl-cellulose to cell medium. For preparation of NSC34 sphere, NSC34 proliferation medium was used. For C2C12 spheroid preparation, either C2C12 growth or differentiation medium were used depending on the type of the utilized C2C12 culture. Each 25μl droplet contained 1000 cells. For 20 spheres a total 500 ml volume of cell suspension was prepared. Then, cell suspension was divided evenly into non-adherent

plastic square petri dishes. Petri dishes were placed upside down, to make the droplets hang and finally, the dish was filled with 10ml of dH_2O. Spheres were harvested next day and seeded into 3D collagen scaffolds.

2.7. NSC34 and C2C12 3D co-culture

2.7.1. Development of the 3D co-culture

In 3D co-culture experiments only NSC34 (-) cells were used. NSC34 and C2C12 co-culture was performed inside type I Collagen (C) and Collagen-glycosaminoglycan (CG) scaffolds. To optimize the co-culture, parameters as cell concentration, cell state - differentiated / undifferentiated, cell morphology - seeding as single cells or spheres were examined. As it was implied through literature (Jiang et al., 2003; Arnold et al., 2012; Demestre et al., 2015; Vilmont et al., 2016; Happe et al, 2017; Cvetkovic et al., 2017), the muscle cells were seeded first to scaffold in order to prepare the environment for NSC34 cells. The NSC34 differentiation medium, supplemented with ITS was chosen as the co-culture medium, as NSC34 cells were more sensitive.

Stained C2C12 or $C2C12_D$ were seeded in varying concentrations (1×10^3 - 5×10^3) into collagen I scaffolds as single cells. The next day, C2C12 or $C2C12_D$ spheres that were generated the previous night, were seeded in remaining collagen I scaffolds of the device. Each device comprises 6 scaffolds. In case of the undifferentiated C2C12, cells were differentiated on the scaffold by supplementing the C2C12 differentiation medium at the Day 1 and Ara-C at the Day 3 to eliminate the non-fused myoblasts. Right after C2C12 differentiation (Day 6), NSC34 cells were seeded and the medium was switched to the NSC34 differentiation medium supplemented with ITS. In case of $C2C12_D$, cells were seeded to the device with the C2C12 differentiation medium until NSC34 were seeded into wells. Then, medium was as previously switched to NSC34 differentiation medium. Wells containing monocultures of C2C12 or NSC34 cells kept as negative controls. Cells were co-cultured approximately for one week, depending on the experiment.

2.7.2. Staining Protocol

In most of the experiments C2C12 cells were stained with CellTracker™ Orange CMRA Dye (Thermo fisher scientific C34551) and thus excided red fluorescence. On the other hand, NSC34 underwent in most of the times staining with CellTracker™ Green CMFDA Dye (5-chloromethylfluorescein diacetate) (Thermo fisher scientific C7025) exciding green fluorescence. Cells were stained with CellTracker Dyes either before detachment from the growing substrate (Nunc™ Delta dish) or after seeding on the scaffolds. Specifically, medium was removed from the dish and cells were rinsed once with PBS. Then, dye was added in a serum-free buffer to the culture. This was followed by 30-60 minutes incubation at 37°C, protected from light. Then, cells were washed two times with PBS. Finally, PBS was replaced with fresh prewarmed media. After staining, cells were detached from the surface and either transferred to the scaffolds or used for the generation of spheres. The same protocol was followed when cells were stained directly inside scaffolds. To determine the best concentration of the stain solution and the best incubation time, C2C12 cells were stained with 10 μM or 20 μM CellTracker™ Orange CMRA Dye and incubated for 30', 45' and 60' respectively.

Moreover, staining with CalceinAM (Thermo fisher scientific, C3100MP) to label live cells (green fluorescent) and Propidium iodide (PI) (Thermo fisher, scientific P1304M) to detect dead cells in a population (red-fluorescent nuclear and chromosome counterstain), as it is not permeant to live cells, were also performed at the last step of co-culture. Hoechst® nucleic acid stain (Thermo fisher scientific, H1399) (blue fluorescence when bound to dsDNA) to stain the nuclei of cells was also used, before imaging. The staining protocol is exactly the same to the previously described CellTracker staining protocol.

2.7.3. Image acquisition and Analysis

Images were acquired on a Zeiss Axio Inverted Microscope, while analysis was performed with Image-J software.

2.7.4. C2C12 Transfection

In order to develop a stable C2C12 cell line that would emit fluorescence, thereby enabling easy detection of the C2C12 cells in co-culture models, undifferentiated C2C12 cells were transfected with mDsRED plasmid (Clontech, 632466) using the Lipofectamine 2000 reagent (Invitrogen Life Tech) or FuGENE 6 (Promega) kits. Following the manufacturer's instructions, both standard and reversed transfections were performed. mDsRED plasmid was a kind gift of Professor Papamatheakis lab (IMBB-FORTH). Briefly, C2C12 cells were plated in various cell densities (2.500, 5.000, 10.000 cells) in a 96-well plate one day prior to transfection. Different ratios (μl:μg) of Lipofectamine 2000 / FuGENE 6 reagents to mDsRED plasmid DNA were then used for transfection of according to the manufacturer's protocol. The reagent:DNA ratios varied from 3:1 to 6:2. For the selection of transfected cells kill curves with increasing concentrations of Neomycin (3-7mg/ml) and G418 (0.5-3mg/ml) antibiotics were performed (Figure 2.7.4). Cells were selected for up to 2 weeks and medium was changed every 2-3 days. CHO and HEK293T cells were used as controls of transfection.

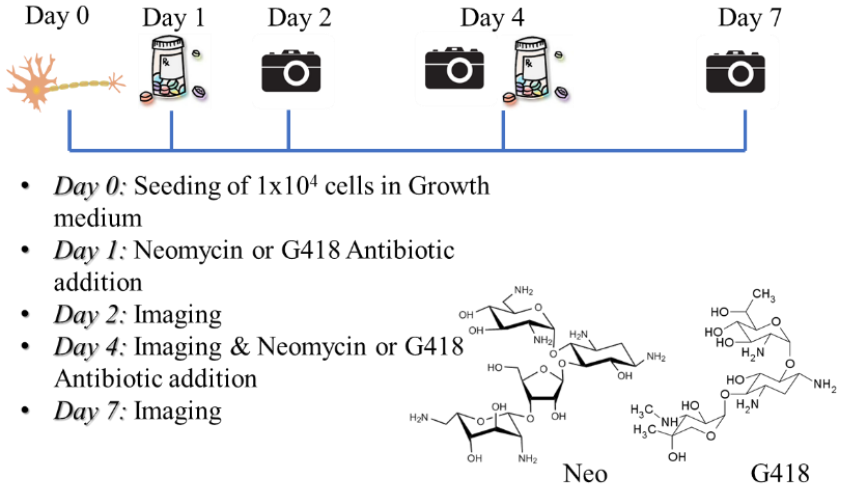

***Figure 2.7.4.*: Neomycin and G418 selection protocol for transfected C2C12.** *C2C12 cultures were maintained for one week and medium was refreshed every 2 days.*

2.7.5. Lentiviral Transduction

Escherichia coli stored in 10% glycerol solution at -80°C that contained packaging and envelope lentiviral plasmids Delta8.91(Department of Medicine, University of Crete) and pMD2.G (Addgene, 12259) were a kind gift of Professor Sourvinos (Department of Medicine, University of Crete). LeGO-C2-mCherry Plasmid (Addgene, 27339) was a kind gift of Professor Papamatheakis lab (IMBB-FORTH). Single *E. coli* bacteria colony for each of the three plasmids was obtained from standard LB-agar-ampicillin plates and was used to prepare a suspension culture. Suspension cultures were further subjected to plasmid isolation using the NucleoSpin® Plasmid method (Macherey-Nagel) and the he QIAGEN Plasmid Midi Kit. DNA purity and concentration were evaluated with Nanodrop measurement. Transient transfection of HEK293T cells with all the three plasmids was performed with both Lipofectamine 2000/FuGENE 6 reagents in 10cm^2 culture dish. HEK293T cells were at 80% confluency 24h prior to transfection. Supernatant was harvested after 48h, 72h and 96h, filtered by 0.45μm filter, aliquoted and stored at -80°C. C2C12 cells were seeded in 24-well plate 24h before transduction at a low density. Next day, viral supernatant for was added to C2C12 culture and stayed for 24-48h. 5-8 μg/ml of polybrene was as well

supplied to further promote lentiviral transduction, which was performed. After 24-48h cells were observed using a Zeiss Axio Inverted Microscope.

Chapter 3: Results

3.1. Characterization of the expression and response of neurotrophin receptors in NSC34 cells grown in 2D

3.1.1. Expression of $p75^{NRT}$ and TrkB Neurotrophin Receptors in $NSC34_D$

To study neurotrophin signaling and use NSC34 cell line as TrkB generic model, the expression of TrkB as well $p75^{NRT}$ should have been confirmed. Literature reports that both NSC34 and $NSC34_D$ express TrkB as well $p75^{NRT}$ receptors (Turner et al., 2004; Matusica et al., 2008). C2C12 cells is as well expressing $p75^{NRT}$ neurotrophin receptors (Reddypalli et al., 2005). Thus, initially, we began examining the expression of TrkB as well $p75^{NRT}$ receptors by immunoblotting analysis. Lysates were harvested from 6-well plate cultures from NSC34 (-), $NSC34_D$ (-) and C2C12 cells and equally loaded onto 10% SDS-polyacrylamide gel. Total protein was quantified by the BCA protein method. Results, shown in Figure 3.1.1.1, showed that both NSC34 and $NSC34_D$ express $p75^{NRT}$ receptors, while in C2C12 expression of $p75^{NRT}$ was lower.

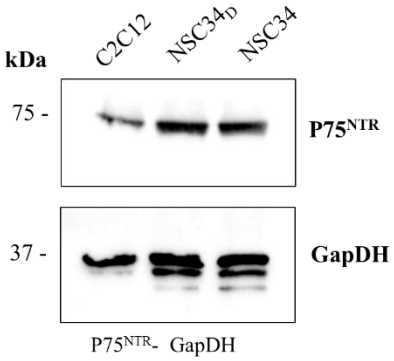

***Figure 3.1.1.1.*: Characterization of $p75^{NRT}$ neurotrophin receptor expression in NSC34 cells.** *Both NSC34 and $NSC34_D$ as well as C2C12 express $p75^{NRT}$.*

Moreover, both NSC34 and $NSC34_D$ cells express TrkB, with $NSC34_D$ showing higher TrkB expression. In contrast to C2C12, $C2C12_D$ demonstrated to possess TrkB receptors, though the number is really low. Results demonstrated in Figure 3.1.1.2.

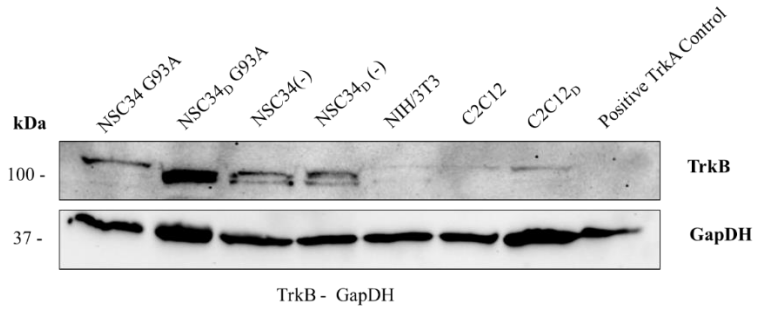

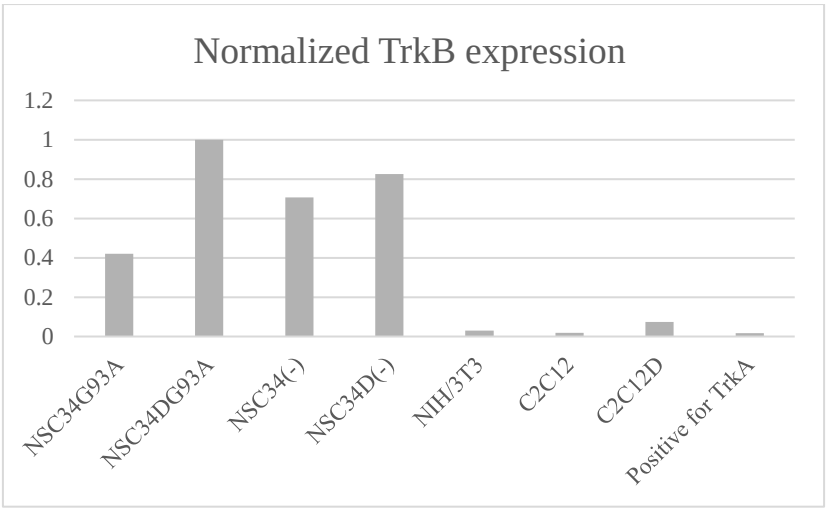

***Figure 3.1.1.2.*: Characterization of TrkB neurotrophin receptor expression in NSC34 and C2C12 cell line.** *Both NSC34 and NSC34$_D$ cells express TrkB receptor.*

3.1.2. NSC34 response to NGF, pro-NGF and BDNF stimulation

After confirming that NSC34 cells expressed neurotrophic factors and consequently are responsive to neurotrophins, neurotrophin signaling was studied. Immature neurotrophin pro-NGF and its mature form NGF were added to 2h-serum-deprived NSC34$_D$(-) Matrigel sandwich cell culture and incubated for 30' or 60 minutes. Activation of proteins involved in pathways related to cell survival were tested. Such proteins were the Erk1/2 and Akt proteins. Pro-NGF was expected to act through p75^{NRT} receptors, while NGF to induce no change to these signaling pathways as NSC34 cells are devoid of the high-affinity NGF receptor TrkA (Turner et al., 2004; Matusica et al., 2008). On the other hand, BDNF stimulation was expected to activate those pathways. Cells seemed responsive to neurotrophins. However, as this experiment was performed successfully only once, the effect of each neurotrophin on the Erk or Akt pathways cannot be determined. Data shown in Figure 3.1.2 is preliminary.

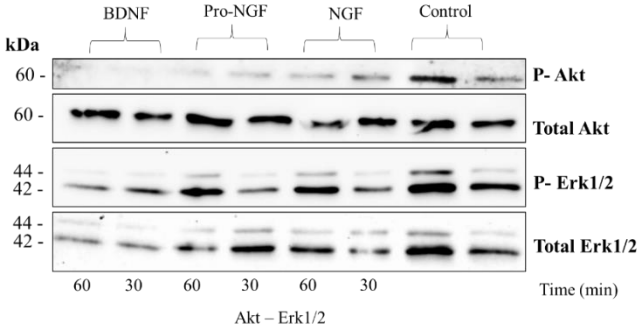

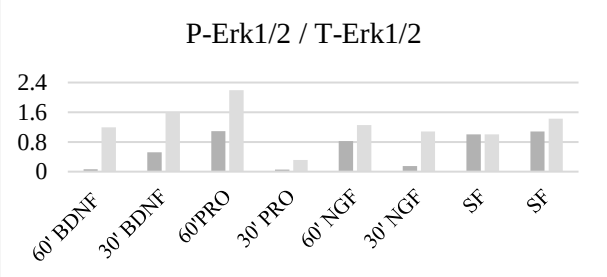

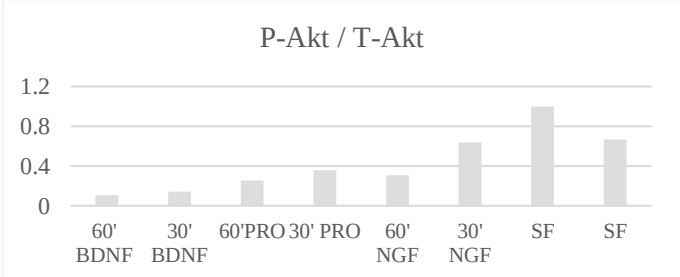

***Figure 3.1.2.*: Characterization of neurotrophic responsiveness of NSC34.** *Immunoblot analysis of NSC34D (-) cell lysates for phospho-p44/42 MAPK (Erk1/2) and phospho-Akt after 30' and 60' stimulation with the mature and immature nerve growth factors (NGF, Pro-NGF) and the brain-derived neurotrophin factor (BDNF).*

Results showed (Figure 3.1.2)

3.1.3. NSC34 response to BNN20 stimulation

In the same manner, the microneurotrophin BNN20 was added to 2h-serum-deprived $NSC34_D$(-) Matrigel sandwich cell culture and incubated for 30' or 60 minutes. Activation of Erk1/2 and Akt proteins involved in survival pathways as well as c-Jun Kinase (JNK) involved in apoptosis and cell death were studied.

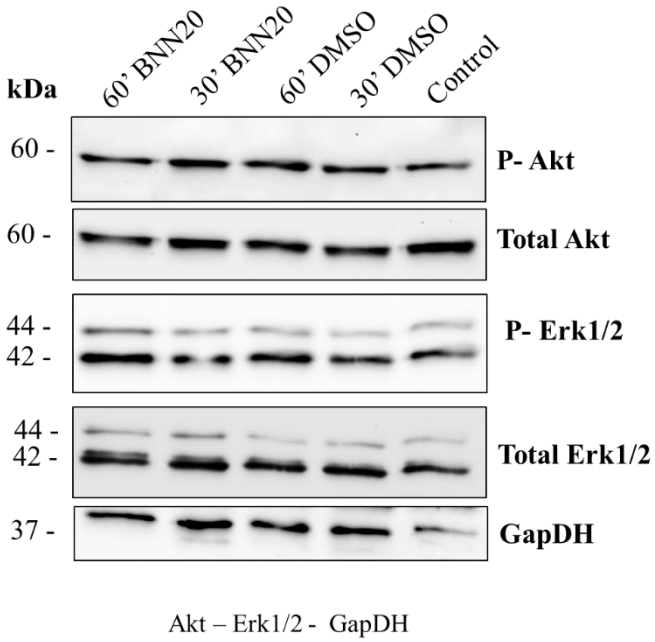

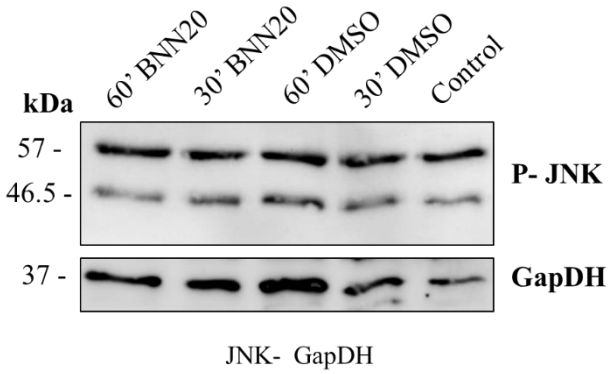

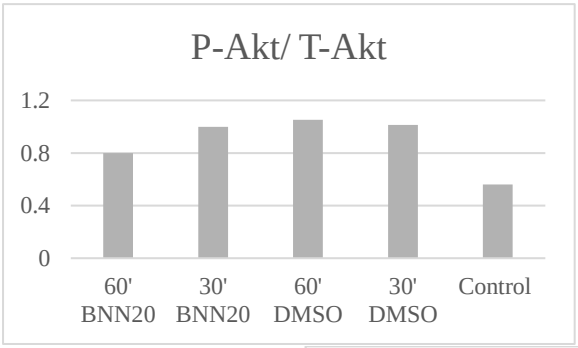

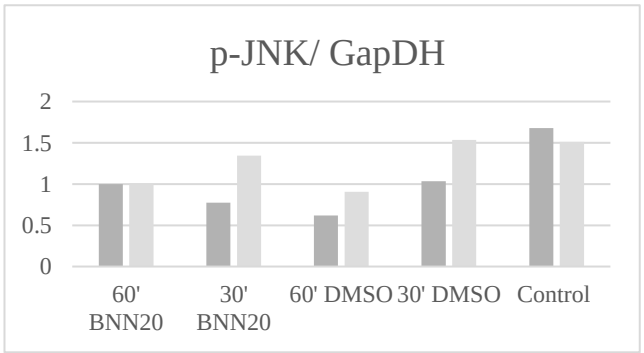

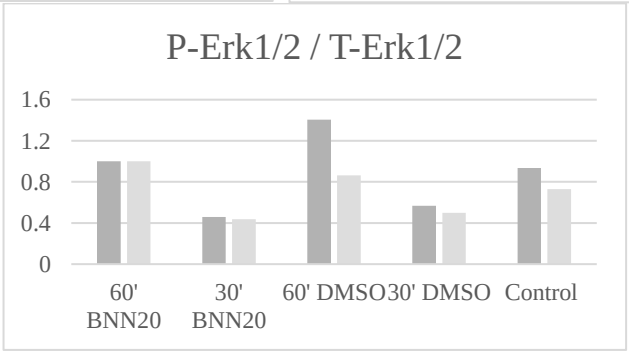

Figure 3.1.3.: ***Characterization of BNN20 neurotrophic responsiveness of NSC34.*** *Immunoblot analysis of NSC34D (-) cell lysates for phospho-p44/42 MAPK (Erk1/2), phospho-SAPK/JNK (Thr183/Tyr185) and phospho-Akt after 30' and 60' stimulation with the BNN20 microneurotrophin.*

Results show (Figure 3.1.3.) a reduction in phospho-SAPK/JNK (Thr183/Tyr185) upon 60 minutes stimulation with BNN20. However, as it is a single biological replicate, results should be proceeded with caution.

3.2. Quantification of NSC34(-) and NSC34(G93A) response to ALS-related stress and drug treatments.

In order to model mechanisms associated with ALS pathogenesis, various compounds – potential stress inducers and potential neuroprotective agents were evaluated in the controlled environment of Matrigel Sandwich culture. The first step was to identify potential stress inducers that would be further incorporated into drug screening studies. The second step included the screening of known neuroprotective compounds to identify potential therapeutics and evaluate the current FDA-approved drugs.

3.2.1. Investigation of the H_2O_2 effect in NSC34 apoptosis

H_2O_2 was used to model the oxidative stress present in ALS pathophysiology. Both NSC34$_D$(-) or NSC34 $_D$ (hSOD1^{G93A}) were exposed to various concentrations of H_2O_2 (Table 2.3.2.). Results showed that both NSC34$_D$(-) or NSC34 $_D$ (hSOD1^{G93A}) responded to oxidative stress. 100 μM concentration H_2O_2 was chosen as the most appropriate for all subsequent neuroprotective treatments, as it resulted in ~20% cell death in NSC34$_D$(-) and ~30% cell death in NSC34 $_D$ (hSOD1^{G93A}). The ~10% variance in cell death was attributed to the mutated SOD1 of the NSC34 $_D$ (hSOD1^{G93A}).

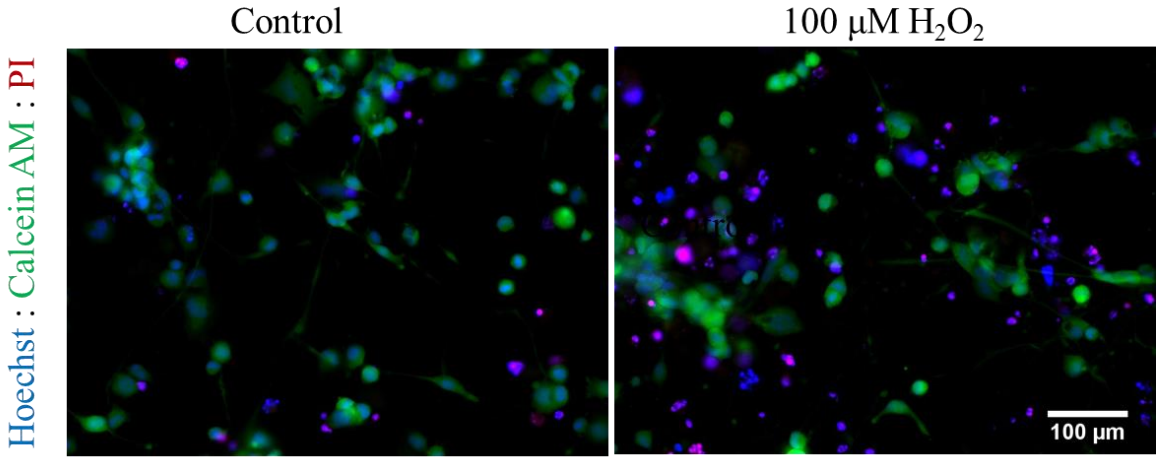

Figure 3.2.1.: ***Induction of the H_2O_2 apoptotic cell death in NSC34$_D$(-) or NSC34 $_D$ (hSOD1^{G93A}).*** *Above: NSC34D(-) after 20h incubation with 100μM of H_2O_2. Cells are stained with the Live-or -Dead staining. Below: NSC34D(-) or NSC34 D (hSOD1^{G93A}) H_2O_2 kill curve.*

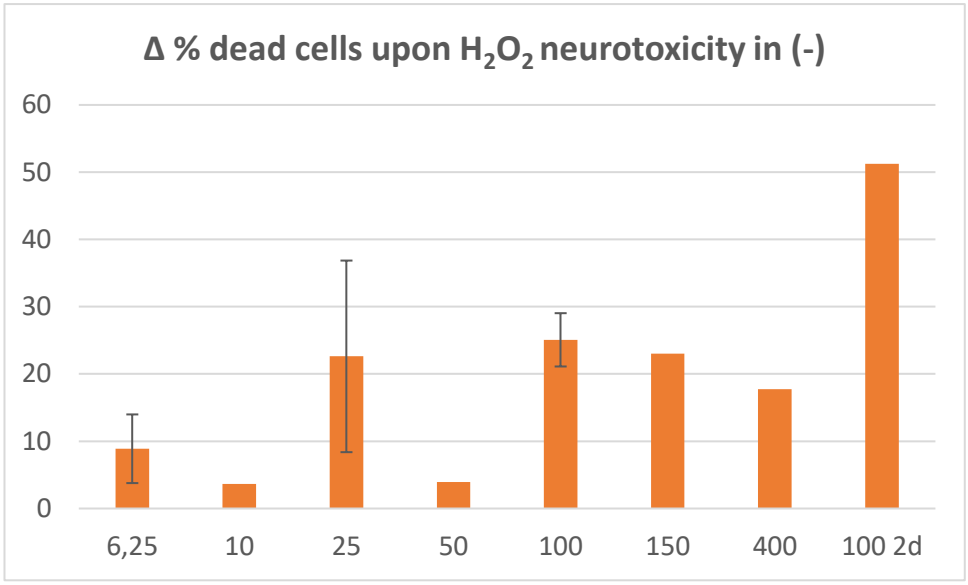

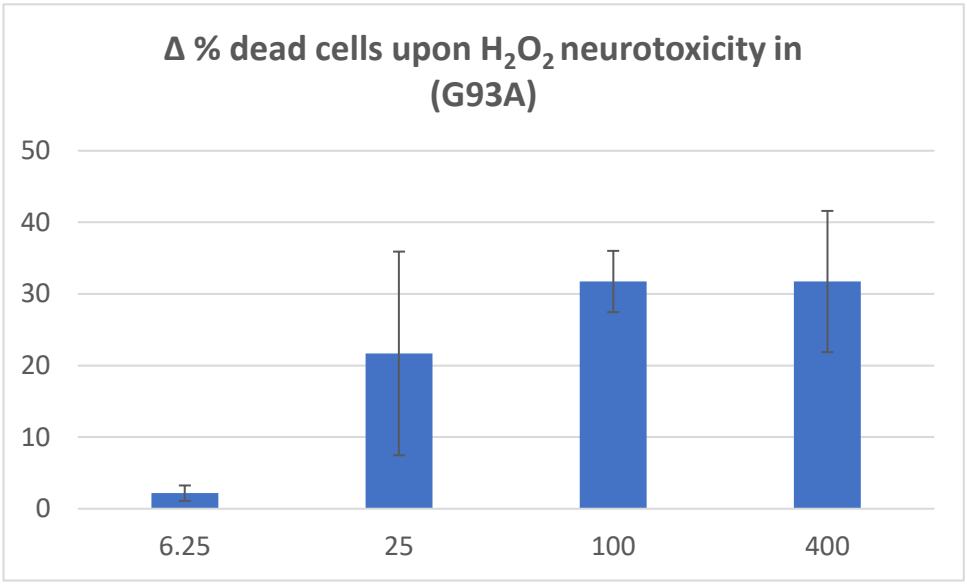

3.2.2. Investigation of the Pro-apoptotic TNFα, INFγ and IL1α cytokine effect in NSC34 apoptosis

Cytokines were used to model the neuroinflammation present in ALS pathophysiology. Both $NSC34_D$(-) or $NSC34_D$ ($hSOD1^{G93A}$) were exposed to various concentrations of TNFα, INFγ and IL1α pro-apoptotic cytokines (Table 2.3.2.). 24h or 48h exposure to INFγ or IL1α had no effect on $NSC34_D$(-) or $NSC34_D$ ($hSOD1^{G93A}$) survival. In contrast, when cells were exposed to 48h TNFα, cell apoptosis was observed in $NSC34_D$(-). A 13.5% increase in cell death compared to control. 24h TNFα cell exposure had no effect in cellular viability of $NSC34_D$(-). Interestingly, lower concentrations of TNFα (15-25 ng/ml) had a significant effect on $NSC34_D$ ($hSOD1^{G93A}$) when exposed for 24h. Such observation did not apply to $NSC34_D$(-), as it is demonstrated by the 24h kill curve (Figure 3.2.2.).

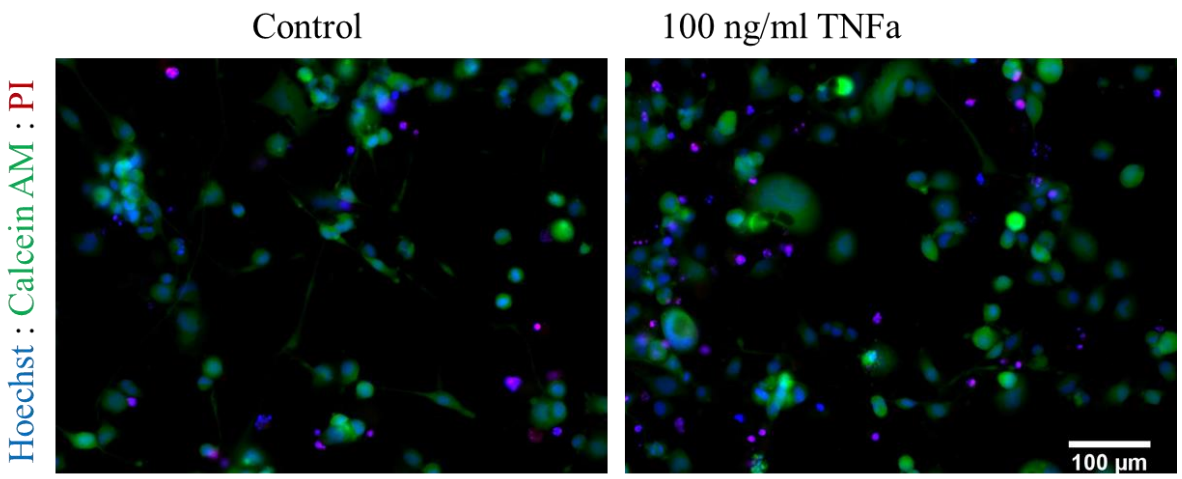

***Figure 3.2.2.*: Induction of TNFα apoptotic cell death in NSC34$_D$(-) or NSC34 $_D$ (hSOD1^{G93A}).** *Above: NSC34$_D$(-) after 18h incubation with 100 ng/ml TNFα. Cells are stained with the Live-or -Dead staining. Below: TNFα kill curve. NSC34$_D$(-) or NSC34 D (hSOD1G93A). Below: TNFα kill curves.*

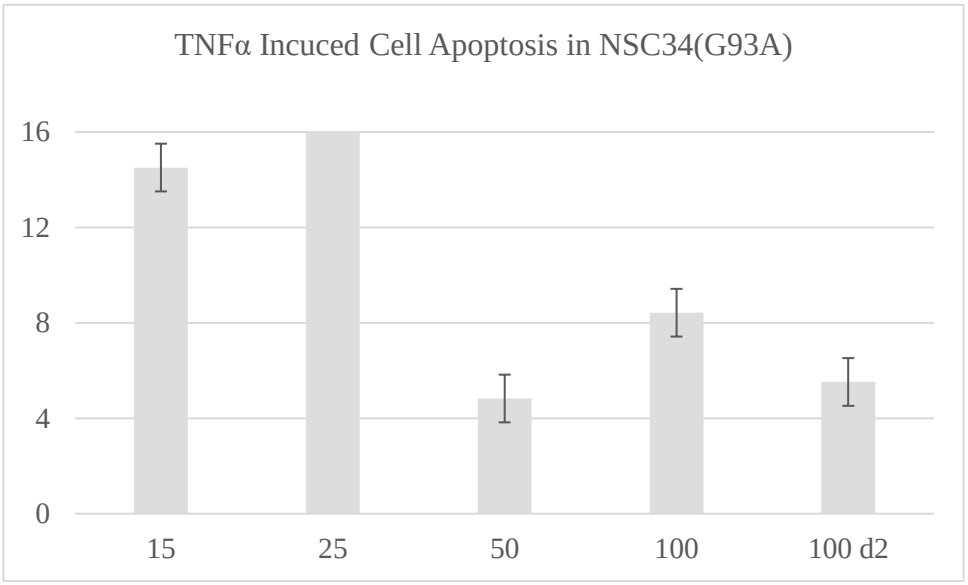

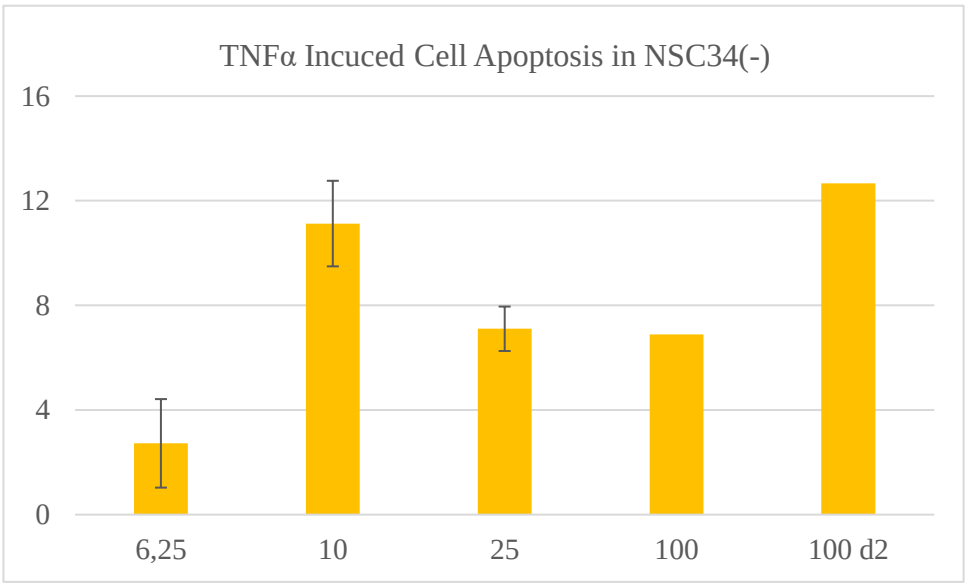

3.2.3. Serum Deprivation effect in NSC34 apoptosis

Results revealed that serum free conditions could induce metabolic cell death. Specifically, 24h serum free deprivation increased cell apoptosis by 10% in both $NSC34_D$ cells, while 48h led to 20% reduction in cell viability.

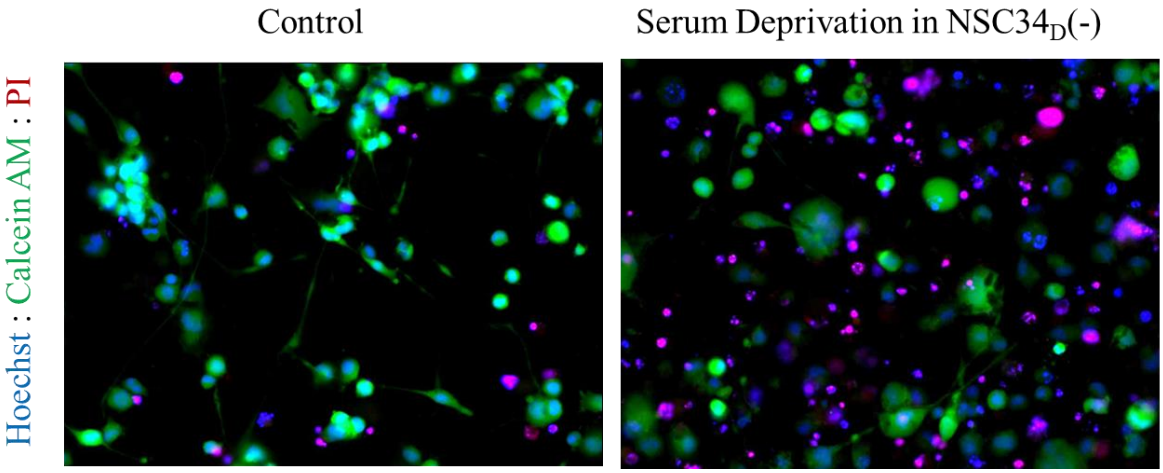

***Figure 3.2.3.1.*: Serum free induced apoptotic cell death in $NSC34_D$(-) or $NSC34_D$ ($hSOD1^{G93A}$).** *Serum deprivation was induced for 48h. Cell death is evident. Cells are stained with the Live-or -Dead staining.*

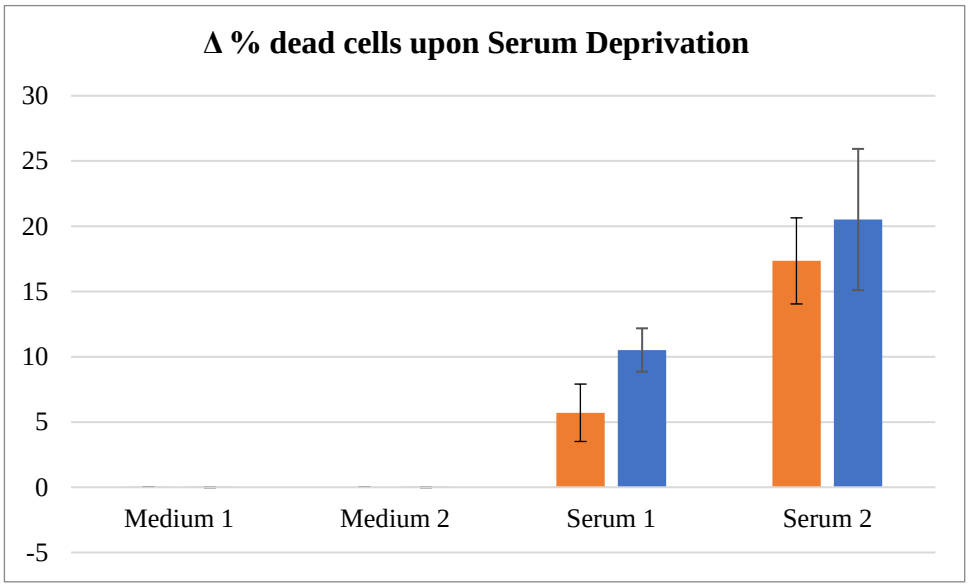

***Figure 3.2.3.2.*: Serum free induced apoptosis in $NSC34_D$(-)or $NSC34_D$ ($hSOD1^{G93A}$).** *$NSC34_D$(-) in orange and $NSC34_D$ ($hSOD1^{G93A}$) in blue respond to serum deprivation in a time dependent manner, as 2 days in serum free medium doubled the apoptosis observed at 1 day.*

3.2.4. Pro-NGF and NMDA and AMPA effect in NSC34 apoptosis

Pro-NGF and NMDA and AMPA were evaluated for their ability to induce cell death. However, neither of these compounds could reduce cellular viability, under these experimental conditions. Specifically, NMDA was induced in various concentrations (0.5-100 μM) to NSC34(-) cells for 24h with no significant changes in cellular viability. No change in viability was as well observed after 48h induction of NMDA to NSC34 (-). Under the same conditions, 48h application of 5-100 μM AMPA to NSC34(-) had also a non-significant effect, although the result was suspicious as the percentage of dead cells was lower than the one of medium (baseline) More experiments are needed to drive conclusions. Pro-NGF exposure to both cell $NSC34_D$(-) or $NSC34_D$ ($hSOD1^{G93A}$) resulted in

no change in cellular viability. It should be mentioned than in NSC34 $_D$ (hSOD1^{G93A}) those simulations were performed only once. Cell death < 10% was not considered as important. To investigate whether such small differences in cell viability, more experiments are needed.

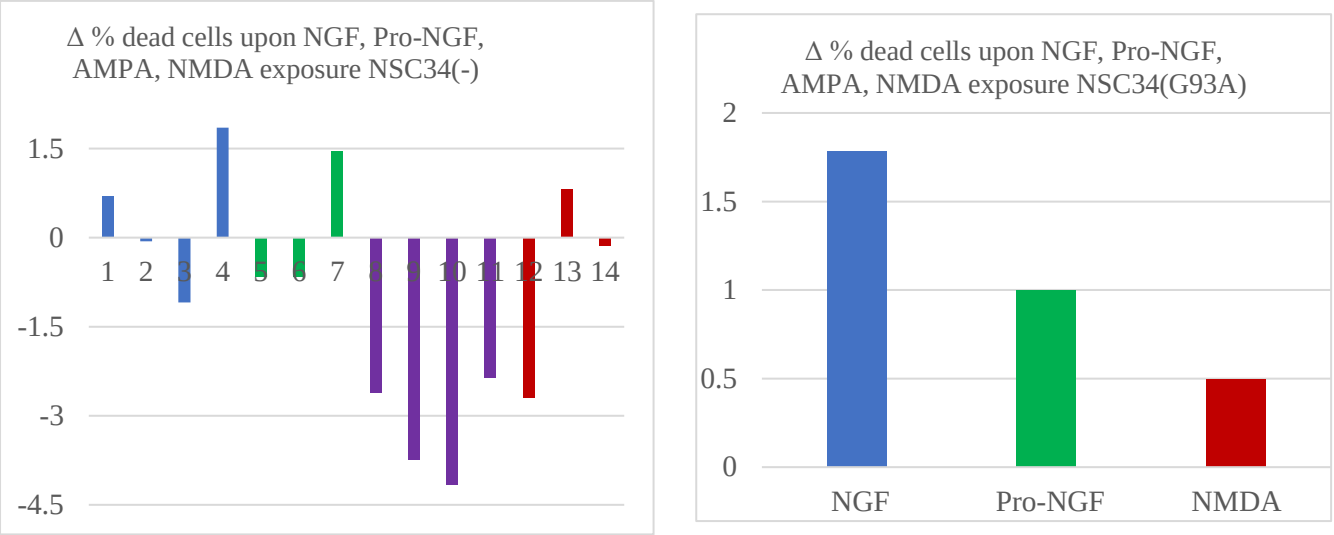

***Figure 3.2.6.*: Exposure of NSC34 cells to NGF, Pro-NGF, NMDA and AMPA.** *(1-4)10, 100, 1000 ng/ml and 100 ng/ml for 44h NGF (blue), (5-7) 10, 100, 1000 ng/ml Pro-NG F(green), (8-11) 50 μM for day, 5, 50, 500 μM for 2 days AMPA (purple), (12-14) 5, 50, 100 μM NMDA (red) respectively. No significant apoptosis is observed upon these stimulations.*

3.2.5. Effect of Edaravone in the reduction of NSC34 apoptosis

The effect of the FDA-approved drug Edaravone on oxidative-induced stress was evaluated in Matrigel Sandwich cultures. Both NSC34$_D$(-) or NSC34 $_D$ (hSOD1^{G93A}) after 4h of serum deprivation were exposed to either- 100 μM of H_2O_2 or 100 μM of H_2O_2 supplemented with 6,25-100 μM of Edaravone for 18-20h. Results showed that neither concentration was able to significantly reduce H_2O_2-induced stress.

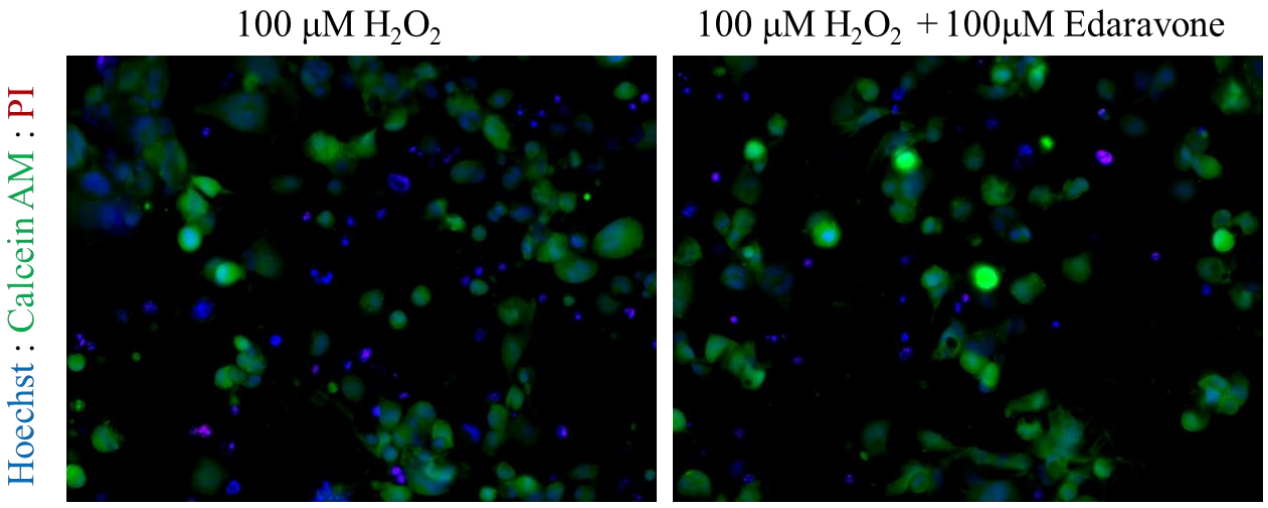

***Figure 3.2.5.*: Induction of H_2O_2 apoptotic cell death in NSC34$_D$(-) or NSC34 $_D$ (hSOD1^{G93A}) and treatment with the FDA-approved drug Edaravone.** *NSC34$_D$(-) after 18h incubation with 100 μM of H_2O_2. or with both 100 μM of H_2O_2 and 100 μM Edaravone. Cells are stained with the Live-or -Dead staining.*

3.2.6. Evaluation of the neuroprotective role of BDNF and BNN20 in the reduction of NSC34 apoptosis

As NSC34 cells are positive for high-affinity BDNF receptor, both BDNF and BNN20 at various concentrations were supplemented into $NSC34_D$(-) or $NSC34_D$ ($hSOD1^{G93A}$) cultures that were exposed to 100 µM of H_2O_2 for 19-20h. However, no difference was observed upon BNN20 or BDNF treatment. (Figure 3.2.6.) More experiments are required to drive a strong conclusion.

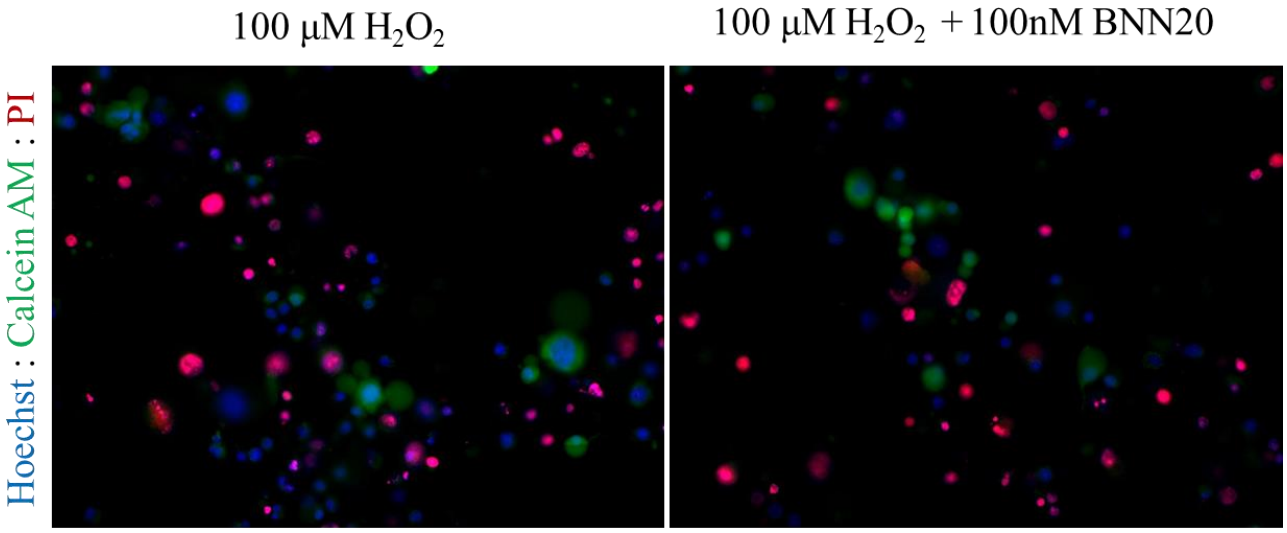

***Figure 3.2.5.*: Induction of H_2O_2 apoptotic cell death in $NSC34_D$(-) or $NSC34_D$ ($hSOD1^{G93A}$) and treatment with the BNN20 microneurotrophin.** *$NSC34_D$(-) after 19h incubation with 100µM of H_2O_2. or with both 100 µM of H_2O_2 and 100 nM of BNN20. Cells are stained with the Live-or -Dead staining.*

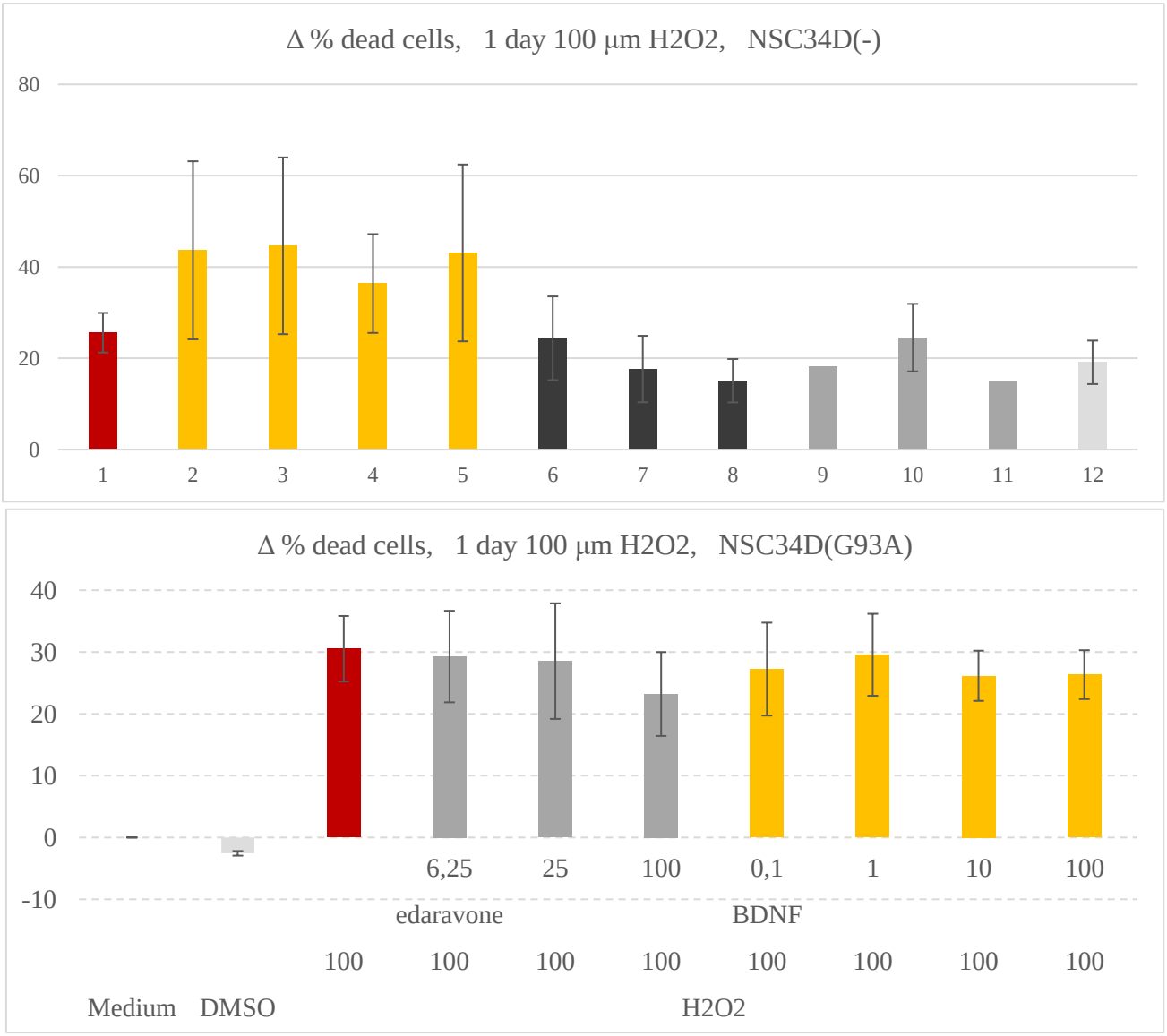

***Figure 3.2.6.*: Overview of Drug evaluation.** *Difference in % of cell death between the % average cell death induced by the compound to % average total cell death induced by the control in NSC34$_D$(-) and NSC34$_D$ (hSOD1^{G93A}). The % average cell death of (1) control, (2-5) 0.1, 1,10,100 ng/ml BDNF, (6-8) 1, 10, 100 nM BNN20, (9-12) 1,56, 6,25, 25, 100 µM Edaravone after 100µM H_2O_2 exposure.*

3.3. Development of a novel 3D NSC34 ALS model based on porous scaffolds.

In contrast to the 2D cell-based screening, 3D systems have more *in vivo* relevance and could be used as predictive tool for the success or failure of a drug screening campaign. Consequently, transition of the 2D ALS model into 3D Porous Collagen I Scaffolds can surpass the limited ability of the current cell culture methodologies. In this project, series of experiments have been conducted using the NSC34 Motor neuron cell line in co-culture with the C2C12 muscle cell line inside Collagen I scaffolds. The first attempts to grown NSC34 cells inside scaffolds were unsuccessful. NSC34 cells were «unhappy» inside the environment of scaffold -cells remained round with no visible axons. The difference between the traditional 2D NSC34 culture and 3D NSC34 was drastic (Figure 3.3.1). To overcome the problem of NSC34 cell attachment, co-culture system between NSC34 cell line and C2C12 muscle cell line was developed and optimized.

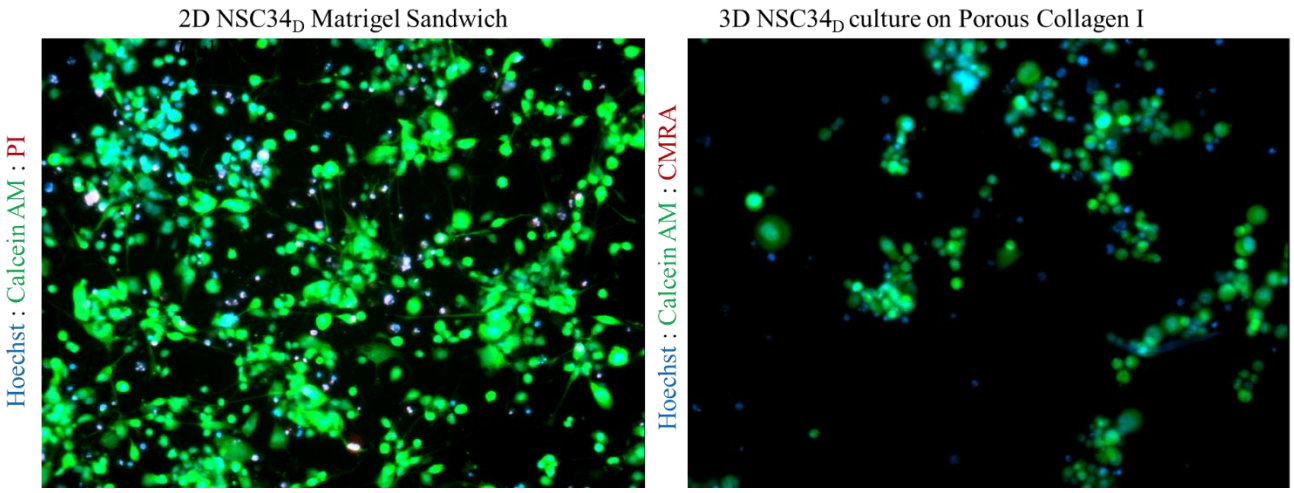

***Figure 3.3.1.:* Difference between 2D NSC34 Matrigel Sandwich culture (Day6) and 3D NSC34 culture (Day 4).** *No formation of axons is evident in 3D Collagen I scaffold. Cells were stained with Live-or Dead staining and visualized with. Zeiss Axio Inverted Microscope, 10x.*

Multiple studies have shown that molecules released for muscle cells can act as tropic factors for motor neurons (Taylor et al, 2007; Madison et al., 2014), affecting positively the formation and elongation of axons. Such factors are the Brain-derived neurotrophic factor (BDNF), the Glial cell line-derived neurotrophic factor (GDNF), the Ciliary neurotrophic factor (CNTF), the neurotrophins 3 and 4/5 (NT3, NT4/5), the hepatic and epidermal growth factors (HGF, EGF), the Insulin-like growth factor 1 (IGF-1), the Fibroblast growth factor (FGF) and cardiotrophin-1. Co-cultures with just extracellular muscle cell vesicles on the motor neuron cells seemed to have a striking effect in terms of neurite outgrowth and survival (Madison et al., 2014). Thus, series of experiments were conducted to firstly evaluate the effect of C2C12 on NSC34 and secondly optimize the co-culture conditions. To evaluate the effect of C2C12 on NSC34 morphology, a co-culture system was developed. As it was implicated through literature, results showed that C2C12 improved the overall morphology of NSC34 (Figure 3.3.2.). Some NSC34 produced long axons throughout the scaffold and co-culture was maintained up to 9 Days.

Next step was to optimize the co-culture condition by testing different parameters. Cells seeded in various densities (1,000 - 5,000 cells of each type) and NSC34:C12C12 ratios to determine the appropriate cell concentration that would result in better NSC34 cell morphology (neurite outgrowth), resembling the 2D NSC34 cultures. Results showed that more than 10^4 total cells on scaffold are difficult to visualize manually. However, to compare cell densities, an accurate method to distinguish the two cell types was needed. Although, C2C12 and $C2C12_D$ were stained with CellTracker™ Orange CMRA Dye a day prior to seeding on scaffold, C2C12 cells were unable to be visualized as dye lost its fluorescence in 2-3 days period. Attempts to stain C2C12 cells after seeding on scaffold, prior to NSC34 seeding also failed, as cells were unable to maintain their fluorescence. Moreover, staining of C2C12 showed that cells were stained unevenly, which was a serious drawback (Figure 3.3.3).

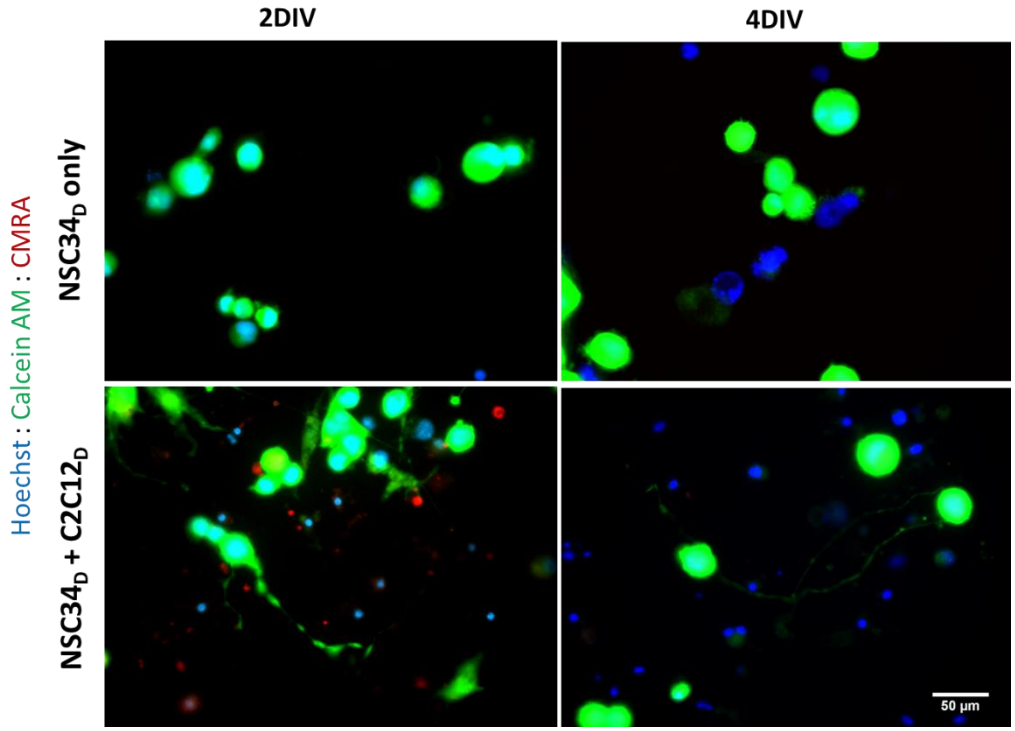

Figure 3.3.2.: ***The effect of C2C12 on NSC34 morphology inside a 3D NSC34 culture.*** *No formation of axons is evident in 3D Collagen I scaffold were evident in absence of C2C12 cells. In contrast, long axons are generated when cells are in co-culture (Day4-4DIV). Cells were stained with CalceinAM, Hoechst, CMRA (C2C12 only) dyes and visualized with. Zeiss Axio Inverted Microscope.*

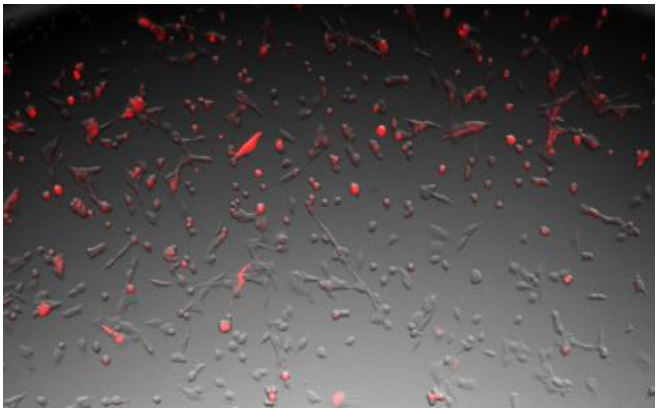

Figure 3.3.3.: ***CellTracker™ Orange CMRA staining of C212 cells in 96-well plate****. Cells where stained with 10 μM concentration for 45'. Higher exposure time to stain was toxic to cells (data not shown).*

Furthermore, results showed that only differentiated cells should be incorporated and cultured in Collagen I scaffolds, as undifferentiated cells, especially C2C12, expanded rapidly disrupting the scaffold (Figure 3.3.4.), thereby deteriorating the visualization procedure. Consequently, undifferentiated cells were excluded from further co-culture. The best results were obtained when both C2C12 and NSC34 were differentiated. This was evaluated by the number of produced axons empirically, due to the inability to distinguish the two cell types in 3D co-culture with certainty. The problem of visualization was faced merely by the generation of spheroid $C2C12_D$ cells (spheres) (Figure 3.3.5.). Spheres contained approximately 1000 cells and retained their shape, after transferring to scaffolds (Figure 3.3.5.). However, the co-culture of single $C2C12_D$ and single cell $NSC34_D$ had better performance (Figure 3.3.6) as more and longer axons were observed after Day 4 (4DIV). However, it is important to mention that in this case the two cell types were too difficult to distinguish.

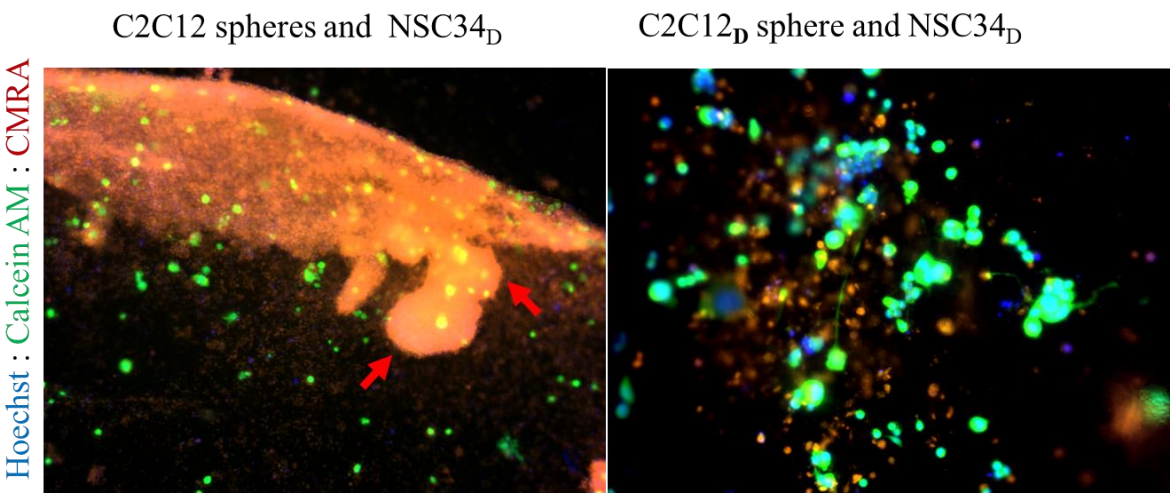

***Figure 3.3.4.:* Single differentiated NSC34D cells in a 3D Collagen I scaffold in co-culture with C2C12 or C2C12D**. *Left: NSC34D cells with spheres of C2C12 (red arrows), where cells spread out of sphere and caused disruption of scaffolds, (rolled over). C2C12 Cell proliferated rapidly covering the surface of the scaffold. The high density of C2C12 enables CMRA dye visualization. Right: NSC34D cells with a sphere of C2C12D that already has spread out (red mass in the middle). Cells were stained with CalceinAM, Hoechst, CMRA (spheres only) prior to imaging.*

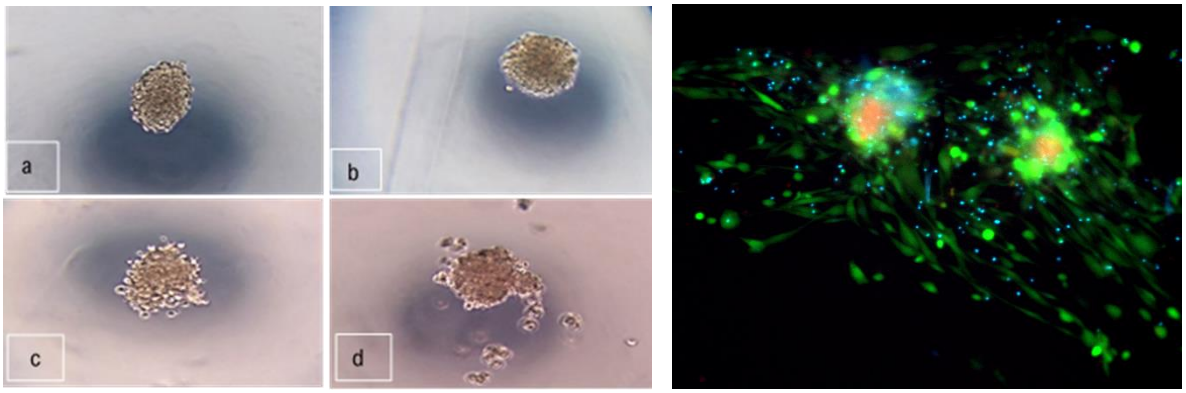

***Figure 3.3.5.:* C2C12 Spheres.** *Left: Cells inside hanging-droplets after 24h. Spheres shown in the a) and b) are generated using undifferentiated C2C12, whereas c) & d) spheres C2C12D. Sphere illustrated in picture d) is not properly formed, due to the excess of cells (>1000) transferred to the 25µl drop (4x lens). Right: C2C12D spheres speeding inside 3D Collagen I scaffold. Spheres were stained with CalceinAM, Hoechst, CMRA prior to imaging (10x).*

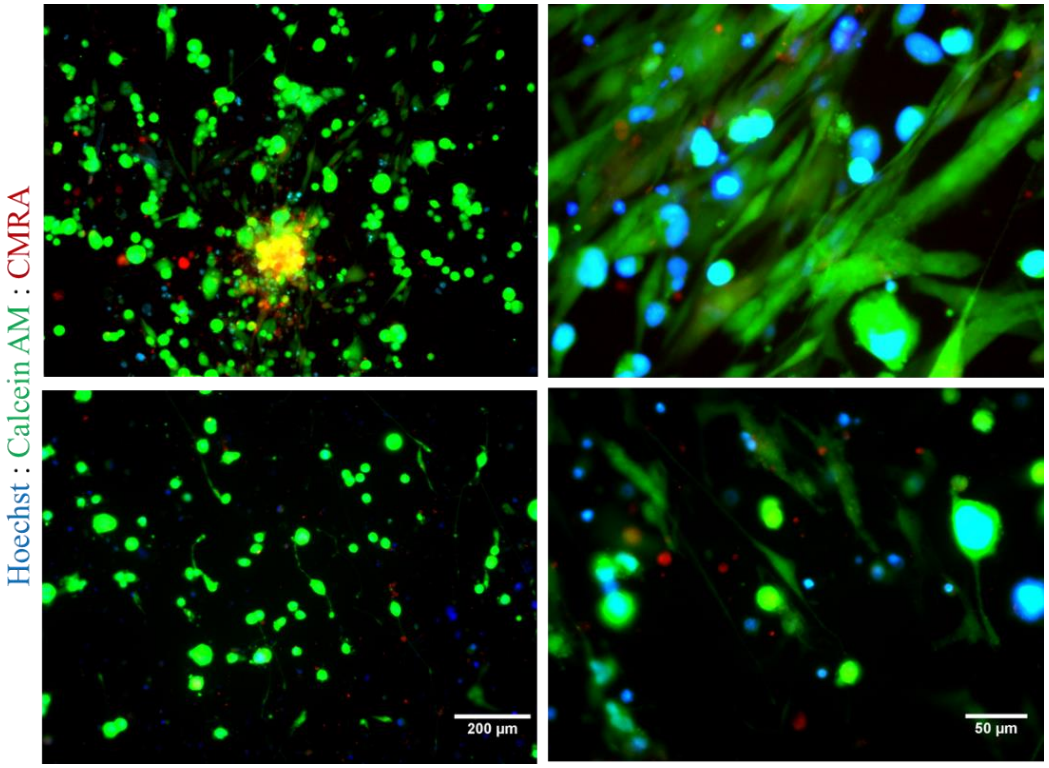

Figure 3.3.6: ***NSC3$_D$ in co-culture with even number of spheres or single cells of C2C12$_D$ inside a 3D collagen scaffold (Day-4DIV).*** *Above: Left: Single cells NSC34$_D$ + Sphere of C2C12$_D$ in 3D Collagen I scaffold. The sphere is located in the middle and surrounded by both NSC34$_D$ and C2C12$_D$ that had spread out of sphere. Right: The surrounding area. Below: Single cells NSC34$_D$ and C2C12$_D$. Cells were stained with CalceinAM, Hoechst, CMRA (C2C12 only) dyes and visualized with Zeiss Axio Inverted Microscope.*

Series of C2C12 transfections with mDsRED using different protocols and Reagents were unsuccessful (low rates in transfection <1%). The most successful transfection was with 5:1 µl:µg of DNA to Lipofectamine 2000 Reagent dilution (Figure 3.3.7.).. Rapid cell proliferation, was as well a major problem during selection. When C2C12 were too confluent, cells differentiated spontaneously. Differentiated cells could not be used in the generation of a stable cell line. Thus, further optimization was performed with cells seeded at really low density (e.g. 2.500 cells per 96-well plate) one day prior to transfection and passaged after transfection. Although the success rate was really low, attempts were made to select cells. To select the stable mDsRed transfected C2C12 cells, 1-1.25 mg/ml G418 determined by performing a kill curve against non-transfected cells (Figure 3.3.8.). However, selection failed as transfected cells died and non-transfected cell developed resistance. Neomycin was excluded as 7mg/ml were needed to kill cells in 7 days (data not shown). C2C12 lentiviral transduction with LeGO-C2-mCherry Plasmid were as well unsuccessful (data not shown).

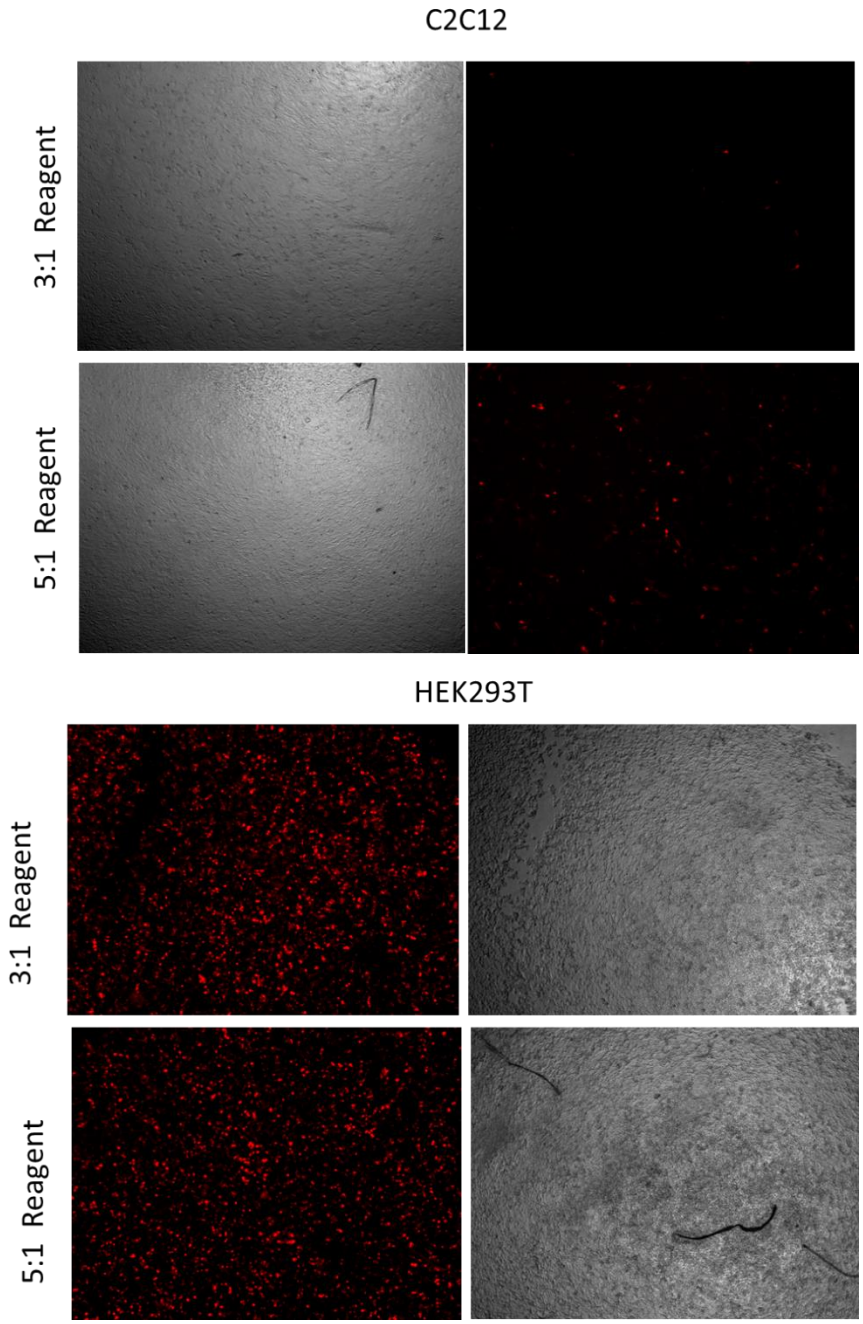

Figure 3.3.7: ***Example of standard transfection of C2C12 cells with Lipofectamine 2000 reagent.*** *3:1 and 5:1 (µl: µg) ratio of Reagent to DNA of mDsRED plasmid dilutions were used to transfect both 10.000 C2C12 AND 10.000 HEK293T cells (Control) in a 96-well plate. Dilutions were performed in Opti-MEM with no antibiotics. 24h after transfection, cells were imagined with Zeiss Axio Inverted Microscope.*

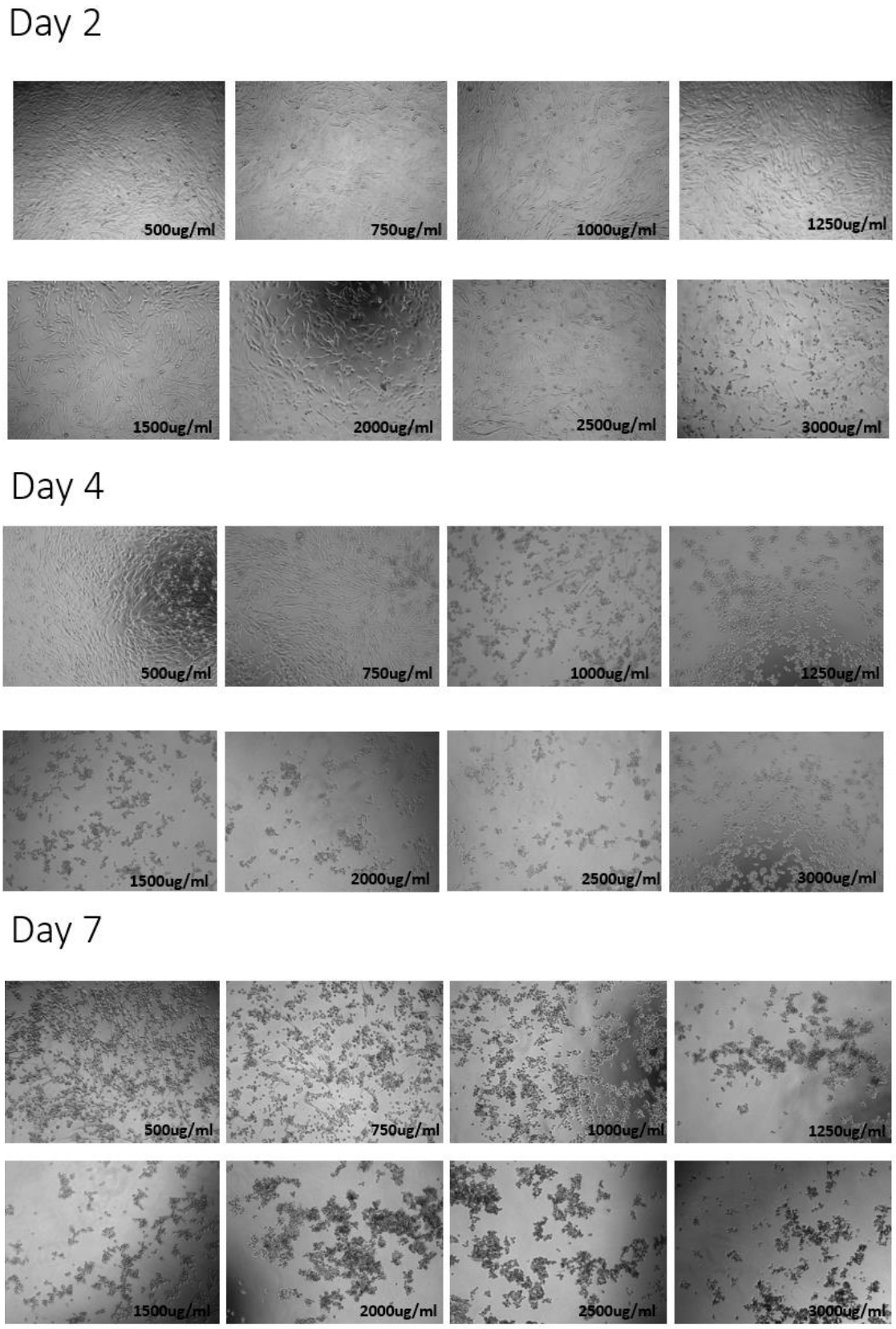

Figure 3.3.8: ***G418 kill curve of C2C12 for 7 days.*** *Cell densities displayed at 2nd, 4th and 7th day of selection. 25mg/ml of G418 were needed to kill C2C12 in 7 days.*

Chapter 4: Discussion and Conclusions

In contrast to the PC12 cell model for TrkA-related studies (Negrini S et al., 2013), generic cellular models for TrkB-related studies do not exist. In this thesis the expression of both TrkB and $p75^{NTR}$ neurotrophin receptors in the $NSC34_D$ cell line was confirmed. $NSC34_D$ cells grown in a recently-developed Matrigel Sandwich culture were responsive to neurotrophin/microneurotrophin exposure, as evaluated by observed effects pro-survival (Erk, Akt) and pro-apoptotic pathways (JNK). The activation of signaling pathways Erk1/2, JNK, AKT was investigated upon pro-NGF, NGF, BNN20 and BDNF treatment. Preliminary immunoblotting results show that $NSC34_D$ cells in Matrigel sandwich culture respond to neurotrophins. These results are consistent findings reported in the B.Sc. thesis of with I. Lapi previous, where BDNF stimulation of $NSC34_D$ reduced Erk phosphorylation, possibly due to the activation of ceramides through the $p75^{NTR}$. $p75^{NTR}$ upon stimulation is able to activate neutral and/or acidic sphingomyelinases that via removal of the sphingomyelin polar head generate ceramide (Blochl et al., 2007). Moreover, NGF stimulation of $p75^{NTR}$ was as well found to elevate intracellular ceramide, thereby deactivating Ras/ERK and PI3-K pathways (Ruvolo et al., 2003). It is worth mentioning, 2h and 4h serum starvation of cells did not completely inactivate these pathways of interest. This can be attributed to Matrigel used in 2D Sandwich culture, which it contains growth factors that could activate survival pathways or even protect cells from further stress induction. Additional studies with a comparison between complete Matrigel and growth factor-reduced Matrigel will be required in the future to resolve the question of whether the signaling events are physiologically relevant.

Based on the *in vitro* NSC34 model for ALS systemic studies recently developed in the IMBB Neural Tissue Engineering lab (Ioanna Lapi, Dr. D. Tzeranis), the response to various neurotoxic ALS-related stimuli on both NSC34(-) and NSC34($hSOD1^{G93A}$) cells was quantified. Various protocols have been applied in order to establish a pro-apoptotic stimulation for drug screening. Up until now three neurotoxic stimuli that show to have the potential to be utilized in pharmacological studies for ALS disease have been identified: a) exposure to 100 μM H_2O_2 for 1 day, b) the TNFα as well as c) Serum derivation that mimic the oxidative stress, neuroinflammation and metabolic stress found in ALS pathophysiology. Treatment with different concentrations of H_2O_2 results in dose-dependent apoptosis in both NSC34(-) and NSC34($hSOD1^{G93A}$). 100 μmM of H_2O_2 leads to ~20% cell death in $NSC34_D$(-) and ~30% cell death in $NSC34_D$ ($hSOD1^{G93A}$). This ~10% increase in cell death could be possibly attributed to mutated SOD1 of the NSC34 D ($hSOD1^{G93A}$). 100 μmM H_2O_2 was selected for further studies to evaluate the ability of various compounds or drugs to reverse adverse effects of effective stress stimuli. However, the most appropriate concentration for TNFα has not yet been found. 48h exposure to 100 ng/ml TNFα led to a 13.5% cell death response in NSC34(-) and 7% in NSC34($hSOD1^{G93A}$). 7% in NSC34($hSOD1^{G93A}$) cannot be considered as statistically significant and more experiment are needed to verify the statistical significance of this result. Consistent with literature, TNFα alone is unable to facilitate cell death alone under physiological concentration (He et al., 2002; Wen et al., 2006; D'Ambrosi et al., 2009). Wen et al., 2006, attributed this finding to limited amount of TNFR1 that immature NSC34 possess (Wen et al., 2006). Other potential stress inducers NMDA, AMPA that were used to mimic excitotoxicity did not induce apoptosis under the previously mentioned conditions. Experiments with more concentrations and time durations are needed to establish the effect of NMDA and AMPA. Glutamate may as well be included in next experiments, though it is known that NSC34 cells does not express all the glutamate receptors found in primary mouse motor neurons (Hounoum et al., 2016). Therefore, only unphysiological concentrations (10 mM) of glutamate facilitated cell death. Serum deprivation was able to induce 10% cell death per day in both NSC34(-) and NSC34($hSOD1^{G93A}$). Thus, an interesting experiment would be to treat cells with the drug Riluzole that was found to increase glucose uptake and energy production by directly activating AMPK and inducing the intracellular translocation of GLUT1 and GLUT3 glucose transporter (Daniel et al., 2013). Additionally, other cytokines IL1α and INFγ that were used to model

neuroinflammation or Pro-NGF did not facilitate cell death under the tested conditions. Higher concentration or time duration may be needed to observe an effect. It is worth mentioning that maybe the reason behind the incapability of the potential neurotoxic compounds to induce cell death was due to Matrigel. As Matrigel contains growth factors, those growth factors could possibly induce further neuroprotection.

Moreover, utilizing the controlled environment of this system we evaluated the efficacy of candidate ALS treatments (BNN20) and FDA-approved drugs (Edaravone, Riluzole) in response to a neurotoxic stimulus. Moreover, potential neuroprotective agents BDNF, CTNF, GDNF were as well investigated in reversing the H_2O_2 induced oxidative damage. Preliminary data shows that NGF did not induce apoptosis, while Edaravone in high concentration sees to affect negatively cell viability. More experiment with BDNF and BNN20 should be conducted in the future as for now, their neuroprotective effect was not able to reverse the H_2O_2-induced apoptosis. In conclusion, it important to mention that although results are preliminary, experiments show biological repeatability as similar results that we obtained through different image processing procedures. Statistical analysis of data should also take place.

Another goal of this thesis was to transfer the previous 2D NSC34 model into a 3D culture model based on Porous Collagen-I scaffolds. 3D NSC34 model would recapitulate more accurately the *in vivo* cell conditions, and hence would be more appropriate for pharmacological studies. However, when NSC34 (-) cells were seeded in Porous Collagen-I scaffolds, no cell attachment to porous scaffold was observed. Cells remained round with no axons. Multiple studies have shown that muscle cells release neurotrophins (BDNF, GDNF, CNTF, NT3, NT4/5) and growth factors (HGF, EGF, FGF) that act as trophic factors for motor neurons (Taylor et al, 2007; Madison et al., 2014) improving motor neurons morphology. When motor neuron cells were incubated with extracellular muscle cell vesicles, cells demonstrated increase in neurite outgrowth and survival (Madison et al., 2014). In our case, the incorporation of C2C12 in 3D NSC34 model was fundamental for obtaining viable motor neurons with significant number of elongated axons. The resulted co-culture was then optimized for several parameters including cell state (differentiated or undifferentiated), number, ratio and morphology (spheres or single cells). The differentiation of the C2C12 inside the device was challenging. Difficulties arise in controlling the number of rapidly proliferating cells that can cover the whole surface of the scaffold. On the other hand, the differentiation inside the 2D cultures prior to the 3D transfer, offers a more convenient and controlled way to seed C2C12 cells inside the 3D device. The question whether those cells should be transferred as spheres or as single cells remain still unknown. In order to answer it, more experiments using both spheres and single cells should be conducted. However, we speculate it depends on the need of the experiment as both morphologies have advantages and disadvantages. Spheres offer a more delicate way to transfer the cells and also work as 3D environment on their own. Using spheres is easier to distinguish different kinds of cells in co-cultures. Experimental findings imply that seeding both cell types as single cells is slightly more effective in neurite outgrowth. However, it should be mentioned that seeding 1000 cells is not equal as seeding just a sphere of 1000 cells. Based on the fact that the core is highly apoptotic and hypoxic, the equivalent number of spheres to single cells should be taken into consideration. The layers of cells observed during microscopy provide evidence that cells are not just lying on the surface but are found inside the scaffolds, while, the longevity of co-culture (up to 2 weeks) that environment created inside the scaffold favors cell survival. However, due to longevity of co-culture the fluorescent signal of the muscle cells became weaker, making cells detection and separation difficult. C2C12 was not stained properly with CMRA dye, hence, cell types could not be distinguished and no quantification could be done. An attempt to generate genetically engineered C2C12 cells, though unsuccessful, has been as well made. The need of genetically engineered C2C12 cells are essential to perform more experiment that could analyzed with appropriate use of programs that offer fully automated morphological analysis, such as Neurite Quant. More experiments in order to determine which relative cell concentration is the most favorable

for the neurite outgrowth and survival, as well as supplementation of neurotrophic factors to the culture should be performed in future.

Taking everything into account, the repeatability of the 2D experiments indicate that NSC34 cell line-based-on-system-level experimental platform can be utilized in both ALS and pharmacological TrkB-mediated signaling studies. On the other hand, genetically engineered C2C12 cells are essential for statistical analysis of the co-culture systems. 3D co-culture is a promising system that could be modified in future to incorporate Embryonic-derived motor neurons or iPSCs for the potential development of ALS-on-Chip model.

Acknowledgements

First and foremost, I want to express my deepest gratitude to my supervisor Professor A. Gravanis for giving me the opportunity to work in his lab and to Dr. D. Tzeranis for his guidance, support and especially patience. Moreover, I would like to thank the rest of my thesis committee members: Professor I. Charalampopoulos, and Professor I. Zaganas for their feedback, encouragement and insightful comments. I would especially like to thank Dr. E. Deligianni for High Content Microscopy imaging and data analysis, Dr. M. Tseliou for lentiviral production, and K. Iordanidou for collaboration on performing all 2D experiments. Last but not least, I would like to extend my appreciation to all my labmates for their knowledge, experience, and partnership.

References

1. Acsadi, G., Lee, I., Li, X., Khaidakov, M., Pecinova, A., Parker, G. C., & Hüttemann, M. (2009). Mitochondrial dysfunction in a neural cell model of spinal muscular atrophy. Journal of Neuroscience Research, 87(12), 2748–2756. https://doi.org/10.1002/jnr.22106
2. Al-Chalabi, A., Van Den Berg, L. H., & Veldink, J. (2017). Gene discovery in amyotrophic lateral sclerosis: Implications for clinical management. Nature Reviews Neurology, 13(2), 96–104. https://doi.org/10.1038/nrneurol.2016.182
3. Almokhtar, M., Wikvall, K., Ubhayasekera, S. J. K. A., Bergquist, J., & Norlin, M. (2016). Motor neuron-like NSC-34 cells as a new model for the study of vitamin D metabolism in the brain. Journal of Steroid Biochemistry and Molecular Biology, 158, 178–188. https://doi.org/10.1016/j.jsbmb.2015.12.010
4. Andersen, P. M. (2000). Genetic factors in the early diagnosis of ALS. Amyotrophic Lateral Sclerosis and Other Motor Neuron Disorders, 1(0), 31-42. doi:10.1080/14660820052415899.
5. Andersen, P., Sims, K., Xin, W., Kiely, R., Oneill, G., Ravits, J., Brown, J. R. (2003). Sixteen novel mutations in the Cu/Zn superoxide dismutase gene in amyotrophic lateral sclerosis: a decade of discoveries, defects and disputes. Amyotrophic Lateral Sclerosis and Other Motor Neuron Disorders, 4(2), 62-73. doi:10.1080/14660820301188.
6. Arnold, A., Christe, M., & Handschin, C. (2012). A Functional Motor Unit in the Culture Dish: Co-culture of Spinal Cord Explants and Muscle Cells. Journal of Visualized Experiments, (62). doi:10.3791/3616
7. Barber, S. C., & Shaw, P. J. (2010). Oxidative stress in ALS: Key role in motor neuron injury and therapeutic target. Free Radical Biology and Medicine, 48(5), 629-641. doi:10.1016/j.freeradbiomed.2009.11.018.
8. Barber, S. C., Higginbottom, A., Mead, R. J., Barber, S., & Shaw, P. J. (2009). An in vitro screening cascade to identify neuroprotective antioxidants in ALS. Free Radical Biology and Medicine, 46(8), 1127–1138. https://doi.org/10.1016/j.freeradbiomed.2009.01.019
9. Benavente, F., Pinto, C., Parada, M., Henríquez, J. P., & Osses, N. (2012). Bone morphogenetic protein 2 inhibits neurite outgrowth of motor neuron-like NSC-34 cells and up-regulates its type II receptor. Journal of Neurochemistry, 122(3), 594–604. https://doi.org/10.1111/j.1471-4159.2012.07795.x

10. Benkler, C., Ben-Zur, T., Barhum, Y., & Offen, D. (2013). Altered astrocytic response to activation in SOD1G93A mice and its implications on amyotrophic lateral sclerosis pathogenesis. Glia, 61(3), 312–326. https://doi.org/10.1002/glia.22428
11. Bensimon, G., Lacomblez, L., and Meininger, V. (1994). A controlled trial of riluzole in amyotrophic lateral sclerosis. ALS/Riluzole Study Group. N. Engl. J. Med. 330, 585–591. doi: 10.1056/NEJM199403033300901
12. Bhakar, A. L., Howell, J. L., Paul, C. E., Salehi, A. H., Becker, E. B., Said, F., et al. (2003). Apoptosis induced by p75NTR overexpression requires Jun kinase- dependent phosphorylation ofBad. J. Neurosci. 23, 11373–11381.
13. Blasco, H., Mavel, S., Corcia, P., & Gordon, P. (2014). The Glutamate Hypothesis in ALS: Pathophysiology and Drug Development. Current Medicinal Chemistry, 21(31), 3551-3575. doi:10.2174/0929867321666140916120118.
14. Blizzard, C. A., Southam, K. A., Dawkins, E., Lewis, K. E., King, A. E., Clark, J. A., & Dickson, T. C. (2015). Identifying the primary site of pathogenesis in amyotrophic lateral sclerosis - vulnerability of lower motor neurons to proximal excitotoxicity. Disease Models & Mechanisms, 8(3), 215-224. doi:10.1242/dmm.018606
15. Blöchl, A., and R. Blöchl. “A cell-Biological model of p75NTR signaling.” Journal of Neurochemistry, vol. 102, no. 2, 2007, pp. 289–305., doi:10.1111/j.1471-4159.2007.04496.x.
16. Boer, Albertus G De, and Pieter J Gaillard. “Strategies to Improve Drug Delivery Across the Blood-Brain Barrier.” Clinical Pharmacokinetics, vol. 46, no. 7, 2007, pp. 553–576., doi:10.2165/00003088-200746070-00002.
17. Boillée, S., Velde, C. V., & Cleveland, D. (2006). ALS: A Disease of Motor Neurons and Their Nonneuronal Neighbors. Neuron, 52(1), 39-59. doi:10.1016/j.neuron.2006.09.018
18. Bonafede, R., Scambi, I., Peroni, D., Potrich, V., Boschi, F., Benati, D., … Mariotti, R. (2016). Exosome derived from murine adipose-derived stromal cells: Neuroprotective effect on in vitro model of amyotrophic lateral sclerosis. Experimental Cell Research, 340(1), 150–158. https://doi.org/10.1016/j.yexcr.2015.12.009
19. Bosch, L. V., Vandenberghe, W., Klaassen, H., Houtte, E. V., & Robberecht, W. (2000). Ca2 -permeable AMPA receptors and selective vulnerability of motor neurons. Journal of the Neurological Sciences, 180(1-2), 29-34. doi:10.1016/s0022-510x(00)00414-7
20. Bothwell, Mark. “Recent advances in understanding neurotrophin signaling.” F1000Research, vol. 5, 2016, p. 1885., doi:10.12688/f1000research.8434.1.
21. Botsakis, K., Mourtzi, T., Panagiotakopoulou, V., Vreka, M., Stathopoulos, G. T., Pediaditakis, I., . . . Angelatou, F. (2017). BNN-20, a synthetic microneurotrophin, strongly protects dopaminergic neurons in the “weaver” mouse, a genetic model of dopamine-denervation, acting through the TrkB neurotrophin receptor. Neuropharmacology, 121, 140-157. doi:10.1016/j.neuropharm.2017.04.043
22. Brites, D., and Fernandes, A. (2015). Neuroinflammation and depression: microglia activation, extracellular microvesicles and microRNA dysregulation. Front. Cell. Neurosci. 9:476. doi: 10.3389/fncel.2015.00476
23. Brown, R. H., & Al-Chalabi, A. (2017). Amyotrophic Lateral Sclerosis. New England Journal of Medicine, 377(2), 162–172. https://doi.org/10.1056/NEJMra160347
24. Cashman, Neil R., et al. “Neuroblastoma × spinal cord (NSC) hybrid cell lines resemble developing motor neurons.” Developmental Dynamics, vol. 194, no. 3, 1992, pp. 209–221., doi:10.1002/aja.1001940306.
25. Chao, M. V. (2003). Neurotrophins and their receptors: A convergence point for many signalling pathways. Nat. Rev. Neurosci. 4, 299–309. doi: 10.1038/nrn1078
26. Charalampopoulos I, Remboutsika E, Margioris AN, Gravanis A. Neurosteroids as modulators of neurogenesis and neuronal survival. Trends in endocrinology and metabolism: TEM. 2008;19(8):300-307.
27. Charcot J-M, Joffroy A. Deus cas d’atrophie musculaire progressive avec lesions de la substance grise et des faisceaux antéro-latérale. Arch Physiol. 1869;2:354–67. 744–60.
28. Choi, Y. J., Park, J., & Lee, S. (2013). Size-controllable networked neurospheres as a 3D neuronal tissue model for Alzheimers disease studies. Biomaterials, 34(12), 2938-2946. doi:10.1016/j.biomaterials.2013.01.038
29. Clerc, P., Lipnick, S., & Willett, C. (2016). A look into the future of ALS research. Drug Discovery Today, 21(6), 939-949. doi:10.1016/j.drudis.2016.02.002

30. Cleveland, D. W., & Rothstein, J. D. (2001). From charcot to lou gehrig: Deciphering selective motor neuron death in als. Nature Reviews Neuroscience, 2(11), 806-819. doi:10.1038/35097565
31. Conejo, R., & Lorenzo, M. (2001). Insulin signaling leading to proliferation, survival, and membrane ruffling in C2C12 myoblasts. Journal of Cellular Physiology, 187(1), 96-108. doi:10.1002/1097-4652(2001)9999:9999<::aid-jcp1058>3.0.co;2-v
32. Conejo, R., Alvaro, C. D., Benito, M., Cuadrado, A., & Lorenzo, M. (2002). Insulin restores differentiation of Ras-transformed C2C12 myoblasts by inducing NF-κB through an AKT/P70S6K/p38-MAPK pathway. Oncogene, 21(23), 3739-3753. doi:10.1038/sj.onc.1205469
33. Conejo, R., Valverde, A. M., Benito, M., & Lorenzo, M. (2000). Insulin produces myogenesis in C2C12 myoblasts by induction of NF-kB and downregulation of AP-1 activities. Journal of Cellular Physiology, 186(1), 82-94. doi:10.1002/1097-4652(200101)186:1<82::aid-jcp1001>3.0.co;2-r
34. Cookson, M. R., Ince, P. G., & Shaw, P. J. (1998). Peroxynitrite and hydrogen peroxide induced cell death in the NSC34 neuroblastoma x spinal cord cell line: role of poly (ADP-ribose) polymerase. Journal of Neurochemistry, 70(2), 501–508.
35. Corcia, P., Tauber, C., Vercoullie, J., Arlicot, N., Prunier, C., Praline, J., . . . Ribeiro, M. (2012). Molecular Imaging of Microglial Activation in Amyotrophic Lateral Sclerosis. PLoS ONE, 7(12). doi:10.1371/journal.pone.0052941
36. Correia, A. S., Patel, P., Dutta, K., & Julien, J. (2015). Inflammation Induces TDP-43 Mislocalization and Aggregation. Plos One, 10(10). doi:10.1371/journal.pone.0140248.
37. Custer, Sara K., et al. “Altered MRNA Splicing in SMN-Depleted Motor Neuron-Like Cells.” Plos One, vol. 11, no. 10, 2016, doi:10.1371/journal.pone.0163954.
38. Cvetkovic, C., Rich, M. H., Raman, R., Kong, H., & Bashir, R. (2017). A 3D-printed platform for modular neuromuscular motor units. Microsystems & Nanoengineering, 3, 17015. doi:10.1038/micronano.2017.15
39. D’Ambrosi, N., Finocchi, P., Apolloni, S., Cozzolino, M., Ferri, A., Padovano, V., … Volonte, C. (2009). The Proinflammatory Action of Microglial P2 Receptors Is Enhanced in SOD1 Models for Amyotrophic Lateral Sclerosis. The Journal of Immunology, 183(7), 4648–4656. https://doi.org/10.4049/jimmunol.0901212
40. D’Amico, E., Factor-Litvak, P., Santella, R. M., & Mitsumoto, H. (2013). Clinical perspective on oxidative stress in sporadic amyotrophic lateral sclerosis. Free Radical Biology and Medicine, 65(7628), 509–527. https://doi.org/10.1016/j.freeradbiomed.2013.06.029
41. Daniel, B., Green, O., Viskind, O., & Gruzman, A. (2013). Riluzole increases the rate of glucose transport in L6 myotubes and NSC-34 motor neuron-like cells via AMPK pathway activation. Amyotrophic Lateral Sclerosis and Frontotemporal Degeneration, 14(5–6), 434–443. https://doi.org/10.3109/21678421.2013.808226
42. Daud, M. F., Pawar, K. C., Claeyssens, F., Ryan, A. J., & Haycock, J. W. (2012). An aligned 3D neuronal-glial co-culture model for peripheral nerve studies. Biomaterials, 33(25), 5901-5913. doi:10.1016/j.biomaterials.2012.05.008
43. DeFreitas, M. F., McQuillen, P. S., and Shatz, C. J. (2001). A novel p75NTR signaling pathway promotes survival, not death, ofimmunopurified neocortical subplate neurons. J. Neurosci. 21, 5121–5129.
44. Deinhardt, Katrin, and Giampietro Schiavo. “Endocytosis and retrograde axonal traffic in motor neurons.” Biochemical Society Symposium, vol. 72, 2005, pp. 139–150., doi:10.1042/bss0720139.
45. Dejesus-Hernandez, M., Mackenzie, I., Boeve, B., Boxer, A., Baker, M., Rutherford, N., Nicholson, A. M., Finch, N. A., Flynn, H., Adamson, J., Kouri, N., Wojtas, A., Sengdy, P., Hsiung, G. Y., Karydas, A., Seeley, W. W., Josephs, K. A., Coppola, G., Geschwind, D. H., Wszolek, Z. K., Feldman, H., Knopman, D. S., Petersen, R. C., Miller, B. L., Dickson, D. W., Boylan, K. B., Graff-Radford, N. R., Rademakers, R. (2011). Expanded GGGGCC Hexanucleotide Repeat in Noncoding Region of C9ORF72 Causes Chromosome 9p-Linked FTD and ALS. Neuron, 72(2), 245-256. doi:10.1016/j.neuron.2011.09.011
46. Demestre, M., Orth, M., Föhr, K., Achberger, K., Ludolph, A., Liebau, S., & Boeckers, T. (2015). Formation and characterisation of neuromuscular junctions between hiPSC derived motoneurons and myotubes. Stem Cell Research, 15(2), 328-336. doi:10.1016/j.scr.2015.07.005
47. Deng, H., Chen, W., Hong, S., Boycott, K. M., Gorrie, G. H., Siddique, N., Siddique, T., et al. (2011). Mutations in UBQLN2 cause dominant X-linked juvenile and adult-onset ALS and ALS/dementia. Nature, 477(7363), 211-215. doi:10.1038/nature10353

48. Dimos, J. T., Rodolfa, K. T., Niakan, K. K., Weisenthal, L. M., Mitsumoto, H., Chung, W., Eggan, K., et al. (2008). Induced Pluripotent Stem Cells Generated from Patients with ALS Can Be Differentiated into Motor Neurons. Science, 321(5893), 1218-1221. doi:10.1126/science.1158799
49. Doble, A. (1996). The pharmacology and mechanism of action of riluzole. Neurology 47, S233–S241
50. Durham H. D., Dabrouge S., and Cashman N. R. (1993) Evaluation of the spinal cord neuron X neuroblastoma hybrid cell line NSC34 as a model for neurotoxicity testing. Neurotoxicology 14, 387—396
51. Edmondson, R., Broglie, J. J., Adcock, A. F., & Yang, L. (2014). Three-Dimensional Cell Culture Systems and Their Applications in Drug Discovery and Cell-Based Biosensors. ASSAY and Drug Development Technologies, 12(4), 207-218. doi:10.1089/adt.2014.573
52. Eggett, C. J., Crosier, S., Manning, P., Cookson, M. R., Menzies, F. M., Mcneil, C. J., & Shaw, P. J. (2008). Development and Characterisation of a Glutamate-Sensitive Motor Neurone Cell Line. Journal of Neurochemistry, 74(5), 1895-1902. doi:10.1046/j.1471-4159.2000.0741895.x
53. Ekestern, E. (2004). Neurotrophic Factors and Amyotrophic Lateral Sclerosis. Neurodegenerative Diseases, 1(2-3), 88-100. doi:10.1159/000080049.
54. Fang, Y., & Eglen, R. M. (2017). Three-Dimensional Cell Cultures in Drug Discovery and Development. SLAS DISCOVERY: Advancing Life Sciences R&D, 22(5), 456-472. doi:10.1177/1087057117696795
55. Fecto, F. (2011). SQSTM1 Mutations in Familial and Sporadic Amyotrophic Lateral Sclerosis. Archives of Neurology, 68(11), 1440. doi:10.1001/archneurol.2011.250
56. Ferraiuolo, Laura, et al. “Molecular pathways of motor neuron injury in amyotrophic lateral sclerosis.” Nature Reviews Neurology, vol. 7, no. 11, 2011, pp. 616–630., doi:10.1038/nrneurol.2011.152
57. Ferraiuolo, Laura. “The non-Cell-Autonomous component of ALS: newin vitromodels and future challenges: Figure 1.” Biochemical Society Transactions, vol. 42, no. 5, Jan. 2014, pp. 1270–1274., doi:10.1042/bst20140168.
58. Gao, Y., Broussard, J., Haque, A., Revzin, A., & Lin, T. (2016). Functional imaging of neuron–astrocyte interactions in a compartmentalized microfluidic device. Microsystems & Nanoengineering, 2(1). doi:10.1038/micronano.2015.45
59. Gingras, Marie, et al. “Optimized protocols for isolation of primary motor neurons, astrocytes and microglia from embryonic mouse spinal cord.” Journal of Neuroscience Methods, vol. 163, no. 1, 2007, pp. 111–118., doi:10.1016/j.jneumeth.2007.02.024.
60. Glajch, K. E., Ferraiuolo, L., Mueller, K. A., Stopford, M. J., Prabhkar, V., Gravanis, A., … Sadri-Vakili, G. (2016). MicroNeurotrophins improve survival in motor neuron-astrocyte co-cultures but do not improve disease phenotypes in a mutant SOD1 mouse model of amyotrophic lateral sclerosis. PLoS ONE, 11(10), 1–24. https://doi.org/10.1371/journal.pone.0164103
61. Gordon, P. H. (2013). Amyotrophic Lateral: An update for 2013 Clinical Features, Pathophysiology, Management and Therapeutic Trials. Aging and Disease, 4(5), 295–310. https://doi.org/10.14336/AD.2013.0400295
62. Hallbook F. Evolution of the vertebrate neurotrophin and Trk receptor gene families. Current opinion in neurobiology. 1999;9(5):616-621.
63. Happe, C. L., Tenerelli, K. P., Gromova, A. K., Kolb, F., & Engler, A. J. (2017). Mechanically patterned neuromuscular junctions-in-a-dish have improved functional maturation. Molecular Biology of the Cell, 28(14), 1950-1958. doi:10.1091/mbc.e17-01-0046
64. Hardiman, O., Al-Chalabi, A., Chio, A., Corr, E. M., Logroscino, G., Robberecht, W., Berg, L. H. (2017). Amyotrophic lateral sclerosis. Nature Reviews Disease Primers, 3, 17085. doi:10.1038/nrdp.2017.85
65. Haycock, J. W. (2010). 3D Cell Culture: A Review of Current Approaches and Techniques. Methods in Molecular Biology 3D Cell Culture, 1-15. doi:10.1007/978-1-60761-984-0_1
66. He, B.P., Wen, W., Strong, M.J., (2002). Activated microglia (BV-2) facilitation of TNF-alpha-mediated motor neuron death in vitro. J. Neuroimmunol. 128, 31–38.
67. Hemendinger, R. A., Armstrong, E. J., & Brooks, B. R. (2011). Methyl Vitamin B12 but not methylfolate rescues a motor neuron-like cell line from homocysteine-mediated cell death. Toxicology and Applied Pharmacology, 251(3), 217–225. https://doi.org/10.1016/j.taap.2011.01.003
68. Hemendinger, R. A., Armstrong, E. J., Radio, N., & Brooks, B. R. (2012). Neurotoxic injury pathways in differentiated mouse motor neuron-neuroblastoma hybrid (NSC-34D) cells in vitro-Limited effect of riluzole

on thapsigargin, but not staurosporine, hydrogen peroxide and homocysteine neurotoxicity. Toxicology and Applied Pharmacology, 258(2), 208–215. https://doi.org/10.1016/j.taap.2011.10.022
69. Higgins, C. M. J., Jung, C., & Xu, Z. (2003). ALS-associated mutant SODIG93A causes mitochondrial vacuolation by expansion of the intermembrane space by involvement of SODI aggregation and peroxisomes. BMC Neuroscience, 4, 1–14. https://doi.org/10.1186/1471-2202-4-16
70. Hounoum, Blandine Madji, et al. "NSC-34 Motor Neuron-Like Cells Are Unsuitable as Experimental Model for Glutamate-Mediated Excitotoxicity." Frontiers in Cellular Neuroscience, vol. 10, Sept. 2016, doi:10.3389/fncel.2016.00118.
71. Hsu, Y., Chen, C., Wu, S., Jong, Y., & Lo, Y. (2012). Berberine activates Nrf2 nuclear translocation and protects against oxidative damage via a phosphatidylinositol 3-kinase/Akt-dependent mechanism in NSC34 motor neuron-like cells. European Journal of Pharmaceutical Sciences, 46(5), 415-425. doi:10.1016/j.ejps.2012.03.004
72. Hughes, Chris S., et al. "Matrigel: A complex protein mixture required for optimal growth of cell culture." Proteomics, vol. 10, no. 9, 2010, pp. 1886–1890., doi:10.1002/pmic.200900758.
73. Huh, Dongeun, et al. "From 3D cell culture to organs-on-Chips." Trends in Cell Biology, vol. 21, no. 12, 2011, pp. 745–754. doi:10.1016/j.tcb.2011.09.005.
74. Hunter, D., Cashman, N., Morris-Valero, R., Bulock, J., Adams, S., & Sanes, J. (1991). An LRE (leucine-arginine-glutamate)-dependent mechanism for adhesion of neurons to S-laminin. The Journal of Neuroscience, 11(12), 3960-3971. doi:10.1523/jneurosci.11-12-03960.1991
75. Ince, P. G., Clark, B., Holton, J., Revesz, T. & Wharton, S. B. in Greenfield's Neuropathology (eds Love, S. et al.) 947–971 (Hodder Arnold, London, 2008).
76. Jhamandas K. H., Boegman R. J., Beninger R. J., Miranda A. F. and Lipic K. A. (2000) Excitotoxicity ofquinolinic acid: modulation by endogenous antagonists. Neurotox. Res. 2, 139–155
77. Jiang, X. (n.d.). Muscle induces neuronal expression of acetylcholinesterase in neuron-muscle co-culture: transcription regulation mediated by cAMP-dependent signaling. doi:10.14711/thesis-b802015
78. Johann S., Dahm M., Kipp M., Zahn U., Beyer C. (2011). Regulation of choline acetyltransferase expression by 17 β-oestradiol in NSC-34 cells and in the spinal cord. J. Neuroendocrinol. 23, 839–848. 10.1111/j.1365-2826.2011.02192.x
79. Johnson, G., & Moore, S. W. (2013). The Leu-Arg-Glu (LRE) adhesion motif in proteins of the neuromuscular junction with special reference to proteins of the carboxylesterase/cholinesterase family. Comparative Biochemistry and Physiology Part D: Genomics and Proteomics, 8(3), 231-243. doi:10.1016/j.cbd.2013.06.001
80. Johnson, J. O., Mandrioli, J., Benatar, M., Abramzon, Y., Deerlin, V. M., Trojanowski, J. Q., Traynor, B. J., et al. (2010). Exome Sequencing Reveals VCP Mutations as a Cause of Familial ALS. Neuron, 68(5), 857-864. doi:10.1016/j.neuron.2010.11.036
81. Johnson, J. O., Pioro, E. P., Boehringer, A., Chia, R., Feit, H., Renton, A. E., Traynor, B. J., et al. (2014). Mutations in the Matrin 3 gene cause familial amyotrophic lateral sclerosis. Nature Neuroscience, 17(5), 664-666. doi:10.1038/nn.3688
82. Kabashi, E., Valdmanis, P. N., Dion, P., Spiegelman, D., Mcconkey, B. J., Velde, C. V., Rouleau, G. A. (2008). TARDBP mutations in individuals with sporadic and familial amyotrophic lateral sclerosis. Nature Genetics, 40(5), 572-574. doi:10.1038/ng.132
83. Kalisch B. E., Jhamandas K., Boegman R. J. and Beninger R. J. (1994) Picolinic acid protects against quinolinic acid-induced depletion of NADPH diaphorase containing neurons in the rat striatum. Brain Res. 668, 1–8
84. Kanjilal, B., Keyser, B. M., Andres, D. K., Nealley, E., Benton, B., Melber, A. A., Ray, R. (2014). Differentiated NSC-34 cells as an in vitro cell model for VX. Toxicology Mechanisms and Methods, 24(7), 488–494. https://doi.org/10.3109/15376516.2014.943442
85. Keilhoff, G., Lucas, B., Fansa, H., & Fansa, H. (2016). Selected gene profiles of stressed NSC-34 cells and rat spinal cord following peripheral nerve reconstruction and minocycline treatment. Experimental and Therapeutic Medicine, 11(5), 1685–1699. https://doi.org/10.3892/etm.2016.3130

86. Keilhoff, G., Lucas, B., Pinkernelle, J., Steiner, M., & Fansa, H. (2014). Effects of cerebrolysin on motor-neuron-like NSC-34 cells. Experimental Cell Research, 327(2), 234–255. https://doi.org/10.1016/j.yexcr.2014.06.020
87. Kim, H. J., Kim, N. C., Wang, Y., Scarborough, E. A., Moore, J., Diaz, Z., . . . Taylor, J. P. (2013). Mutations in prion-like domains in hnRNPA2B1 and hnRNPA1 cause multisystem proteinopathy and ALS. Nature, 495(7442), 467-473. doi:10.1038/nature11922
88. Kim, Y. H., Choi, S. H., Davanzo, C., Hebisch, M., Sliwinski, C., Bylykbashi, E., Kim, D. Y., et al. (2015). A 3D human neural cell culture system for modeling Alzheimers disease. Nature Protocols, 10(7), 985-1006. doi:10.1038/nprot.2015.065
89. Kipnis, J., Cohen, H., Cardon, M., Ziv, Y., & Schwartz, M. (2004). T cell deficiency leads to cognitive dysfunction: Implications for therapeutic vaccination for schizophrenia and other psychiatric conditions. Proceedings of the National Academy of Sciences, 101(21), 8180-8185. doi:10.1073/pnas.0402268101.
90. Kirby, J., Halligan, E., Baptista, M. J., Allen, S., Heath, P. R., Holden, H., Shaw, P. J. (2005). Mutant SOD1 alters the motor neuronal transcriptome: implications for familial ALS. Brain, 128(7), 1686-1706. doi:10.1093/brain/awh503.
91. Kunze, A., Lengacher, S., Dirren, E., Aebischer, P., Magistretti, P. J., & Renaud, P. (2013). Astrocyte-neuron co-culture on microchips based on the model of SOD mutation to mimic ALS. Integrative Biology (United Kingdom), 5(7), 964–975. https://doi.org/10.1039/c3ib40022k
92. Kwiatkowski, T. J., Bosco, D. A., Leclerc, A. L., Tamrazian, E., Vanderburg, C. R., Russ, C., Davis, A., Gilchrist, J., Kasarskis, E. J., Munsat, T., Valdmanis, P., Rouleau, G. A., Hosler, B. A., Cortelli, P., de Jong, P. J., Yoshinaga, Y., Haines, J. L., Pericak-Vance, M. A., Yan, J., Ticozzi, N., Siddique, T., McKenna-Yasek, D., Sapp, P. C., Horvitz, H. R., Landers J. E., Brown, R. H. (2009). Mutations in the FUS/TLS Gene on Chromosome 16 Cause Familial Amyotrophic Lateral Sclerosis. Science, 323(5918), 1205-1208. doi:10.1126/science.1166066
93. Laib, A. M., Bartol, A., Alajati, A., Korff, T., Weber, H., & Augustin, H. G. (2009). Spheroid-based human endothelial cell microvessel formation in vivo. Nature Protocols, 4(8), 1202-1215. doi:10.1038/nprot.2009.96
94. Lazaridis, I., Charalampopoulos, I., Alexaki, V. I., Avlonitis, N., Pediaditakis, I., Efstathopoulos, P., et al. (2011). Neurosteroid dehydroepiandrosterone interacts with nerve growth factor (NGF) receptors, preventing neuronal apoptosis. PLoS Biol. 9:e1001051. doi: 10.1371/journal.pbio.1001051
95. Lee, S., & Huang, E. J. (2017). Modeling ALS and FTD with iPSC-derived neurons. Brain Research, 1656, 88–97. https://doi.org/10.1016/j.brainres.2015.10.003
96. Li, L., Lu, J., Tay, S. S. W., Moochhala, S. M., & He, B. P. (2007). The function of microglia, either neuroprotection or neurotoxicity, is determined by the equilibrium among factors released from activated microglia in vitro. Brain Research, 1159(1), 8–17. https://doi.org/10.1016/j.brainres.2007.04.066
97. Liao, B., Zhao, W., Beers, D. R., Henkel, J. S., & Appel, S. H. (2012). Transformation from a neuroprotective to a neurotoxic microglial phenotype in a mouse model of ALS. Experimental Neurology, 237(1), 147-152. doi:10.1016/j.expneurol.2012.06.011
98. Liu, Z., Zhou, T., Ziegler, A. C., Dimitrion, P., & Zuo, L. (2017). Oxidative Stress in Neurodegenerative Diseases: From Molecular Mechanisms to Clinical Applications. Oxidative Medicine and Cellular Longevity, 2017(Figure 1). https://doi.org/10.1155/2017/2525967
99. Lodge, D. (2009). The history of the pharmacology and cloning of ionotropic glutamate receptors and the development of idiosyncratic nomenclature. Neuropharmacology, 56(1), 6-21. doi:10.1016/j.neuropharm.2008.08.006
100. Lu, J., Duan, W., Guo, Y., Jiang, H., Li, Z., Huang, J., Li, C. (2012). Mitochondrial dysfunction in human TDP-43 transfected NSC34 cell lines and the protective effect of dimethoxy curcumin. Brain Research Bulletin, 89(5-6), 185-190. doi:10.1016/j.brainresbull.2012.09.005
101. MacPherson P. A., Jones S., Pawson P. A., Marshall K. C., McBurney M. W. (1997). P19 cells differentiate into glutamatergic and glutamate-responsive neurons in vitro. Neuroscience 80, 487–499. 10.1016/s0306-4522(97)00102-4

102. Madison, R. D., Mcgee, C., Rawson, R., & Robinson, G. A. (2014). Extracellular vesicles from a muscle cell line (C2C12) enhance cell survival and neurite outgrowth of a motor neuron cell line (NSC-34). Journal of Extracellular Vesicles, 3(1), 22865. doi:10.3402/jev.v3.22865
103. Magrané, J., Cortez, C., Gan, W., & Manfredi, G. (2013). Abnormal mitochondrial transport and morphology are common pathological denominators in SOD1 and TDP43 ALS mouse models. Human Molecular Genetics, 23(6), 1413-1424. doi:10.1093/hmg/ddt528
104. Maier, Oliver, et al. "Differentiated NSC-34 motoneuron-like cells as experimental model for cholinergic neurodegeneration." Neurochemistry International, vol. 62, no. 8, 2013, pp. 1029–1038., doi:10.1016/j.neuint.2013.03.008.
105. Maruyama, H., Morino, H., Ito, H., Izumi, Y., Kato, H., Watanabe, Y., Kawakami, H., et al. (2010). Mutations of optineurin in amyotrophic lateral sclerosis. Nature, 465(7295), 223-226. doi:10.1038/nature08971
106. Matsuda, T. (1999). STAT3 activation is sufficient to maintain an undifferentiated state of mouse embryonic stem cells. The EMBO Journal, 18(15), 4261-4269. doi:10.1093/emboj/18.15.4261
107. Matsumoto, A., Okada, Y., Nakamichi, M., Nakamura, M., Toyama, Y., Sobue, G., Okano, H. (2006). Disease progression of human SOD1 (G93A) transgenic ALS model rats. Journal of Neuroscience Research, 83(1), 119-133. doi:10.1002/jnr.20708.
108. Matsumoto, A., Yoshino, H., Yuki, N., Hara, Y., Cashman, N. R., Handa, S., & Miyatake, T. (1995). Erratum to "Ganglioside characterization of a cell line displaying motor neuron-like phenotype: GM2 as a possible major ganglioside in motor neurons". Journal of the Neurological Sciences, 134(1-2), 219-220. doi:10.1016/0022-510x(95)00267-x
109. Matusica D, Fenech MP, Rogers ML, Rush RA. (2008). Characterization and use of the NSC-34 cell line for study of neurotrophin receptor trafficking. J Neurosci Res 86:553–65.
110. McDonough JH, Shih TM. (1997). Neuropharmacological mechanisms of nerve agent-induced seizure and neuropathology. Neurosci Biobehav Rev 21:559–79
111. Mcgonigle, P., & Ruggeri, B. (2014). Animal models of human disease: Challenges in enabling translation. Biochemical Pharmacology, 87(1), 162-171. doi:10.1016/j.bcp.2013.08.006
112. Menzies, F. M. (2002). Mitochondrial dysfunction in a cell culture model of familial amyotrophic lateral sclerosis. Brain, 125(7), 1522-1533. doi:10.1093/brain/awf167
113. Mishra, P. S., Dhull, D. K., Nalini, A., Vijayalakshmi, K., Sathyaprabha, T. N., Alladi, P. A., & Raju, T. R. (2016). Astroglia acquires a toxic neuroinflammatory role in response to the cerebrospinal fluid from amyotrophic lateral sclerosis patients. Journal of Neuroinflammation, 13(1), 1–14. https://doi.org/10.1186/s12974-016-0698-0
114. Mitsumoto, Hiroshi, et al. "The effects of ciliary neurotrophic factor on motor dysfunction in wobbler mouse motor neuron disease." Annals of Neurology, vol. 36, no. 2, 1994, pp. 142–148., doi:10.1002/ana.410360205.
115. Moisse, K., & Strong, M. J. (2006). Innate immunity in amyotrophic lateral sclerosis. Biochimica et Biophysica Acta (BBA) - Molecular Basis of Disease, 1762(11-12), 1083-1093. doi:10.1016/j.bbadis.2006.03.001.
116. Moreno-Martet, M., Mestre, L., Loría, F., Guaza, C., Fernández-Ruiz, J., & De Lago, E. (2012). Identification of receptors and enzymes for endocannabinoids in NSC-34 cells: Relevance for in vitro studies with cannabinoids in motor neuron diseases. Neuroscience Letters, 508(2), 67–72. https://doi.org/10.1016/j.neulet.2011.12.020.
117. Moscoso, L. M., & Sanes, J. R. (1995). Expression of four immunoglobulin superfamily adhesion molecules (L1, Nr-CAM/Bravo, neurofascin/ABGP, and N-CAM)in the developing mouse spinal cord. The Journal of Comparative Neurology, 352(3), 321-334. doi:10.1002/cne.903520302
118. Musarò, Antonio. "Understanding ALS: new therapeutic approaches." FEBS Journal, vol. 280, no. 17, Mar. 2013, pp. 4315–4322., doi:10.1111/febs.12087. Richardson, K., Allen, S. P., Mortiboys, H., Grierson, A. J., Wharton, S. B., Ince, P. G., . . . Heath, P. R. (2013). The Effect of SOD1 Mutation on Cellular Bioenergetic Profile and Viability in Response to Oxidative Stress and Influence of Mutation-Type. PLoS ONE, 8(6). doi:10.1371/journal.pone.0068256.

119. Negrini, S., et al. “NGF signaling in PC12 cells: the cooperation of p75NTR with TrkA is needed for the activation of both mTORC2 and the PI3K signalling cascade.” Biology Open, vol. 2, no. 8, 2013, pp. 855–866., doi:10.1242/bio.20135116.
120. Nykjaer, A., Lee, R., Teng, K. K., Jansen, P., Madsen, P., Nielsen, M. S., . . . Petersen, C. M. (2004). Sortilin is essential for proNGF-induced neuronal cell death. Nature, 427(6977), 843-848. doi:10.1038/nature02319
121. Oosthuyse, B., Moons, L., Storkebaum, E., Beck, H., Nuyens, D., Brusselmans, K., Van Dorpe, J., Hellings, P., Gorselink, M., Heymans, S., et al. (2001). Deletion of the hypoxia-response element in the vascular endothelial growth factor promoter causes motor neuron degeneration. Nat. Genet. 28(2), 131–138. doi:10.1038/88842
122. Orrell, Richard W., et al. “A systematic review of antioxidant treatment for amyotrophic lateral sclerosis/Motor neuron disease.” Amyotrophic Lateral Sclerosis, vol. 9, no. 4, 2008, pp. 195–211., doi:10.1080/17482960801900032.
123. Osaki, T., Uzel, S. G. M., & Kamm, R. D. (2018). Microphysiological 3D model of amyotrophic lateral sclerosis (ALS) from human iPS-derived muscle cells and optogenetic motor neurons. Science Advances, 4(10), eaat5847. https://doi.org/10.1126/sciadv.aat5847
124. Pandya, R. S., Zhu, H., Li, W., Bowser, R., Friedland, R. M., & Wang, X. (2013). Therapeutic neuroprotective agents for amyotrophic lateral sclerosis. Cell Mol Life Science, 70(24), 4729–4745. https://doi.org/10.1007/s00018-013-1415-0.Therapeutic
125. Pasinelli, P., & Brown, R. H. (2006). Molecular biology of amyotrophic lateral sclerosis: insights from genetics. Nature Reviews Neuroscience, 7(9), 710-723. doi:10.1038/nrn1971.
126. Pediaditakis, I., Efstathopoulos, P., Prousis, K. C., Zervou, M., Arevalo, J. C., Alexaki, V. I., et al. (2016). Selective and differential interactions of BNN27, a novel C17-spiroepoxy steroid derivative, with TrkA receptors, regulating neuronal survival and differentiation. Neuropharmacology 111, 266–282. doi: 10.1016/j.neuropharm.2016.09.007
127. Pediaditakis, I., Iliopoulos, I., Theologidis, I., Delivanoglou, N., Margioris, A. N., Charalampopoulos, I., et al. (2015). Dehydroepiandrosterone: an ancestral ligand of neurotrophin receptors. Endocrinology 156, 16–23. doi: 10.1210/en. 2014-1596
128. Pediaditakis, Iosif, et al. “BNN27, a 17-Spiroepoxy Steroid Derivative, Interacts With and Activates p75 Neurotrophin Receptor, Rescuing Cerebellar Granule Neurons from Apoptosis.” Frontiers in Pharmacology, vol. 7, 2016, doi:10.3389/fphar.2016.00512.
129. Perkins M. N. and Stone T. W. (1982) An iontophoretic investigation of the actions of convulsant kynurenines and their interaction with the endogenous excitant quinolinic acid. Brain Res. 247, 184–187
130. Petersen, O. W., Ronnov-Jessen, L., Howlett, A. R., & Bissell, M. J. (1992). Interaction with basement membrane serves to rapidly distinguish growth and differentiation pattern of normal and malignant human breast epithelial cells. Proceedings of the National Academy of Sciences, 89(19), 9064-9068. doi:10.1073/pnas.89.19.9064
131. Petrov, D., Mansfield, C., Moussy, A., & Hermine, O. (2017). ALS clinical trials review: 20 years of failure. Are we any closer to registering a new treatment? Frontiers in Aging Neuroscience, 9(MAR), 1–11. https://doi.org/10.3389/fnagi.2017.00068
132. Philips, Thomas, and Jeffrey D. Rothstein. “Rodent Models of Amyotrophic Lateral Sclerosis.” Current Protocols in Pharmacology, Jan. 2015, doi:10.1002/0471141755.ph0567s69.
133. Pinto, S., Cunha, C., Barbosa, M., Vaz, A. R., & Brites, D. (2017). Exosomes from NSC-34 cells transfected with hSOD1-G93A are enriched in mir-124 and drive alterations in microglia phenotype. Frontiers in Neuroscience, 11(MAY). https://doi.org/10.3389/fnins.2017.00273
134. Prause, J., Goswami, A., Katona, I., Roos, A., Schnizler, M., Bushuven, E., Weis, J. (2013). Altered localization, abnormal modification and loss of function of Sigma receptor-1 in amyotrophic lateral sclerosis. Human Molecular Genetics, 22(8), 1581-1600. doi:10.1093/hmg/ddt008
135. Prell, T., Lautenschläger, J., Witte, O. W., Carri, M. T., & Grosskreutz, J. (2012). The unfolded protein response in models of human mutant G93A amyotrophic lateral sclerosis. European Journal of Neuroscience, 35(5), 652-660. doi:10.1111/j.1460-9568.2012.08008.x

136. Reddypalli, Shailaja, et al. “p75NTR-Mediated Signaling Promotes the Survival of Myoblasts and Influences Muscle Strength.” Journal of Cellular Physiology, vol. 204, no. 3, 2005, pp. 819–829., doi:10.1002/jcp.20330.
137. Reichardt, L. F. “Neurotrophin-Regulated signalling pathways.” Philosophical Transactions of the Royal Society B: Biological Sciences, vol. 361, no. 1473, 2006, pp. 1545–1564., doi:10.1098/rstb.2006.1894.
138. Rembach A., Turner B. J., Bruce S., Cheah I. K., Scott R. L., Lopes E. C., et al. . (2004). Antisense peptide nucleic acid targeting GluR3 delays disease onset and progression in the SOD1 G93A mouse model of familial ALS. J. Neurosci. Res. 77, 573–582. 10.1002/jnr.20191
139. Ren, M., Du, C., Acero, E. H., Tang-Schomer, M. D., & Özkucur, N. (2016). A biofidelic 3D culture model to study the development of brain cellular systems. Scientific Reports, 6(1). doi:10.1038/srep24953
140. Renton, A. E., Chiò, A., & Traynor, B. J. (2013). State of play in amyotrophic lateral sclerosis genetics. Nature Neuroscience, 17(1), 17-23. doi:10.1038/nn.3584
141. Renton, A.E., Majounie, E., Waite, A., Simón-Sánchez, J., Rollinson, S., Gibbs, J.R., Schymick, J.C., Laaksovirta. H., van Swieten, J.C., Myllykangas, L., Kalimo, H., Paetau, A., Abramzon, Y., Remes, A.M., Kaganovich, A., Scholz, S.W., Duckworth, J., Ding, J., Harmer, D.W., Hernandez, D.G., Johnson, J.O., Mok, K., Ryten, M., Trabzuni, D., Guerreiro, R.J., Orrell, R.W., Neal, J., Murray, A., Pearson, J., Jansen, I.E., Sondervan, D., Seelaar, H., Blake, D., Young, K., Halliwell, N., Callister, J.B., Toulson, G., Richardson, A., Gerhard, A., et al. (2011). A hexanucleotide repeat expansion in C9ORF72 is the cause of chromosome 9p21-linked ALS-FTD. Neuron. 72(2), 257-68. doi:10.1016/j.neuron.2011.09.010
142. Richardson, K., Allen, S. P., Mortiboys, H., Grierson, A. J., Wharton, S. B., Ince, P. G., . . . Heath, P. R. (2013). The Effect of SOD1 Mutation on Cellular Bioenergetic Profile and Viability in Response to Oxidative Stress and Influence of Mutation-Type. PLoS ONE, 8(6). doi:10.1371/journal.pone.0068256
143. Robberecht, W., & Philips, T. (2013). The changing scene of amyotrophic lateral sclerosis. Nature Reviews Neuroscience, 14(4), 248-264. doi:10.1038/nrn3430
144. Rosen, D. (1993). Erratum: Mutations in Cu/Zn superoxide dismutase gene are associated with familial amyotrophic lateral sclerosis. Nature, 364(6435), 362-362. doi:10.1038/364362c0
145. Rothstein, Jeffrey D. “Edaravone: A new drug approved for ALS.” Cell, vol. 171, no. 4, 2017, p. 725., doi:10.1016/j.cell.2017.10.011.
146. Rutherford, N. J., Zhang, Y., Baker, M., Gass, J. M., Finch, N. A., Xu, Y., Stewart, H., Kelley, B.J., Kuntz, K., Crook, R.J., Sreedharan, J., Vance, C., Sorenson, E., Lippa, C., Bigio, E.H., Geschwind, D.H., Knopman, D.S., Mitsumoto, H., Petersen, R.C., Cashman, N.R., Hutton, M., Shaw, C.E., Boylan, K.B., Boeve, B., Graff-Radford, N.R., Wszolek, Z.K., Caselli, R.J., Dickson, D.W., Mackenzie, I.R., Petrucelli., L., Rademakers, R. (2008). Novel Mutations in TARDBP (TDP-43) in Patients with Familial Amyotrophic Lateral Sclerosis. PLoS Genetics, 4(9). doi:10.1371/journal.pgen.1000193
147. Ryu, H., Jeon, G. S., Cashman, N. R., Kowall, N. W., & Lee, J. (2011). Differential expression of c-Ret in motor neurons versus non-neuronal cells is linked to the pathogenesis of ALS. Laboratory Investigation, 91(3), 342–352. https://doi.org/10.1038/labinvest.2010.203
148. Saccon, R. A., Bunton-Stasyshyn, R. K. A., Fisher, E. M. C., & Fratta, P. (2013). Is SOD1 loss of function involved in amyotrophic lateral sclerosis? Brain, 136(8), 2342–2358. https://doi.org/10.1093/brain/awt09
149. Serio, A., & Patani, R. (2017). Concise Review: The Cellular Conspiracy of Amyotrophic Lateral Sclerosis. Stem Cells. doi:10.1002/stem.2758
150. Shibata, N., Hirano, A., Kobayashi, M., Sasaki, S., Takeo, K., Matsumoto, S., Asayama, K. (1994). Superoxide dismutase-like immunoreactivity in Lewy body-like inclusions of sporadic amyotrophic lateral sclerosis. Neuroscience Letters, 179(1-2), 149-152. doi:10.1016/0304-3940(94)90956-3.
151. Sholl D. A. (1956). The measurable parameters of the cerebral cortex and their significance in its organization. Prog. Neurobiol. 2, 324–333. 10.1016/s0079-6123(08)62112-3
152. Simian, M., & Bissell, M. J. (2016). Organoids: A historical perspective of thinking in three dimensions. The Journal of Cell Biology, 216(1), 31-40. doi:10.1083/jcb.201610056
153. Smith, I., Haag, M., Ugbode, C., Tams, D., Rattray, M., Przyborski, S., Whalley, B. J., et al. (2015). Neuronal-glial populations form functional networks in a biocompatible 3D scaffold. Neuroscience Letters, 609, 198-202. doi:10.1016/j.neulet.2015.10.044

154. Sreedharan, J., Blair, I. P., Tripathi, V. B., Hu, X., Vance, C., Rogelj, B., Ackerley, S., Durnall, J. C., Williams, K. L., Buratti, E., Baralle, F., de Belleroche, J., Mitchell, J. D., Leigh, P. N., Al-Chalabi, A., Miller, C. C., Nicholson, G., Shaw, C. E. (2008). TDP-43 Mutations in Familial and Sporadic Amyotrophic Lateral Sclerosis. Science, 319(5870), 1668-1672. doi:10.1126/science.1154584
155. Subramaniam, J. R., Lyons, W. E., Liu, J., Bartnikas, T. B., Rothstein, J., Price, D. L., Wong, P. C. (2002). Mutant SOD1 causes motor neuron disease independent of copper chaperone–mediated copper loading. Nature Neuroscience, 5(4), 301-307. doi:10.1038/nn823.
156. Taylor, A. R., Gifondorwa, D. J., Newbern, J. M., Robinson, M. B., Strupe, J. L., Prevette, D., Milligan, C. E., et al. (2007). Astrocyte and Muscle-Derived Secreted Factors Differentially Regulate Motoneuron Survival. Journal of Neuroscience, 27(3), 634-644. doi:10.1523/jneurosci.4947-06.2007
157. Taylor, J. P., & Cleveland, D. W. (2017). HHS Public Access, 539(7628), 197–206. https://doi.org/10.1038/nature20413.Decoding
158. Todd, A. G., Astroski, J. W., Lin, H., . . . Androphy, E. J. (2016). Altered mRNA Splicing in SMN-Depleted Motor Neuron-Like Cells. Plos One, 11(10). doi:10.1371/journal.pone.0163954
159. Tortarolo, M., Lo Coco, D., Veglianese, P., Vallarola, A., Giordana, M. T., Marcon, G., Bendotti, C. (2017). Amyotrophic Lateral Sclerosis, a Multisystem Pathology: Insights into the Role of TNF α. Mediators of Inflammation, 2017. https://doi.org/10.1155/2017/2985051
160. Tseng, Y., Chen, C., Jong, Y., Chang, F., & Lo, Y. (2016). Loganin possesses neuroprotective properties, restores SMN protein and activates protein synthesis positive regulator Akt/mTOR in experimental models of spinal muscular atrophy. Pharmacological Research, 111, 58-75. doi:10.1016/j.phrs.2016.05.023
161. Turner, B. J., Murray, S. S., Piccenna, L. G., Lopes, E. C., Kilpatrick, T. J., & Cheema, S. S. (2004). Effect of p75 neurotrophin receptor antagonist on disease progression in transgenic amyotrophic lateral sclerosis mice. Journal of Neuroscience Research, 78(2), 193-199. doi:10.1002/jnr.20256
162. Urushitani, M., Kurisu, J., Tsukita, K., & Takahashi, R. (2002). Proteasomal inhibition by misfolded mutant superoxide dismutase 1 induces selective motor neuron death in familial amyotrophic lateral sclerosis. Journal of Neurochemistry, 83(5), 1030-1042. doi:10.1046/j.1471-4159.2002.01211.x
163. Urushitani, M., Sik, A., Sakurai, T., Nukina, N., Takahashi, R., & Julien, J. P. (2006). Chromogranin-mediated secretion of mutant superoxide dismutase proteins linked to amyotrophic lateral sclerosis. Nature Neuroscience, 9(1), 108–118. https://doi.org/10.1038/nn1603
164. Usuki S, Ren J, Utsunomiya I, Cashman NR, Inokuchi J, Miyatake T. GM2ganglioside regulates the function of ciliary neurotrophic factor receptor inmurine immortalized motor neuron-like cells (NSC-34).Neurochem Res2001;26: 375–82
165. Uzel, S. G., Platt, R. J., Subramanian, V., Pearl, T. M., Rowlands, C. J., Chan, V., Kamm, R. D., et al. (2016). Microfluidic device for the formation of optically excitable, three-dimensional, compartmentalized motor units. Science Advances, 2(8). doi:10.1126/sciadv.1501429
166. Van Damme, P., Robberecht, W., & Van Den Bosch, L. (2017). Modelling amyotrophic lateral sclerosis: progress and possibilities. Disease Models & Mechanisms, 10(5), 537–549. https://doi.org/10.1242/dmm.029058
167. Vance, C., Rogelj, B., Hortobagyi, T., Vos, K. J., Nishimura, A. L., Sreedharan, J., Shaw, C. E. et al. (2009). Mutations in FUS, an RNA Processing Protein, Cause Familial Amyotrophic Lateral Sclerosis Type 6. Science, 323(5918), 1208-1211. doi:10.1126/science.1165942
168. Velde, C. V., Mcdonald, K. K., Boukhedimi, Y., Mcalonis-Downes, M., Lobsiger, C. S., Hadj, S. B., . . . Cleveland, D. W. (2011). Misfolded SOD1 Associated with Motor Neuron Mitochondria Alters Mitochondrial Shape and Distribution Prior to Clinical Onset. PLoS ONE, 6(7). doi:10.1371/journal.pone.0022031
169. Veyrat-Durebex, C., Corcia, P., Dangoumau, A., Laumonnier, F., Piver, E., Gordon, P. H., . . . Blasco, H. (2013). Advances in Cellular Models to Explore the Pathophysiology of Amyotrophic Lateral Sclerosis. Molecular Neurobiology, 49(2), 966-983. doi:10.1007/s12035-013-8573-9
170. Vicario, A., Kisiswa, L., Tann, J. Y., Kelly, C. E., and Ibáñez, C. F. (2015). Neuron- type-specific signaling by the p75NTR death receptor is regulated by differential proteolytic cleavage. J. Cell Sci. 128, 1507–1517. doi: 10.1242/jcs.161745

171. Vilmont, V., Cadot, B., Ouanounou, G., & Gomes, E. R. (2016). A system for studying mechanisms of neuromuscular junction development and maintenance. Journal of Cell Science, 129(14). doi:10.1242/jcs.194613
172. Wang, L., Gutmann, D. H., & Roos, R. P. (2010). Astrocyte loss of mutant SOD1 delays ALS disease onset and progression in G85R transgenic mice. Human Molecular Genetics, 20(2), 286-293. doi:10.1093/hmg/ddq463
173. Wen, W., Sanelli, T., Ge, W., Strong, W., & Strong, M. J. (2006). Activated microglial supernatant induced motor neuron cytotoxicity is associated with upregulation of the TNFR1 receptor. Neuroscience Research, 55(1), 87–95. https://doi.org/10.1016/j.neures.2006.02.004
174. Wichterle, H., & Peljto, M. (2008). Differentiation of Mouse Embryonic Stem Cells to Spinal Motor Neurons. Current Protocols in Stem Cell Biology. doi:10.1002/9780470151808.sc01h01s5
175. Wiese, Stefan, et al. "Isolation and enrichment of embryonic mouse motoneurons from the lumbar spinal cord of individual mouse embryos." Nature Protocols, vol. 5, no. 1, 2009, pp. 31–38., doi:10.1038/nprot.2009.193.
176. Wijesekera, L. C., & Leigh, P. N. (2009). Amyotrophic lateral sclerosis. Orphanet Journal of Rare Diseases, 4(1), 3. doi:10.1186/1750-1172-4-3
177. Xiao, S., McLean, J., & Robertson, J. (2006). Neuronal intermediate filaments and ALS: A new look at an old question. Biochimica et Biophysica Acta - Molecular Basis of Disease, 1762(11–12), 1001–1012. https://doi.org/10.1016/j.bbadis.2006.09.003
178. Xu, R., Wu, C., Zhang, X., Zhang, Q., Yang, Y., Yi, J., . . . Tao, Y. (2011). Linking hypoxic and oxidative insults to cell death mechanisms in models of ALS. Brain Research, 1372, 133-144. doi:10.1016/j.brainres.2010.11.056
179. Yaffe D, Saxel O. Serial passaging and differentiation of myogenic cells isolated from dystrophic mouse muscle. Nature 1977; 270:725- 727.
180. Yang, L., Lindholm, K., Konishi, Y., Li, R., Shen, Y., (2002). Target depletion of distinct tumor necrosis factor receptor subtypes reveals hippocampal neuron death and survival through different signal transduction pathways. J. Neurosci. 22, 3025–3032.
181. Yim, M. B., Kang, J. H., Yim, H. S., Kwak, H. S., Chock, P. B., & Stadtman, E. R. (1996). A gain-of-function of an amyotrophic lateral sclerosis-associated Cu,Zn-superoxide dismutase mutant: An enhancement of free radical formation due to a decrease in Km for hydrogen peroxide. Proceedings of the National Academy of Sciences, 93(12), 5709-5714. doi:10.1073/pnas.93.12.5709.
182. Yu, R. K., Tsai, Y., & Ariga, T. (2012). Functional Roles of Gangliosides in Neurodevelopment: An Overview of Recent Advances. Neurochemical Research, 37(6), 1230-1244. doi:10.1007/s11064-012-0744-y
183. Zahavi, E. E., Ionescu, A., Gluska, S., Gradus, T., Ben-Yaakov, K., & Perlson, E. (2015). A compartmentalized microfluidic neuromuscular co-culture system reveals spatial aspects of GDNF functions. Journal of Cell Science, 128(6), 1241-1252. doi:10.1242/jcs.167544
184. Zielasek, J., Hartung, H.P., (1996). Molecular mechanisms of microglial activation. Adv. Neuroimmunol. 6, 191–220

Appendix

Overview of the 2D Experiments Performed Using in Matrigel Sandwich Cell Culture.

					Image analysis					
Stimulus	Amount	Duration (days)	n(bio)	Experiments	mean (% Live Healthy)	mean (% Δ Live Healthy)	sem (% Δ Live Healthy)	mean (% Dead)	mean (% Δ Dead)	sem (% Δ Dead)
Medium		1	11	3,5,7,8,9,	35,3	0,0	0,0	24,3	0,0	0,0
		2	2	18,21	33,8	0,0	0,0	24,7	0,0	0,0
Serum free		1	4	12,13,19,	35,5	-4,3	2,2	30,2	5,7	2,2
		2	2	18,21	27,9	-5,9	1,5	42,1	17,3	3,3
NGF	10	1	1	12	54,9	2,4		26,8	0,7	
	100	1	1	12	52,5	-0,1		26,1	-0,1	
	1000	1	1	12	55,6	3,1		25,0	-1,1	
	100	2	2	18,21	32,2	-1,6	2,8	26,6	1,8	3,4
pro-NGF	100	1	2	12,13	47,6	0,9	1,1	24,5	-0,7	0,1
	1000	1	1	12	53,8	1,3		25,5	-0,7	
	100	2	2	18,21	32,8	-1,1	2,6	26,2	1,5	3,7
BDNF	0,1	1	2	19,23	28,9	-2,4	3,9	23,9	0,1	1,0
	1	1	2	19,23	27,9	-4,9	6,7	24,5	0,6	3,4
	10	1	3	17,19,23	33,3	-1,7	2,7	18,7	-0,8	0,7
	100	1	2	19,23	30,6	-2,2	6,2	23,0	-0,9	2,1
	100	2	1	21	29,0	-2,1		23,2	-2,5	
IL1α	0,1	1	1	11	41,5	3,8		20,9	-2,8	
	1	1	1	11	40,0	2,4		20,8	-2,9	
	10	1	1	11	37,4	-0,3		22,5	-1,3	
	100	1	1	11	37,1	-0,6		23,8	0,0	
	10	2	2	18,21	31,1	-2,7	3,1	26,4	1,7	3,2
INFγ	0,1	1	1	11	39,6	2,0		21,8	-1,9	
	1	1	1	11	40,5	2,9		20,8	-2,9	
	10	1	1	11	37,0	-0,7		21,8	-1,9	
	100	1	1	11	38,1	0,5		23,5	-0,2	
	25	2	2	18,21	30,6	-3,2	2,2	25,3	0,6	1,4
TNFa	6,25	1	1	5	22,5	-4,8		27,5	2,7	
	10	1	1	4	16,2	-1,4		37,0	11,1	
	25	1	2	4,5	19,0	-3,5	1,2	32,4	7,1	1,7
	100	1	2	4,5	18,4	-4,1	0,6	32,2	6,9	1,6
	100	2	2	18,21	27,3	-6,5	0,2	37,4	12,7	0,8
AMPA	50	1	1	13	45,0	4,1		21,6	-2,6	
	5	2	1	18	28,6	-7,9		20,0	-3,7	
	50	2	1	18	28,7	-7,8		19,6	-4,2	
	500	2	1	18	29,0	-7,6		21,4	-2,4	
NMDA	5	1	1	12	55,4	2,8		23,4	-2,7	
	50	1	1	12	45,7	-6,9		26,9	0,8	
	100	1	2	12,13	46,0	-0,8	0,1	25,0	-0,1	0,5
DMSO	0,15%	1	3	8,9,13	36,4	-1,0	2,0	27,6	1,4	0,6
	0,60%	1	1	16	52,2	1,1		9,9	-3,0	
	1,00%	1	3	17,22,25	35,1	1,5	0,9	19,9	-0,6	0,7
H2O2	6,25	1	2	5,8	29,1	0,4	8,9	36,2	8,9	5,1
	10	1	1	4	20,9	3,3		29,5	3,6	
	25	1	3	4,5,8	18,2	-6,8	7,4	49,4	22,6	14,2
	50	1	2	3,16				31,9	3,9	
	100	1	10	3,7,8,13,	16,8	-17,3	2,2	49,4	25,1	4,0
	150	1	1	3				51,0	23,0	
	400	1	1	8	15,5	-14,6		47,6	17,7	
	100	2	1	21	2,0	-29,1		77,0	51,3	
BNN20	1	1	3	17,22,25	34,5	1,0	1,1	19,2	-1,3	2,1
	10	1	2	22,25	28,3	-2,3	1,8	18,6	-6,8	1,8
	100	1	4	16,17,22,	33,1	-0,4	4,3	16,3	-4,2	2,2
Edaravone	6	1	1	8	34,8	4,7		36,4	6,5	
	25	1	1	8	34,0	3,9		36,5	6,7	
	100	1	2	7,8	37,6	-2,2	0,5	35,7	9,2	5,9
	400	1	1	8	33,3	3,2		41,3	11,5	
Medium		1	5	3,20,24,2	49,6	0,0	0,0	25,9	0,0	0,0
		2	2	18,26	38,0	0,0	0,0	23,1	0,0	0,0
Serum free		1	3	24,27,28	42,2	-10,4	2,6	33,7	10,5	1,7
		2	1	18	23,6	-4,9	14,1	43,6	20,5	5,4
NGF	100	2	2	18,26	39,4	1,4	2,4	24,9	1,8	0,9
pro-NGF	100	2	2	18,26	39,3	1,2	1,4	24,1	1,0	1,7
BDNF	0,1	1	2	27,28	49,8	-1,4	1,8	28,9	1,7	1,7
	1	1	2	27,28	50,3	-1,3	0,5	30,0	2,8	0,7
	10	1	2	27,28	49,0	-2,6	1,7	31,5	4,3	1,4
	100	1	2	27,28	45,2	-6,4	4,3	35,9	8,7	4,2
	100	2	1	26	37,1	3,6		13,0	2,4	
IL1α	10	2	2	18,26	38,9	0,8	1,0	24,8	1,7	1,1
INFγ	25	2	2	18,26	41,7	3,6	0,7	23,3	0,1	4,3
TNFa	15	1	1	3				43,7	14,5	
	25	1	1	3				46,8	17,6	
	50	1	1	3				34,0	4,8	
	100	1	1	3				37,6	8,4	
	100	2	2	18,26	36,6	-1,5	3,0	28,6	5,5	1,0
NMDA	100	2	1	26	33,3	-0,2		11,1	0,5	
DMSO	0,40%	1	2	20,24	45,6	-2,3	0,2	20,3	-2,6	0,4
H2O2	6,25	1	3	5,20,24	48,6	0,7	0,6	25,0	2,2	1,1
	25	1	3	5,20,24	38,0	-9,9	10,8	44,5	21,7	14,2
	100	1	4	20,24,27,	23,4	-24,5	2,6	57,9	31,7	4,3
	400	1	2	20,24	22,5	-25,4	2,2	54,6	31,7	9,9
Edaravone	6,25	1	2	20,24	43,6	-4,4	0,4	24,9	2,1	1,1
	25	1	2	20,24	39,8	-8,1	3,5	25,4	2,5	0,4
	100	1	2	20,24	40,1	-7,8	4,3	28,9	6,1	4,0